University of Stavanger

FACULTY OF SCIENCE AND TECHNOLOGY

MASTER'S THESIS

Study programme/specialisation: **Petroleum Engineering** **(Drilling Technology)**	**Spring semester, 2018** **Open** / ~~Confidential~~
Author: **Mari Røstvig Tveit**	**Digital submission** ~~(signature of author)~~
Programme coordinator: **Mahmoud Khalifeh** Supervisor(s): **Mahmoud Khalifeh (UiS), Tor Nordam (SINTEF Ocean)**	
Title of master's thesis: **Understanding Leakage Rates in Permanently Abandoned Wells by Studying Natural Hydrocarbon Seepages**	
Credits: **30 ECTS**	
Keywords: **Permanent plug and abandonment** **Natural hydrocarbon seepages** **Oil / gas seeps** **Fate analysis** **Leaking wells**	Number of pages: 144 + supplemental material/other: 0 Stavanger, **15th June 2018**

Spring | 18

Understanding Leakage Rates in Permanently Abandoned Wells by Studying Natural Hydrocarbon Seepages

By Mari Røstvig Tveit

This work is submitted in partial fulfillment of
the requirements for the degree of Master of Science (MSc)
within Petroleum Engineering at the University of Stavanger

To Leon,

For knowing before myself that I would love engineering

ABSTRACT

Permanent plug and abandonment (PP&A) of wells is steadily becoming more important on the Norwegian Continental Shelf (NCS), as a large number of fields are approaching end of their productive life. Combining operational, material, and qualification challenges, it is evident that risk of leaks exists from permanently abandoned wells. To ensure the protection of our environment, well integrity standard NORSOK D-010 constitutes zero leak acceptance criteria; however, natural hydrocarbon seepages are occurring all over the world on a daily basis. To evaluate the fate of leaking oil and/or gas from abandoned wells, two real cases from the NCS, one historical gas leak (Field A) and one theoretical oil leak (Field B), have been subject to fate analysis, executed using software from SINTEF Ocean's Marine Environmental Modeling Workbench (MEMW). For Field A, it is found that approximately 95 to 99% of the leaking gas dissolves while rising through the water column. The fraction of gas transported to atmosphere is a function of the initial gas bubble size and ambient temperature. The fate of oil is more complex than gas, but results show that due to its persistent nature, released oil will be able to travel more than hundred kilometers away from the release point. Due to this dispersion, concentrations, the main factor controlling toxicity, will be greatly diluted. Fate of oil is dependent on chemical composition; lighter compounds will evaporate to the atmosphere, while heavy compounds will be deposited on the seafloor. Evaporation, sedimentation and biodegradation are the main contributing mechanisms in fate analysis of oil.

ACKNOWLEDGEMENTS

I would like to express my gratitude to the number of people that made this work possible:

- First and foremost, I would like to sincerely thank my supervisor at the University of Stavanger, Mahmoud Khalifeh; for believing in me, for always being available and for always making me feel welcome in your office. I really enjoyed my time!
- To Tor Nordam, my co-supervisor at SINTEF Ocean; thank you for teaching me the software, for providing me with scripts and for your kindness and willingness to help.
- To SINTEF Ocean; for providing me with access to your excellent software, thank you, I am very grateful.
- To Ivar Blaauw, Lars Hovda and the rest of the team at ConocoPhillips; thank you for all of your time and input, from start to finish. This work has benefited a lot from our conversations.
- To all PAF members; for inviting me to present my work at your meeting, thank you for your time and interesting discussion.
- To Øystein Arild and Hans Petter Lohne; for providing me with useful input when pitching the idea of the project, thank you.
- To Martin Hovland; thank you for sharing your knowledge with me and helping me put things in a larger perspective.

Lastly, I would like to thank my family for all of their love and support throughout the years. The biggest thank you of all goes to Andreas; for your continuous support, encouragement, humour and tough love, I would never have been able to complete this work without you. I love you!

Mari Tveit

Stavanger 2018

TABLE OF CONTENTS

ABSTRACT ii

ACKNOWLEDGEMENTS iii

LIST OF FIGURES viii

LIST OF TABLES xi

NOMENCLATURE xii

1. INTRODUCTION 1

1.1 Permanent Plug & Abandonment 1

1.1.1 Plug and abandonment activities in the North Sea 1

1.1.2 Regulatory authorities 2

1.1.3 Regulatory authorities in the North Sea 2

1.2 Well barrier 3

1.2.1 Well barrier materials 5

1.2.2 Barrier failure modes 6

1.2.2.1 Leakage through the bulk material 7

1.2.2.2 Leakage around the bulk material 7

1.2.2.3 Shift in barrier position 8

1.2.3 Well barrier verification 9

1.3 Challenges in permanent plug and abandonment 12

1.3.1 Leaks through permanently abandoned wells 13

1.4 Objectives of the thesis 15

1.5 Methodology 16

2. NATURAL HYDROCARBON SEEPAGES 17

2.1 Terminology 19

2.1.1 Seep and seepage 19

2.1.2 Macro-seeps vs. microseepage 20
2.1.3 Origin of hydrocarbon seepages 20
2.1.4 Classifying seeping gas 21
2.1.5 Degradation of natural gas 23
2.1.6 How seeps affect the seabed 25
2.2 Natural hydrocarbon seepage in Norway and in the North Sea 26
2.2.1 Tommeliten seep area 27
2.3 Oil and gas seeps in North America 29
2.3.1 Seeps offshore California 29
2.3.2 The Gulf of Mexico 30
3. METHODOLOGY 32
3.1 Fate modeling 32
3.2 Case studies 36
3.2.1 Field A 37
3.2.2 Field B 40
3.3 Software 41
3.3.1 The OSCAR model 41
3.3.2 The Gastrack model 42
3.3.3 Model conventions and concepts 42
3.3.4 Scientific background of model 43
3.4 Model parameters 43
3.4.1 Number of particles 44
3.4.2 Concentration grid dimensions (xyz) 44
3.4.3 Time step 45
3.5 Input parameters 46
3.5.1 Release site 46
3.5.2 Time and duration of simulation and release 47
3.5.3 Release profile 48
3.5.4 Bubble / droplet size 49

3.5.4.1 Gas bubbles 50
3.5.4.2 Oil droplets 51
3.5.5 Environmental parameters 54
4. RESULTS AND DISCUSSION 56
4.1 Simulation process 56
4.2 Case A – Field A 57
4.2.1 Determining grid size for simulation 57
4.2.2 Determining duration of simulation 60
4.2.3 Mass balance results and its dependence on bubble size 61
4.2.4 Leak rate sensitivity analysis 65
4.2.5 Comparing the results with natural seeps at Tommeliten 65
4.2.6 Factors affecting atmospheric transport of methane 67
4.2.7 Environmental effects of natural gas in the atmosphere 69
4.2.8 Environmental effects of natural gas in the sea 71
4.3 Case B 75
4.3.1 Mass balance results 75
4.3.1.1 Droplet size sensitivity analysis 78
4.3.1.2 Leak rate sensitivity analysis 80
4.3.1.3 Seasonal variations 82
4.3.2 Ultimate fate of oil 82
4.3.3 Oil persistence in the sediments 86
4.3.4 Concentration analysis – determining grid size 87
4.3.5 Leak rates and resulting concentrations 89
4.3.6 Environmental effects of evaporated oil 93
4.3.7 Environmental effects of oil in the water column 93
4.3.8 Environmental effects of oil in the sediments 99
4.4 Acceptable leak rates? 103
4.5 Implications of the work for PP&A 105
5. CONCLUSION 106

6. SUGGESTIONS FOR FUTURE WORK....108

REFERENCES....111

APPENDIX A – FIELD A TEMPERATURE DATA....119

APPENDIX B – PYTHON PROGRAMMING SCRIPTS....120

APPENDIX C – MASS BALANCE RESULTS....125

APPENDIX D – MASS BALANCE RESULTS DAY 90....128

LIST OF FIGURES

Fig. 1.1 Well barrier extended from formation to formation, as visualized by NORSOK D-010 (2013). 4
Fig. 1.2 Well barrier schematics as shown in NORSOK D-010 (2013). 4
Fig. 1.3 Potential leak paths for cement plug and/or annular cement, including channeling, microannuli and mudcake due to poorly executed cementing operations. 6
Fig. 1.4 Forces acting on a barrier. 9
Fig. 1.5 Status in temporary abandoned wells summarized by the PSA. 15

Fig. 2.1 Map of reported oil and gas seeps, onshore and offshore, created from global data sets. 17
Fig. 2.2 Photographs of natural seepages. 18
Fig. 2.3 Temperature windows for the generation of different hydrocarbons. 21
Fig. 2.4 Classifying natural gas by isotopic signatures and component ratios. 22
Fig. 2.5 Gas seepage offshore Virginia, north of Washington Canyon, USA.. 25
Fig. 2.6 Locations of selected macro seeps in the North Sea 26
Fig. 2.7 Seismic image of salt diapir and gas in sediments in the Tommeliten seep area. 28
Fig. 2.8 Tar from natural seeps floating in the ocean offshore Point Conception, California 30
Fig. 2.9 Weathered oil found on Port Aransas Beach, Texas, sample ca. 1 cm 31

Fig. 3.1 Fate of naturally seeping oil and gas. 33
Fig. 3.2 Monitoring of leaking gas wells at Field A, January to June. 38
Fig. 3.3 Monitoring of leaking gas wells at Field A, January to November. 39
Fig. 3.4 OSCAR start page interface for new release scenario. 46
Fig. 3.5 Seasonal variations in sea temperature by the formation of a thermocline in Mid-Latitudes. 48
Fig. 3.6 Oil droplet size distribution, OSCAR default settings. 52
Fig. 3.7 Temperature and salinity profiles for the water column, winter data on the left, summer data on the right. Data applicable for Field B. 55

Fig. 4.1 Simulation process.....56
Fig. 4.2 Surface gas mass fluxes for 100m x 100m grid, W-08 and W-16. 58
Fig. 4.3 Surface gas mass fluxes for different grid sizes, W-16. 59
Fig. 4.4 Surface gas mass fluxes for different grid sizes, W-08. 59
Fig. 4.5 Cross sectional views to evaluate escaping gas at times t. 60
Fig. 4.6 Gas mass flux variation according to different bubble sizes. 62
Fig. 4.7 Cross sectional view of gas releases with different bubble sizes 64
Fig. 4.8 Changes in methane percentage and bubble diameter as functions of initial bubble size.66
Fig. 4.9 Gas exchange in seep bubble.....67
Fig. 4.10 Los Angeles skyline seen through the smog 71
Fig. 4.11 Example of mass balance results from OSCAR. 75
Fig. 4.12 Mass balance results day 1. 76
Fig. 4.13 Mass balance results day 90. 77
Fig. 4.14 Example of 200km x 200km size grid in the North Sea.....78
Fig. 4.15 Mass balance results in winter as function of droplet size. 79
Fig. 4.16 Mass balance results in summer as function of droplet size. 79
Fig. 4.17 Mass balance as function of leak rate, winter.....81
Fig. 4.18 Mass balance as function of leak rate, summer. 81
Fig. 4.19 Final mass balance according to season and droplet size. 83
Fig. 4.20 Minimum and maximum values of final mass balance fractions. 84
Fig. 4.21 Mass balance as function of time following a five day oil release, winter. 85
Fig. 4.22 Mass balance as function of time following a five day oil release, summer. 85
Fig. 4.23 Mass balance for one year following a five day release. 86
Fig. 4.24 Maximum concentrations for different droplets sizes and grids. 88
Fig. 4.25 Mean concentrations for different droplet sizes and grids. 89
Fig. 4.26 Maximum concentrations following the release scenarios as function of time [days]....91
Fig. 4.27 Maximum concentrations, comparison between leak rates. 92
Fig. 4.28 Mean concentrations, comparison between leak rates. 92
Fig. 4.29 Zones of biological effect as a function of dissolved oil in mg/l. 95

Fig. 4.30 Maximum concentration maps for a) all compounds, b) naphtalenes at a random time t 98
Fig. 4.31 Sediment concentrations.....100
Fig. 4.32 Sediment deposition of different oil compounds grouped by carbon numbers.....102

LIST OF TABLES

Table 2.1 Simplified notation for natural gas components 23
Table 2.2 Leak rate conversion. 39

Table 3.1 Solubility of selected aromatics and oils. 35

Table 4.1 Mean gas mass flux rate and fractions of gas released to atmosphere and gas dissolved, as function of bubble sizes. 63
Table 4.2 Fractions of gas released to atmosphere and gas dissolved, as function of leak rates. 65
Table 4.3 Contribution of leaking gas to ocean acidification. 73
Table 4.4 Mass balance fractions. 75
Table 4.5 Mass balance results, for a 5 day release, 90 day simulation. 82
Table 4.6 Mean and maximum concentrations for different grid sizes. 88
Table 4.7 Mean and maximum concentration following the release scenarios. 90
Table 4.8 Resulting zones of biological effects following the different oil release scenarios. 96

NOMENCLATURE

A	Area
D	Diameter
d	Day
D_{min}	Minimum diameter
D_{max}	Maximum diameter
g	Gravitational acceleration
hr	Hour
k	Permeability
L	Length
min	Minute
mPa·s	Millipascal-seconds, denotes viscosity
P_h	Force, exerted by hydrostatic pressure
P_p	Force, exerted by pressure
ppm	Parts per million
ppb	Parts per billion
P_w	Force, exerted by self weight
q	Volumetric Flowrate
R	Radius
Sm^3	Standard cubic meter
t	Metric ton (1000 kg)
y	Year
μ	Viscosity
μm	Micrometer
ρ_f	Density of fluid
ρ_p	Density of particle

Abbreviations

AOMs	Anaerobic Oxidizers of Methane
BTEX	Benzene, Toluene, Ethyl-benzene and Xylenes
CBL	Cement Bond Log
COP	Coal Oil Point
CT	Coiled Tubing
DEA	Danish Energy Agency
DPZ	Distinct Permeable Zone
GHSZ	Gas Hydrate Stability Zone
GoM	Gulf of Mexico
LOT	Leak Off Test
MDAC	Methane-Derived Authigenic Carbonates
MEMW	Marine Environmental Modeling Workbench
MPC	Maximum Permissible Concentration
NCS	Norwegian Continental Shelf
NPD	Norwegian Petroleum Directorate
OBM	Oil Based Mud
OPC	Ordinary Portland Cement
OSCAR	Oil Spill Contingency And Response
P&A	Plug and Abandonment
PAHs	Polycyclic Aromatic Hydrocarbons
PP&A	Permanent Plug and Abandonment
PSA	Petroleum Safety Authority (Norwegian)
PWC	Perforate, Wash and Cement
R&D	Research and Development
ROV	Remotely Operated Vehicle
SAR	Synthetic-aperture radar
SCA	Short-Chained Alkane
TOC	Top of cement
UKCS	UK Continental Shelf

VDL	Variable Density Log
WBE	Well Barrier Element
WBM	Water Based Mud
WBS	Well Barrier Schematic

CHAPTER 1

INTRODUCTION

1.1 Permanent Plug & Abandonment

When a well has fulfilled its intended purpose, and it is not to be re-used or re-entered, it becomes a candidate for Permanent Plug & Abandonment (PP&A). Different regulatory authorities have different requirements to be fulfilled when plugging and abandoning a well, and operators need to comply with the local standards. Although there are some discrepancies in different parts of the world, for instance regarding plug length, the common intention of permanent well abandonment is to achieve the following (Campbell and Smith 2013):

- Isolate and protect all freshwater zones.
- Isolate all potential future commercial zones.
- Maintain well integrity in an eternal perspective.
- Cut pipe to an agreed level below seabed or ground and remove all surface equipment.

In other words, operators shall leave the well in a condition such that both the downhole and surface conditions are protected. Generally, most regulatory authorities require placement of two independent, permanent well barriers for hydrocarbon sources or abnormally pressurized zones and one permanent well barrier for non-hydrocarbon potentials to ensure well integrity is maintained (NORSOK D-010 2013, Oil & Gas UK 2012a). Well integrity is defined as the "*application of technical, operational and organizational solutions to reduce risk of uncontrolled release of formation fluids throughout the life cycle of a well*" (NORSOK D-010 2013). The Plug & Abandonment (P&A) operation thus depends not only on advanced technologies, but also on human factors.

1.1.1 Plug and abandonment activities in the North Sea

After gas was discovered at the Groningen field in the Netherlands in 1959, exploration activities intensified in the North Sea. In 1965, the first British discovery of gas was made in the West Sole Field, followed by the Danish oil discovery in 1966 at the Kraka field and the first viable

Norwegian oil discovery in 1969 at Ekofisk (Nordsøfonden 2018, Ministry of Petroleum and Energy 2013, University of Aberdeen 2006). In the following years a number of major discoveries were made, and approximately 12,000 wells have since been drilled in the North Sea (Liversidge et al. 2006). As the oil and gas industry has matured, more and more of these fields are now reaching end of their productive life, and the number of wells ready for permanent abandonment is rapidly increasing. In 2014, a report estimated that the PP&A of the current wells on the UK Continental Shelf (UKCS) alone would require over 140 years of working time, without any working downtime (DECOM North Sea 2014). Since PP&A is costly work, with no financial return, the industry is applying major effort on developing and implementing new technology. Moving towards rigless abandonment to reduce day rates, and using new technology that reduces operational time are the two areas with the greatest focus and cost saving potential (Campbell and Smith 2013).

1.1.2 Regulatory authorities

Even though oil and gas industries are active around the world, few countries have publically available regulations considering PP&A. The most highly regulated areas for well abandonment are the North Sea and the Gulf of Mexico (GoM), both areas with long oil and gas production history, fields near reaching the end of their productive lives and ageing infrastructure. The regulations and recommended practices give descriptions on qualification of materials, operational procedures and verification requirements (Smith et al. 2011). The contrast is significant to some countries, such as Italy, Ukraine, Angola and Australia, whose regulations only state the goals of P&A operations, while again other countries, such as Venezuela, Russia, Oman, Saudi-Arabia and Egypt, have no known or publically available legislation considering P&A, leaving the full responsibility to the operators (Diaz 2017). Even though well integrity and environmental protection can be viewed as a global matter, no global standards for P&A exist yet.

1.1.3 Regulatory authorities in the North Sea

The North Sea is divided into several sectors, with the four most active petroleum producing sectors being the Norwegian, United Kingdom, Dutch and Danish sector. Each country has its own regulatory authorities, and they are the Norwegian Petroleum Directorate (NPD), The Health

and Safety Executive, the Dutch Supervision of Mines and the Danish Energy Agency (DEA), respectively (Fronks 2002, IEA GHG 2009). All of these authorities require zero leak acceptance criteria for permanently abandoned wells, and cement is the prime barrier material used. However, the means for which one is to obtain this criterion is not conclusive, as the regulatory authorities have different requirements for the well barriers – particularly regarding the length of the cement plug. For instance, the Norwegian and Dutch well integrity standards both require 100 m of cement in open hole, or 50 m of cement to be placed on top of a mechanical plug, while the UK guidelines generally states that 500 ft of cement should be placed, with a minimum window of good quality cement of 100 ft (30.48 m) (Liversidge et al. 2006, NORSOK D-010 2013, Oil & Gas UK 2012a).

1.2 Well barrier

A well barrier is best described as an envelope, consisting of one or several Well Barrier Elements (WBEs) that together prevent uncontrolled fluid flow from the reservoir into the well, other formations or the external environment. The barrier shall prevent fluid flow in both vertical and lateral direction. When abandoning a well permanently, the barriers must maintain a permanent seal. A permanent barrier must thus be designed in such a way that it is able to withstand the maximum anticipated loads and maximum differential pressure and temperature that it may be exposed to in an eternal perspective. The barrier must extend across the full cross section of the well, from formation to formation, and include all annuli, as shown in Fig. 1.1. This concept can also be shown by Well Barrier Schematics (WBS), such as the two examples shown in Fig. 1.2 of permanently abandoned wells with one and two potential reservoirs, respectively.

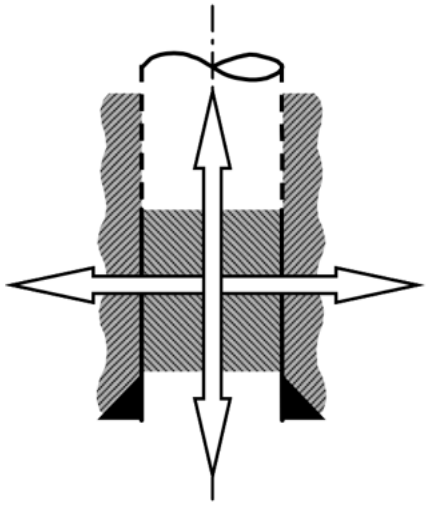

Fig. 1.1 Well barrier extended from formation to formation, as visualized by NORSOK D-010 (2013).

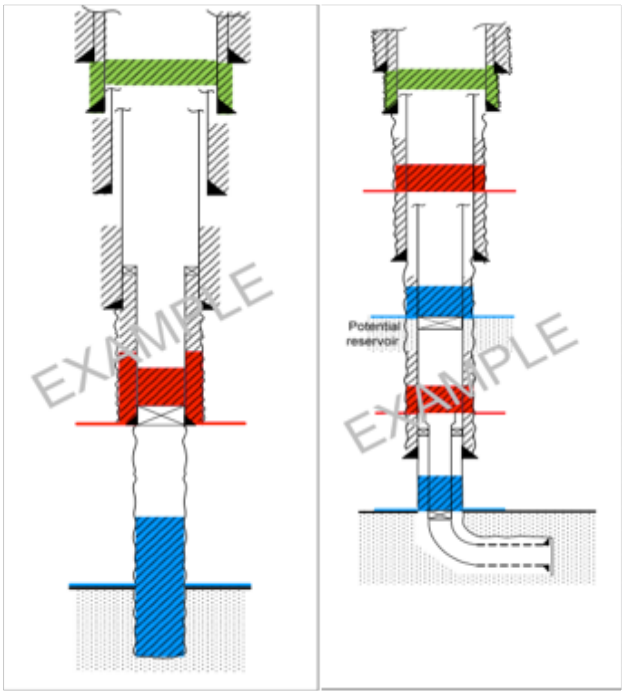

Fig. 1.2 Well barrier schematics as shown in NORSOK D-010 (2013).

1.2.1 Well barrier materials

Ordinary Portland Cement (OPC) is currently and historically the prime material used for permanent barriers in well abandonment, as it has previously been considered to have similar properties to the cap rock that it is replacing (Oil & Gas UK 2012b). This is however not the case, and drawbacks regarding its properties and durability persuades researches to search for alternatives. Until new materials are available for use on a large scale, OPC is still the main barrier material used.

Portland cement is an example of hydraulic cement, which sets and develops compressive strength as a result of hydration – a chemical reaction between water and the compounds present in cement. The hydration process can also occur when the cement slurry is submerged in water, and the development of strength is predictable, uniform and relatively rapid. Set cement has low permeability and is near insoluble in water. By using different cement additives, systems for well cementing can be designed for a wide range of temperatures and pressures, from permafrost conditions below freezing point, to 350 °C [700 °F] and pressures in deep wells exceeding 200 MPa [30.000 psi]. Therefore, OPC is used in almost all well cementing operations (Nelson and Guillot 2006). These properties, in addition to being an inexpensive material, make cement a good candidate for use as barrier material. However, other materials can also function as a barrier, if they fulfill the main requirements of a barrier material (Oil & Gas UK 2012b):

- Very low permeability – to prevent flow of hydrocarbons or over-pressured fluids through the barrier.
- Long-term integrity – long-lasting isolation ability, does not deteriorate over time.
- Non-shrinking – no flow between plug and casing / annulus.
- Ductile – able to accommodate mechanical loads and changes in pressure / temperature.
- Resistance to downhole fluids and gases (CO_2, H_2S, hydrocarbons etc.).
- Able to make a good bond to the casing or formation in which it is placed.

OPC does not actually fulfill all these requirements, and this poses some challenges. It cannot withstand high temperature or corrosive environments, which may lead to gas influx unless certain chemicals are added (Vignes 2011). In addition, cement is known for becoming brittle

after setting, and can experience bulk shrinkage during setting, typically in the range of 0.5 – 5.0 % (Salehi et al. 2016, Nelson and Guillot 2006). However, these challenges may be minimized by adding different chemicals known as additives (Lende 2012).

There are many parameters during cementing operations, which may influence the long-term sealing capacity, and consequently affect well integrity. Both barrier materials and operational parameters must be optimized in order to achieve satisfactory results (Barclay et al. 2001). Failure to do so may lead to barrier failure.

1.2.2 Barrier failure modes

There are three potential barrier failure modes: leakage through the bulk material, leakage around the bulk material and shift in barrier position. These failure modes, and their associated root causes, are applicable both to annular cement and cement plugs. A visual presentation of potential leak paths is shown in Fig. 1.3.

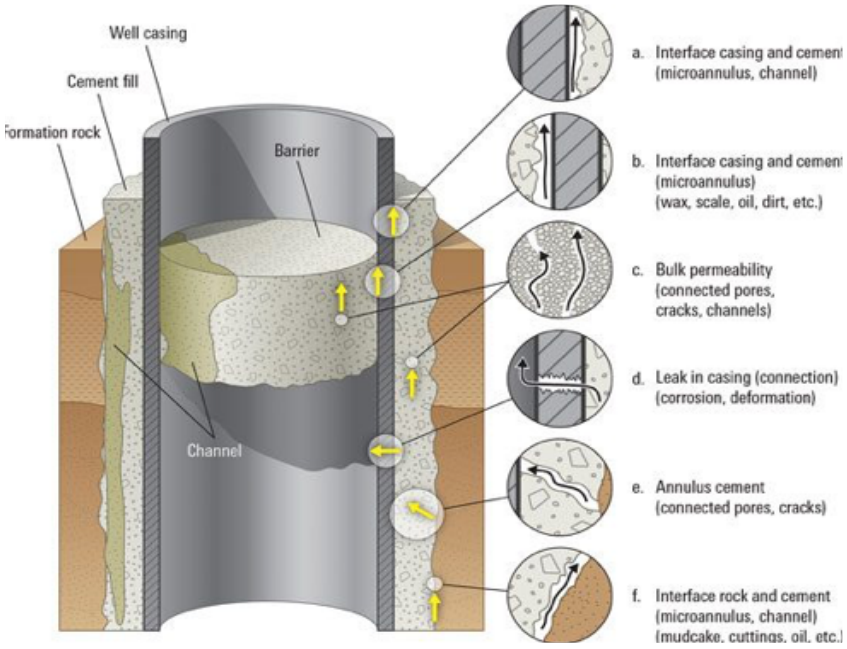

Fig. 1.3 Potential leak paths for cement plug and/or annular cement, including channeling, microannuli and mudcake due to poorly executed cementing operations. Figure reproduced from Schlumberger (2017).

1.2.2.1 Leakage through the bulk material

Leakage through the bulk material, which is most often a cement plug, can be described by Darcy's law;

$$q = \frac{kA}{\mu}\frac{\Delta p}{\Delta L}$$

where q is the flow rate of the fluid, k is the permeability of the plug material, A and ΔL are the cross sectional area and the length of the plug, respectively, Δp is the differential pressure across the plug and μ is the viscosity of the fluid. By studying this equation, the flow rate can only be zero if either the permeability and/or pressure difference approaches zero, or if the viscosity of the fluid and/or the length of the plug approaches infinity. The permeability of OPC matrix itself is extremely low, Oil & Gas UK (2012b) deems a typical permeability of 10 micro-Darcy in good-quality cement acceptable, but the effective permeability through a cement plug can be much higher if there are any defects in the plug, such as gas channels, cracks or microannuli (Nelson and Guillot 2006).

Bulk shrinkage of OPC slurry as it sets can create small cracks and gaps that can become flow paths for leaking hydrocarbons. Excessive fluid loss from the slurry to the formation may cause gas intrusion in the cement before setting, and consequently gas channels may form (Barclay et al. 2001). Leakage paths may also form after a successful cementing job, for instance, cracks may form due to changes in tectonic stress, or perhaps due to subsidence of the formation as the reservoir is depleted. Cracking may also occur in wells where temperature and pressure fluctuations are present, such as gas producing wells. In other words, there are several mechanisms in play that may compromise the quality of the cement plug and may cause flow paths to form, both during and after cementing operations (Nelson and Guillot 2006).

1.2.2.2 Leakage around the bulk material

A well-known failure mode causing leakages around a cement plug is the presence of a microannulus. During setting, as it is an exothermal reaction, cement will exert heat to its surroundings, and thereby might cause the casing to expand. After the cement has set and

temperature drops, the casing may shrink and cause stress in the cement plug, which again may crack or form a microannulus. In addition to the temperature variation, bulk shrinkage of the cement may also contribute to the microannulus, and even small microannuli can become effective flow paths around a cement plug (Nelson and Guillot 2006).

To avoid leakage around the cement plug, emphasis should be placed on creating a good hydraulic bonding between the cement and the adjacent casing or formation (Khalifeh et al. 2018). A hydraulic bond is defined as the bond between the cement and the casing or formation that will help to prevent the flow of fluids through the interface (Evans and Carter 1962). In order to create a good bonding, the cement slurry must make good contact with the surface of the casing or the formation. Consequently, removal of drilling fluid, filter cake and other pollutants such as barite, washed out formation and swarf is very important. If hole cleaning is not adequate, this can cause leakage paths to form around the plug (Barclay et al. 2001). The strength of the hydraulic bond also depends on other factors, such as temperature and pressure, properties of the cement slurry and type of casing material (Khalifeh et al. 2018). Evans and Carter (1962) investigated the relationship between the different factors and the resulting bond strength, and concluded that a mud layer at the interface between cement and casing, ergo insufficient hole cleaning, was the factor that caused the maximum reduction in hydraulic bonding strength.

Even though one manages to create a good hydraulic bond when placing the cement, this may fail with time, and this process is called “debonding”. Debonding can be a result of many processes and factors, including changes in the tectonic stresses in the formation, subsidence, pressure decrease during production, pressure increase after PP&A, stimulation practices, cement shrinkage with time or temperature fluctuations (Thiercelin et al. 1998, Nelson and Guillot 2006).

1.2.2.3 Shift in barrier position

The mechanism that preserves the barrier’s position in the well is shear bond strength. The bond strength must be strong enough to resist the forces exerted on the barrier, which include downward acting forces caused by the barriers self-weight (P_w) and the hydrostatic pressure above it (P_h), and the upward acting force from the reservoir pressure (P_p), as illustrated in Fig.

1.4. As a depleted reservoir often will experience a pressure build up after abandonment, and PP&A is conducted with an eternal perspective, the initial reservoir pressure is safe to use as the final reservoir pressure in calculations (Mainguy et al. 2007).

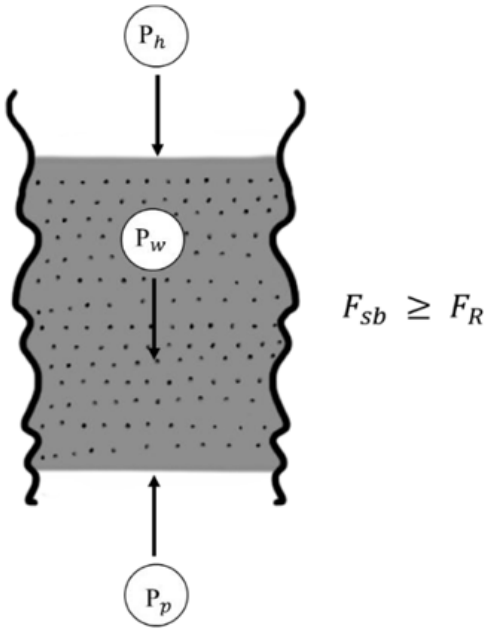

Fig. 1.4 Forces acting on a barrier. Figure reproduced from Khalifeh (2017).

The shear bond strength between the cement and the casing or formation depends on the nature of the contact surfaces and the reaction characteristics of the materials. Other factors affecting the shear bond strength include borehole temperature and pressure, contamination of slurry, whether the formation or casing has been contaminated with water-based mud (WBM) or oil-based mud (OBM) and types of cement additives (Khalifeh et al. 2018).

1.2.3 Well barrier verification

As PP&A is conducted with an eternal perspective, it is important to be able to verify the quality of the barriers. This is also addressed in the well integrity standards, where different testing procedures are often specified. The verification processes may differ with different plug and well configurations.

Typically, in a PP&A operation, the starting point is assessing the current status of the well. By examining the number and location of potential reservoirs the well has penetrated, the number of plugs and their depth placement intervals must be decided. It is desirable to execute the PP&A as cost efficiently as possible, while still maintaining long-term well integrity. If it is possible to use the existing casings strings and primary casing cement as well barrier elements, the cost of a plug will amount only to the cost of placing an additional cement plug inside the casing. To evaluate this possibility, the Top Of Cement (TOC) behind the casing string must be located, so that the length of the cemented interval can be found. If the length of the interval is sufficient for placing a barrier, and located within the appropriate depth window for a barrier, the quality of the primary cement must be examined.

There are different types of logs used to evaluate cement quality, including temperature logs, sonic logs, Cement Bond Logs and (CBL) and Variable Density Logs (VDL), and one can either evaluate the logs from the primary cementing operations or run new logs before PP&A. In addition, original cementing reports describing operational parameters, such as volumes pumped, returns, differential pressure, slurry rate and density etc., are used to check the quality of cement (Khalifeh 2017). CBL and VDL logs can also be used in un-cemented intervals to assess if formation can be used as an annulus barrier element, as naturally creeping shale may form a tight seal around the casing strings (Williams et al. 2009). The challenge with using CBL and VDL logs to evaluate sealing quality of primary cement or creeping formation, is that the interpretation of the logs is qualitative, not quantitative. The results are dependent on calibration factors and subject to personal interpretation, and hence, different personnel may come to different conclusions. Another parameter affecting the accuracy of CBL and VDL logs, is the downhole conditions. Wellbore inclination, casing eccentricity and potential defects will all affect the output from the logs, which are initially designed for an ideal case of centralized use in a wellbore of uniform size. These shortcomings in both data acquisition and interpretation accuracy have sparked a trend of evaluating new logging tools and methods, the most promising ones including acoustic logs, X-ray measurements and Neutron-Neutron logs. However, none of the alternative methods are commercially used for cement evaluation yet (Khalifeh et al. 2017).

Should the annular barrier element be deemed of good quality, the typical next steps in creating a barrier are retrieving the tubing inside the casing, pump a viscous pill or set a mechanical plug as a foundation for a cement plug, and pump as much cement as required by the appropriate well integrity standard. If the logs reveal non-existent or compromised annular barrier element, a new formation-to-formation barrier needs to be placed, and this usually requires section milling or Perforate Wash and Cement technique (PWC). In both cases, the position and sealing capability of the finished barrier must be tested and verified after completion.

For cement barriers placed in open hole, the top of the cement plug is dressed off after setting and the TOC is identified by tagging. NORSOK D-010 (2013) requires no further barrier verification, while Oil & Gas UK (2012a) states that cement barriers in open hole should also be verified by a weight test, typically 10 to 15 klbs on drillpipe, or otherwise limited to tools and geometry of the wellbore if test is performed with wireline, coiled tubing or stinger. For cement plugs in cased hole, tagging is also used to evaluate the TOC, unless the cement has a mechanical plug foundation and the TOC can easily be calculated from the volume of cement. The sealing capability of the cement plug is evaluated by means of pressure testing (Aguilar et al. 2016). A pressure test is performed by applying a minimum of 500 psi above the estimated leak off pressure below the barrier, to check whether it is able to withstand the pressure without any loss of fluids through the barrier. It is important to evaluate and stay below the burst strength of the casing, to avoid damaging the well while performing the test. A negative pressure test, or an in-flow test, is performed by lowering the pressure in the well so that at least the maximum pressure differential expected after PP&A is experienced, and monitor the pressure to see if there are any inflow to the well. In the case where the cement plug has a mechanical foundation that has already been pressure tested, there is no point in pressure testing the plug itself (NORSOK D-010 2013, Oil & Gas UK 2012a).

The method of pressure testing a barrier, gives a qualitative result of whether the barrier is able to withstand a certain differential pressure or not without fluids flowing through the barrier. However, these tests of the functional requirements cannot be correlated with the requirements for plug length. Even though recommended standards state that a barrier should contain 50 m or

100 ft of good cement, the pressure test cannot describe the quality throughout the barrier, as it is a simple test of yes or no. In a worst-case scenario, a 50 m plug could contain as little as 1 m of good cement, and this would still be enough to keep the pressure. In a long-term perspective however, due to pure statistics, this plug would be more prone to failure in the future. In other words, the current barrier verification process does not yield quantitative information, and will therefore not be very useful in evaluating the leak potential of an abandoned well.

1.3 Challenges in permanent plug and abandonment

PP&A is a challenging field. In addition to the comprehensive well integrity standards, there are several other factors that may pose a challenge, from the planning phase and all throughout the execution and verification phases.

One challenge that may arise in the planning phase is the ability to assess the current status of the well, as there might be relevant data lacking in the documentation of old wells. Also, well conditions may have changed, due to e.g. tectonic stresses exerted by the formation and subsidence after depletion of the reservoir. For instance, the seabed above the Ekofisk chalk reservoir has subsided several meters since the start of production in 1971, causing major casing deformation (Schwall and Denney 1994). This causes problems when entering the well with tools or when trying to pull equipment out of hole. Depletion may also cause changes in formation strength, making old pressure plots from the drilling phase unreliable (Khalifeh et al. 2013).

During the execution phase, successful placement of the barriers is essential for obtaining the desired results. High temperatures downhole, unconsolidated formations, swarf handling, insufficient hole cleaning and formation porosity are some factors that may complicate the placement. As previously discussed, there are also several parameters affecting the sealing capabilities of the plugs after successful placement, and with an eternal perspective, there might be parameters out of our control that may affect the well integrity in the future (Barclay et al. 2001, Khalifeh et al. 2013).

Another challenge in PP&A on the NCS (and in other parts of the world) is simply the amount of work left. Executing all the necessary PP&A with today's strict regulations and available technology will mean substantial operational time. To attempt to avoid this, Norwegian operator Equinor is currently awaiting start up of almost all PP&A operations until 2020, with the peak activity expected after 2030, hoping that new, time and cost saving technology will be available by then (Ottøy 2017). Several companies are currently researching new, innovative PP&A solutions trying to meet this demand, one of them using a combination of bismuth and thermite to melt the wellbore and surrounding cap rock together in one, permanent seal (Carragher and Fulks 2018). Progress is also being made moving towards rigless abandonment. For instance, Halliburton recently plugged and abandoned 13 wells successfully in one single campaign on the NCS, using only coiled tubing (CT) for all operational steps such as milling, washing, placing mechanical plugs and cementing (Thomson 2018). Other ways to increase efficiency are also being investigated, and in one ongoing Norwegian project, a national open-source P&A database is being developed, to ease the obtainment of information on the NCS (Myrseth et al. 2017).

With the increasing focus on reducing operational time, and the testing of new technology, some may argue that the risk of leaks is increasing. And indeed, at the Plug and Abandonment Forum in October 2017, the Norwegian Petroleum Safety Agency (PSA) emphasized the operators' need to be focused on verification and HSE when using new technology and methods, and suggested that failure to provide sufficient documentation might lead to new requirements regarding post PP&A monitoring and development of contingency intervention plans (Gundersen 2017).

1.3.1 Leaks through permanently abandoned wells

In the current revision, NORSOK D-010 (2013) does not require any monitoring system for permanently abandoned wells. In other words, when the operators permanently plug and abandon a well, they do a visual examination and monitor the pressures over some time to make sure that the well was successfully abandoned without any leakages. After cutting and retrieving the wellhead, and decommissioning the platform and other seabed equipment such as pipelines, they leave the site with a goal to leave it looking like its previous, natural state. In the hypothetical scenario where only 1 m of cement out of 50 m is of good quality, how long would it take before

the pressure would build up and/or the barrier would be degraded, allowing a leak to propagate upwards in the well? And would this ever be detected? A small leak from an anonymous well without monitoring would emerge from the seafloor as a small stream of gas bubbles or oil droplets, which would most likely dissolve and disperse in the sea without reaching the surface, and without being noticed. This makes one wonder just how many possible leaking wells are going under our radar.

In 2015, a public study was published aiming to quantify methane leakage from abandoned wells in the North Sea. A survey of three permanently abandoned exploration wells was performed on the south-western flank of the Utsira high in the Norwegian sector of the North Sea, and leakages of shallow, biogenic gas was proven in all three wells, specifically wells 15/9-13, 16/4-2 and 16/7-2. The total annual seabed emissions from the three wells were estimated to be approximately 24 tons (Vielstädte et al. 2015). The finding sparked an interest for assessing total emissions from all abandoned wells, and a follow up study was presented in 2017, estimating that 33 ± 6 % of all wells in the North Sea have the potential for leaking shallow gas, releasing between 3,000 – 17,000 t of methane to the seabed each year (Vielstädte et al. 2017). However, this study is based on statistics and a limited number of field observations, so the numbers are subject to uncertainty.

Even though there is no organized monitoring of permanently abandoned wells, the PSA is closely monitoring well integrity in temporary abandoned wells. Even though the requirements for temporary and permanent plug and abandonment differ in some aspects, for instance in approved well barrier elements, the experiences from these monitored wells can help with the understanding of the way barriers are degraded, and in turn help improve the abandonment standards. As can be seen by Fig. 1.5**,** with numbers adapted from Gundersen (2016), the idea of a potential leak in permanently abandoned well is not unlikely.

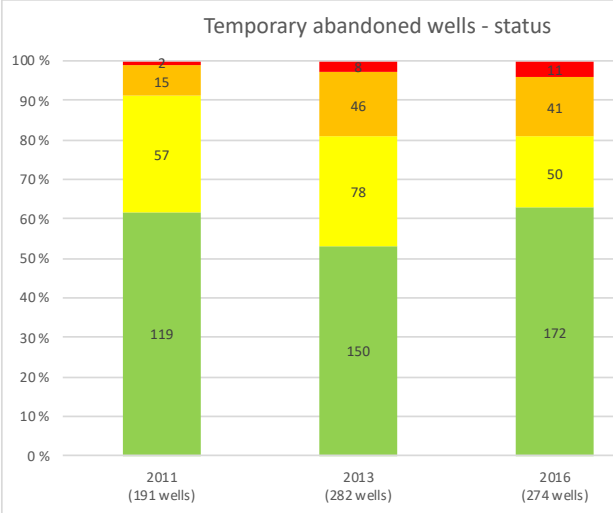

Red	One barrier failure and the other is degraded / not verified, or leak to surface
Orange	One barrier failure and the other is intact, or a single failure may lead to leak to surface
Yellow	One barrier degraded, the other is intact
Green	Healthy well - no or minor issue

Fig. 1.5 Status in temporary abandoned wells summarized by the PSA.

1.4 Objectives of the thesis

On the NCS and in the North Sea, regulations have defined zero leak acceptance criteria for permanently abandoned wells. However, how to proceed if a leak occurs, is unclear. As PP&A is indeed intended to be permanent, and the wellhead is removed in the last stage, installing well control equipment and re-entering a leaking well to do a re-abandonment would be practically impossible. Remediating a leak from an unknown source after all cement plugs are set, perhaps over several formations with flow potential, would be time consuming, difficult and extremely costly. As todays regulations does not address this topic, the current work is therefore meant to serve as a source of information to help with decision analysis, in case a small hydrocarbon leak from a permanently abandoned well is detected. By evaluating the possible consequences of a leak, the regulators will have more facts to base their regulations on, and the zero leak criteria might be re-evaluated. When applying a zero leak tolerance, this may suppress necessary research on the consequences, and limit communication between operators and regulatory authorities, and the decisions are made based on working standard, not risk evaluation. Ultimately, the objectives of this thesis is to help the industry form new, more specific standards and evaluation procedures in the case of leaking, abandoned wells.

1.5 Methodology

To be able to evaluate the consequences of a leaking well, some real and theoretical examples on leaks on the NCS are investigated in this thesis. The intention behind the zero leak philosophy of well integrity standards such as NORSOK D-010 (2013) is to ensure that the petroleum industry make no harm on our environment. However, natural hydrocarbon seepages occur around the world, including on the NCS, on a daily basis (Etiope 2015, Judd and Hovland 2007). The goal of this thesis is to model and investigate the fate of a small hydrocarbon leak from an abandoned well and compare it to a natural seep, to make a contribution to the discussion of whether doing no harm to the environment necessarily means allowing zero leak. To achieve this, a review of natural hydrocarbon seepages is presented in chapter 2. In chapter 3, the basics of fate modeling are presented, along with the chosen case studies and a presentation of the software used for this thesis. Results are presented in chapter 4, intertwined with discussion on possible environmental effects. After the conclusions in chapter 5, suggestions for future work are presented in chapter 6. In total, all the chapters together aim to help answer the following question:

Does doing zero harm on our environment necessarily mean requiring zero leakage criteria?

CHAPTER 2

NATURAL HYDROCARBON SEEPAGES

All around the world, hydrocarbons are naturally and spontaneously emerging at the surface, both onshore and offshore. A map of reported seeps is shown in Fig. 2.1.

Fig. 2.1 Map of reported oil and gas seeps, onshore and offshore, created from global data sets. Reproduced from CGG Geoconsulting (2015).

Tales of natural seeps can be found in ancient literature, including in the bible. When Noah was instructed by God to build the ark, he used tar to caulk the hull; "Make for yourself an ark of gopher wood; you shall make the ark with rooms, and shall cover it inside and out with pitch" (Genesis 6:14). Seeping gas in the Baba Gurgur field in Iraq, shown in Fig. 2.2a, has been burning in The Eternal Fire for 2,500 years, and is home for ancient practices and worship. It is clear that natural oil and gas seepages have been observed, and used, by humans for thousands of years. Native Americans, amongst them Karankawa Indians, living in what is now known as Texas, used tar washed up on the beaches from offshore seeps in the GoM to caulk their boats and waterproof baskets (Newcomb Jr. 2002). European explorers reported on bitumen and tar deposits onshore and offshore early in the 16th century in North, Central and South America, and

European immigrants used seeping oil from tar pits, as shown in Fig. 2.2b, to grease their wagon wheels and to burn in oil lamps (Geyer and Sweet 1972). Offshore seeps have been documented by camera in the recent years, and two examples of seeps from the GoM are shown in Fig. 2.2c and Fig. 2.2d.

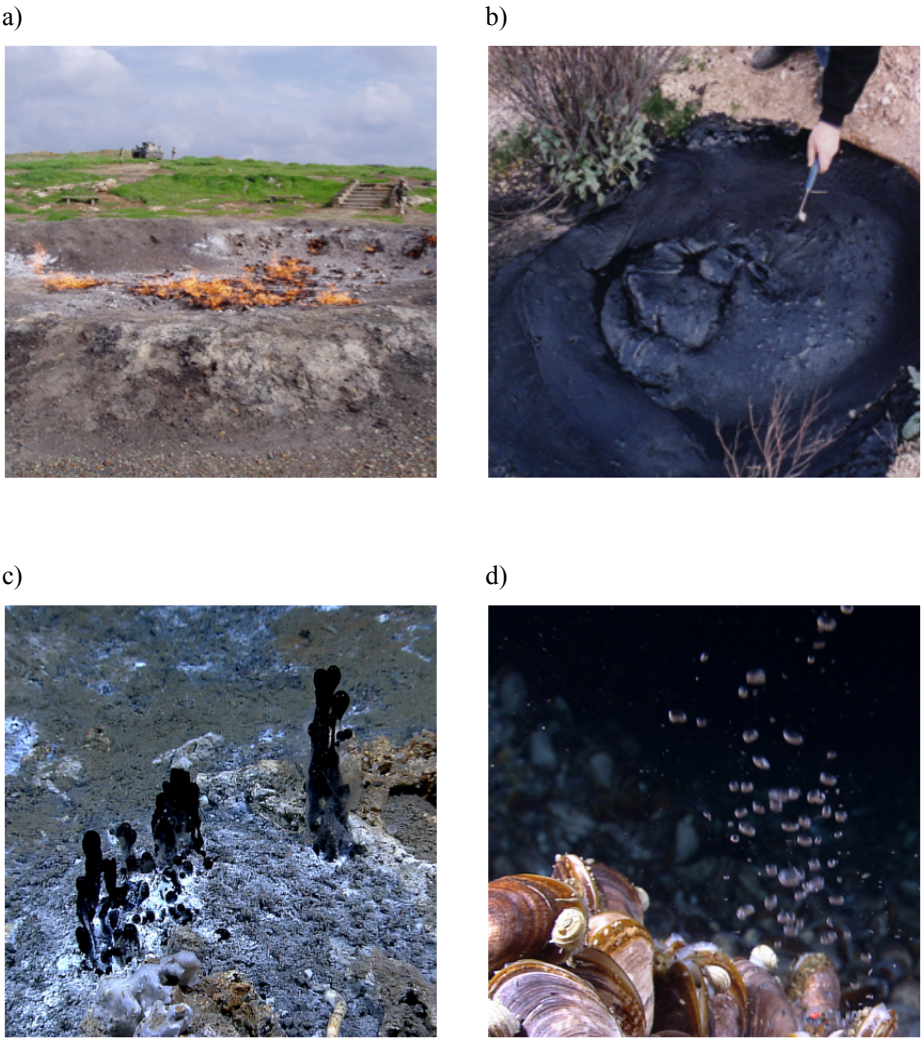

Fig. 2.2 Photographs of natural seepages. a) The eternal fire of Baba Gurgur in Iraq, photograph by Hill (2006). b) The McKittrick tar seep in California, emerging gas bubbles ignited by lighter. Photograph by Lldenke (2000). c) Oil seeping from the seafloor in the GoM. d) Natural gas seeping through a mussel bed in the GoM, photograph of c) and d) by NOAA Okeanos Explorer Program (2012).

In the beginning of the oil industry, all exploration activities were dominated by wells being dug or drilled near natural seeps. In what is now the Yenangyaong field in Burma, oil production started as early as 1800 from 500 hand-dug wells. The name of the field is said to mean "Town through which flows a river of oil", which is clear evidence that surface seeps sparked the production activities in the area. The same pattern can be seen in the Middle East, where old maps of western Iran will show many names with Naft in them. This word means "oil", and invariably marks the locations of seeps. Up until 1949, every field in Iran was associated with surface oil or gas seeps (Link 1952). Even though technology has progressed and there are now more sophisticated means for exploration activities, studying natural hydrocarbon seepages is still used for identifying potential new commercial sources of petroleum (Logan et al. 2010).

As one of the goals of this thesis is to understand the consequences of leaking wells on the NCS by reviewing the phenomenon of natural hydrocarbon seepages, only areas of offshore seepage will be investigated in the current work. A few examples will be more closely examined to retrieve relevant information on the nature and behavior of seeps.

2.1 Terminology

When reviewing literature on hydrocarbon seepages, there are some important terms that need to be defined.

2.1.1 Seep and seepage

The terms *seep* and *seepage* are often used to denote the same phenomenon, although their definitions are different. In general, the term seep should only be used to indicate a fluid emerging from a point source, with a flow rate that can be expressed as mass per time, for instance grams day^{-1}. The term seepage, on the other hand, is used to provide information on the flow rate from an areal source, and thus the flow rate can be expressed as mass per area per time, for instance grams m^{-2} day^{-1} (Etiope 2015). In the dictionary, the word seepage is defined as a geological activity or phenomenon, whereas the word seep is the action of the fluid emerging at

seabed or ground. In other words, oil and gas may seep through a vent at the seafloor, whilst the general activity in the area is defined as oil or gas seepage.

2.1.2 Macro-seeps vs. microseepage

Macro-seeps produce focused streams of gas bubbles or oil droplets that rise through the water column towards the surface, and consequently, a macro-seep can be both visually and acoustically detected (Hovland et al. 2012). Microseepage is a more widespread dispersed exhalation of gas, and is usually detected by taking samples of either pore water in the sediments, or the seawater above the expected seepage area, and measuring the content of dissolved gas. Microseepage is evidence of a permeable subsurface where gas can migrate and disperse throughout the subsurface. Where the migration is more focused, and a macro-seep appears, this is generally an indication of a subsurface with fractures or faults that make up migration routes for oil or gas. Note that oil is always defined as seep, there exists no oil microseepage (Etiope 2015).

2.1.3 Origin of hydrocarbon seepages

Conventional oil and gas as we know it in the petroleum industry, are product of the burial of organic matter, typically in sedimentary basins. When organic matter is preserved and subject to deep burial, high temperature in the subsurface will cause the "cracking" of organic matter into lighter compounds, eventually creating oil and gas. This process is called catagenesis, and the resulting oil and gas is named thermogenic hydrocarbon. The process usually takes place in temperatures above 60°C, and the correlating depth is therefore dependent on the temperature at seafloor and the geothermal gradient. When dealing with seeping gas, the origin is not necessarily thermogenic. Natural gas can also be produced by microbial communities in shallow sediments at relatively low temperatures, typically up to 60 – 80°C. The process is called diagenesis, and this shallow gas is commonly known as biogenic or microbial gas (Tissot and Welte 1984). Fig. 2.3 gives an overview of the temperature windows for the formation of the different hydrocarbon substances.

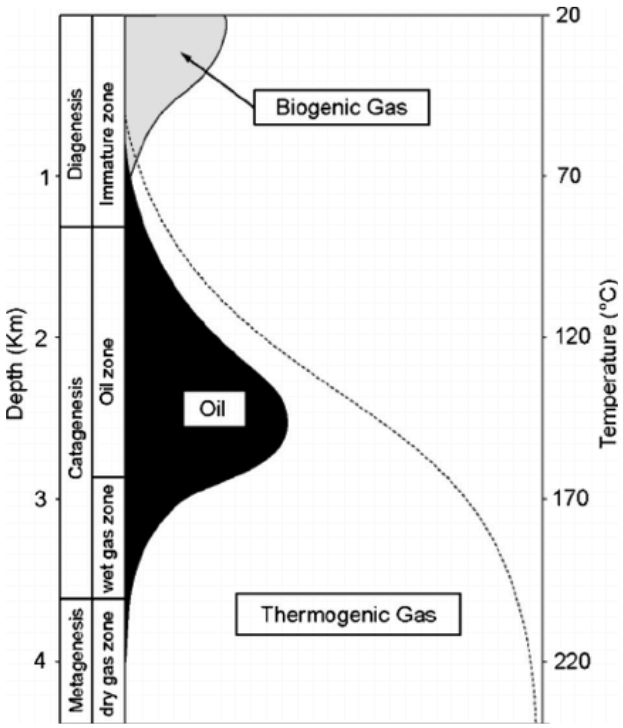

Fig. 2.3 Temperature windows for the generation of different hydrocarbons. Figure reproduced from Tissot and Welte (1984).

As both biogenic and thermogenic gas originate from a biological source, they can be cumulatively termed "biotic". Methane gas can also be created in chemical reactions without presence of organic matter, for instance in magmatic processes (Etiope 2015). However, these "abiotic" gases are outside the scope of this work and will not be discussed further.

2.1.4 Classifying seeping gas

When examining a seep of natural gas, it is desired to know whether the source of the gas is biogenic or thermogenic. The first step for identifying the origin is to examine the composition of the stable isotopes of carbon ($^{13}C/^{12}C$) and hydrogen ($^{2}H/^{1}H$) in methane. These are commonly expressed as $\delta^{13}C$ and $\delta^{2}H$ in ‰ (per mil) relative to the Vienna Pee Dee Belemnite (VPDB) and Vienna Standard Mean Ocean Water (SMOW) standards (Schoell 1980). As the hydrogen isotope ^{2}H is commonly known as Deuterium, $\delta^{2}H$ can also be expressed as δD. Worldwide, the

distributions of hydrogen and carbon isotopes are well defined for thermogenic and biogenic gas. Biogenic gas is generally characterized by $\delta^{13}C$ values lower than −50‰, while thermogenic gas is typically in the range between −45 and −30‰, with highly mature gas reaching values of −20‰. The results of $\delta^{13}C$ and $\delta^{2}H$ are plotted in a Schoell's diagram, Fig. 2.4a, which shows fields of biogenic, thermogenic and mixed source gas.

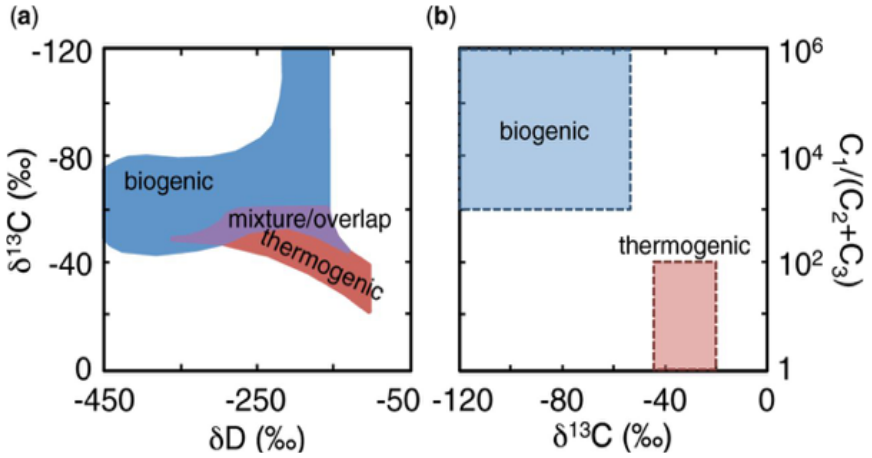

Fig. 2.4 Classifying natural gas by isotopic signatures and component ratios. Figure reproduced from Stolper et al. (2018).

The second step in determining the origin of the gas is to check the relative abundance of light hydrocarbons. Biogenic gas is produced by microbes (Archaea) in the shallow sediments, and the gas is very dry and consists mainly of methane (CH_4). Some ethane (C_2H_6) and trace amounts of propane (C_3H_8) may also be present. In thermogenic gas, which is created by the thermal cracking of larger hydrocarbon molecules, the fraction of heavier compounds will be more pronounced, and the gas may also contain heavier components such as butane (C_4H_{10}), pentane (C_5H_{12}) and hexane (C_6H_{14}). To simplify, the different compounds will from now on be referred to by their carbon number, as specified in Table 2.1.

Table 2.1 Simplified notation for natural gas components

Component	Chemical formula	Simplified notation
Methane	CH_4	C_1
Ethane	C_2H_6	C_2
Propane	C_3H_8	C_3
Butane	C_4H_{10}	C_4
Pentane	C_5H_{12}	C_5
Hexane	C_6H_{14}	C_6

The compositional differences between biogenic and thermogenic gas can be described using the Bernard ratio, $C_1/(C_2+C_3)$ (Bernard et al. 1978). Biogenic gas will normally have a Bernard ratio > 500, and thermogenic gas a Bernard ratio < 100. Note that the typical Bernard ratios vary slightly in literature, ranging from biogenic gas > 1000 to thermogenic gas < 50 (Etiope 2015, Brooks et al. 1979). However, thermogenic gas may in some cases have a Bernard ratio high enough for it to be mistaken as biogenic gas. This occurs when the gas is very dry and highly mature, as a result of the source rock being exposed to deep burial and/or very high temperature at the point of metagenesis, as can be seen from Fig. 2.3. To avoid misinterpreting the Bernard ratio, it is often plotted together with the $\delta^{13}C$ values of methane in what is called a Bernard diagram, shown in Fig. 2.4b. This chart is also often used to evaluate whether the seep may be a mixture of deep, thermogenic sources and shallow, biogenic sources.

2.1.5 Degradation of natural gas

Methane, the most abundant component of natural gas, seeping up through the sediments will undergo different chemical and biological processes. In the anaerobic sediments, anaerobic oxidizers of methane (AOMs) uses seeping methane and sulfate (SO_4^{2-}) from pore-water to create hydrogencarbonate (HCO_3^-), hydrosulfide ion (HS^-) and water (H_2O):

$$CH_4 + SO_4^{2-} \rightarrow HCO_3^- + HS^- + H_2O$$

An excess of methane will result in depletion of pore-water sulfate, excess of bicarbonate and a decrease in pH. In the case of normal supplies of bicarbonate in seawater, the excess carbonate will precipitate to form calcium carbonate ($CaCO_3$). These methane-derived authigenic carbonates (MDAC) are visible near seeps as rocks on the seabed. HS^-, if adequate supply of iron is present, will react and form pyrite (FeS_2). Sulfide not incorporated into pyrite will form hydrogen sulfide (H_2S), a poisonous gas with a characteristic smell of rotten eggs, and this will be utilized by sulfide-oxidizing bacteria, such as *Beggiatoa*. These sorts of bacteria may form large, fluffy, light colored bacterial mats in seepage areas, and is a very common feature of seepage, documented around the world, including the Tommeliten seep area (Judd and Hovland 2007, Niemann et al. 2005).

If not all methane is consumed by the AOMs, the rest will be available for utilization by methane-oxidizing bacteria (methanotrophs) in the top aerobic sediments:

$$CH_4 + 2O_2 \rightarrow CO_2 + 2H_2O$$

This will result in acidification of the local environment, favoring carbonate dissolution (Reeburgh 2007). Methane that "escapes" these bacteria is free to enter the water column in the form of a seep. In Fig. 2.5, a photograph from a gas seepage area offshore Virginia is presented. The white patches are bacterial mats, and quill worms, anemones, pandalid shrimp and a large red crab can also be seen in the area of the seep.

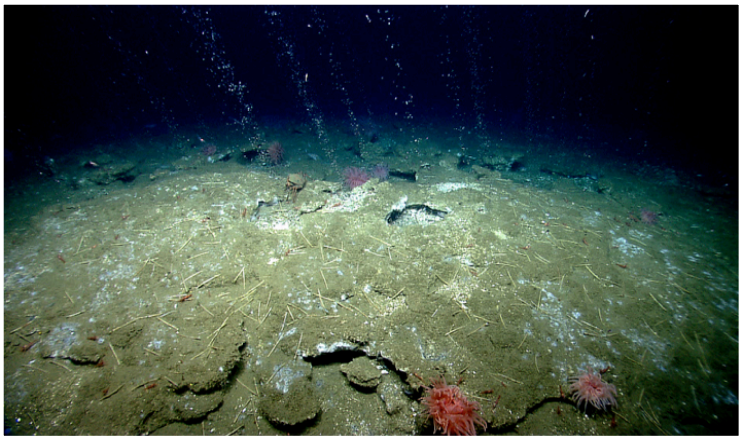

Fig. 2.5 Gas seepage offshore Virginia, north of Washington Canyon, USA. Photograph by NOAA Okeanos Explorer Program (2013).

The heavier components of natural gas undergo similar processes. Aerobic degradation processes on the short-chained alkanes (SCAs) ethane, propane, n-butane and iso-butane (C_2 – C_4) by microorganisms in terrestrial environments have been well known for decades (Musat 2015). The diversity of bacteria and fungi able to degrade gaseous alkanes have been documented around the world, but have only recently been found in marine environments (Shennan Jean 2005). The anaerobic degradation of SCAs in deep-sea marine sediments around hydrocarbon seeps has also been a subject for studies in the past two decades, and anaerobic microorganisms able to degrade SCAs are found to be relatively wide-spread and physiologically diverse (Musat 2015).

2.1.6 How seeps affect the seabed

Wherever oil and gas are escaping from the seafloor, the topography of the seafloor is often affected. Pockmarks, circular or elliptical depressions in the seafloor sediments, are a well-known indicator of seabed fluid flow, and are scattered over the North Sea. They are often associated with gas chimneys on seismic data, evidence of gas seepage. Mud diapirs and mud volcanoes form as a result of oil and/or gas accumulations in the sub seabed, building up pressure and altering the topography of the seabed. Looking for these seabed structures is a good method for localizing seeps (Judd and Hovland 2007).

2.2 Natural hydrocarbon seepage in Norway and in the North Sea

There are no reported oil seeps in Norway or in the North Sea. However, there is evidence of natural gas seepage all along the coast of Norway. Chand et al. (2008) have found an active seepage system on the continental shelf off the coast of Vesterålen that may be leaking from a hydrocarbon reservoir, and there is active gas venting from hydrate systems on the Vestnesa ridge off the western coast of Svalbard (Bünz et al. 2012). Hydrocarbon leakage is also present in the Snøhvit field in the Barents Sea (Mohammedyasin et al. 2016).

Within the central and northern North Sea, there are three well-known macro-seep locations that have been studied over several years, the Tommeliten and the Gullfaks seep areas in the Norwegian sector and the Scanner pockmark seeps in the UK sector (Hovland et al. 2012). The locations of the fields are presented in Fig. 2.6**.**

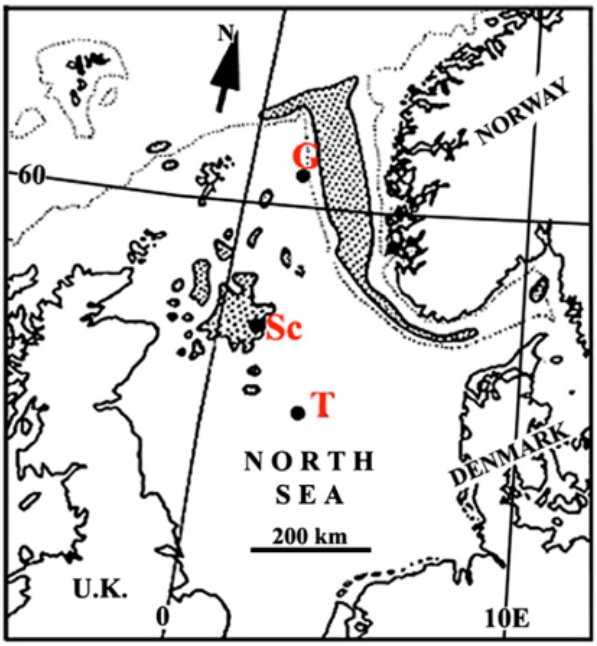

Fig. 2.6 Locations of selected macro seeps in the North Sea, figure reproduced from Hovland (1988).

Even though the number of recorded gas seeps and seepage areas on the NCS is high, the number of flux rate measurements is very small, and this pattern is recognizable all over the world. To measure seep flux rate, a considerable amount of time and money is needed, as measuring equipment needs to be installed over each vent or bubble flux. Common equipment for flux measurements is cameras and funnels. Furthermore, a representative number of vents must be evaluated with a time step large enough to include all spatial and temporal variations (Judd 2004). Such studies have been conducted at the Scanner pockmarks and the Tommeliten seep area, but due to the low activity and small gas mass flux rate at the Scanner pockmarks, emphasis in the current work is placed on the Tommeliten seep area.

2.2.1 Tommeliten seep area

The Tommeliten seep area is located in Norwegian block 1/9, and the gas seepage was first discovered after a routine site survey in 1978. Side scan sonar records indicated that gas emanated as bubbles from the seabed in small, individual vents over a salt diapir structure. The near-circular salt diapir is 3 km wide and located about 1000 m below the seafloor. Due to the diapir piercing the different formations, leakage paths for gas are created. Acoustic scattering and chaotic reflections above the salt diapir constituted evidence of gas-charged sediments, visible on seismic images as shown in Fig. 2.7. Plumes of gas bubbles in the water column were also evident on shallow seismic records, sparking the interest of doing surveys on the seabed (Hovland and Sommerville 1985).

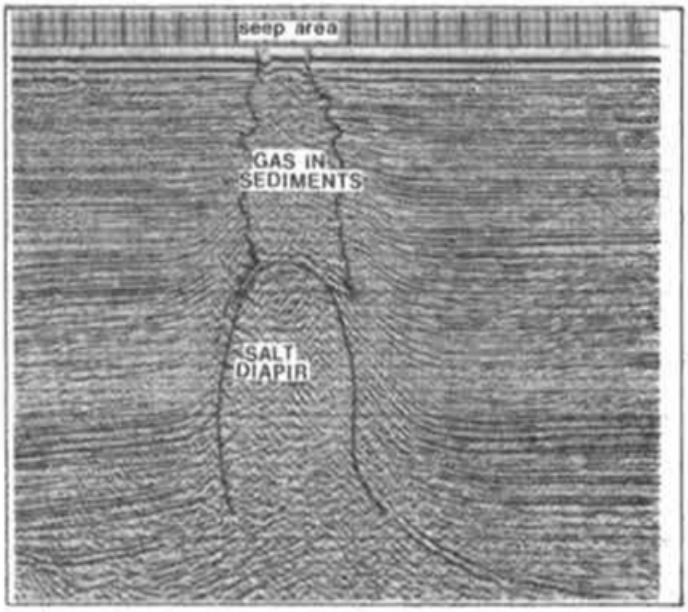

Fig. 2.7 Seismic image of salt diapir and gas in sediments in the Tommeliten seep area, figure reproduced from Hovland and Sommerville (1985).

A detailed survey with a Remotely Operated Vehicle (ROV) over the seep area was conducted in 1983, measuring 10 mm diameter bubbles emerging every 6th second from an estimated 120 vents, making the total gas flow rate ~24 m^3 per day. When released at ambient pressure at 75 m water depth, this corresponds to approximately 51 t/yr. Measured $\delta^{13}C$ values of –45.6‰ and presence of heavier gas molecules up to C5 suggested a thermogenic origin for the gas (Hovland and Sommerville 1985, Hovland et al. 2012). A new survey on the Tommeliten seep field to re-assess the mass flux was published in 2011, and Schneider von Deimling et al. (2011) estimated the total amount of gas released at Tommeliten to be 26.3 t/yr, which is approximately half of the number presented by Hovland and Sommerville (1985). The average diameter of the seeping bubbles was measured at 4.5 mm, and the gas ebullition was of uniform character and size.

2.3 Oil and gas seeps in North America

Two of the most prolific offshore seep areas in the world can be found in North America, namely the Gulf of Mexico and off the coast of California.

2.3.1 Seeps offshore California

It has several times been attempted to quantify the seepage rates offshore California, where abundant natural seeps of both oil and gas are emerging especially along the northern margin of the Santa Barbara Channel. The most intense area of seepage is known as Coal Oil Point (COP), which is located approximately 15 km west of the city of Santa Barbara. Oil is released from the seafloor in water depths ranging from 13 m (within 100 m from shore) to over 50 m (over 2000 m from shore), and large oil slicks extending up to 10 km is common in the area (Mikolaj et al. 1972). The seeping oil is heavy, comprised of ~30 % hydrocarbons and ~70 % resins and asphaltenes, with a specific gravity of more than 0.95 [API gravity of <17°] (Farwell et al. 2009). Early seepage rate estimates in the 1970s ranges between 100 and 35,000 t per year, using primitive measurements and gross extrapolation (Kvenvolden and Cooper 2003). Hornafius et al. (1999) made a more accurate estimation from combining data from seep tents, seep flux buoys floating in the seep area and 50 kHz sonar data, and stated that 23,850 – 27,000 l day^{-1} [150 - 170 bbl day^{-1}] of crude oil is seeping from the COP seeps. A likely estimate of annual seepage was therefore made at 7,800 – 8,900 t. The estimates for total oil seepage offshore California is 17,000 t per year, making the prolific seeps at COP responsible for approximately 50% of the oil seep activity in the region (Kvenvolden and Cooper 2003). There are also prolific gas seeps offshore California, and Hornafius et al. (1999) estimated that between 34,670 and 49,530 t of natural gas escapes the seabed every year. Very often the oil and gas seep through the same vents from the same reservoirs, and the seeps can thus appear either as pure gas bubbles and oil droplets, or as mixtures, such as gas bubbles with an oily coating or gaseous oil droplets. In the COP seep field, seepage primarily appear as oil-coated bubbles (Leifer and Boles 2005).

The prerequisite of these prolific seeps is based on the geology of the reservoirs in the area. All the individual seeps in COP are placed over anticlinal structures containing oil in the Monterey

formation. The overlying Sisquoc formation, the cap rock, is heavily fractured, making it possible for oil and gas to leak from the reservoirs (Hornafius et al. 1999).

Even though the seeping oil is heavy, majority of the oil is transported directly to surface, as the buoyancy of the droplets increase when oil is mixed with gas (Mikolaj et al. 1972). The continuous nature of seepage causes continuous oil slicks on surface, often impacting marine life such as seals and seabirds. After some time on surface, oil is weathered, and remaining tar floating on surface often gathers in lumps, ball-shaped or shaped like a whip as shown in Fig. 2.8. This tar later gets washed up on and pollutes the beaches in the area. Due to their persistence in the environment, depending on the currents, they are able to travel for several hundred kilometers before depositing on far beaches and shorelines as well (SOS California 2018).

Fig. 2.8 Tar from natural seeps floating in the ocean offshore Point Conception, California. Photographs by US Geological Survey (2008).

2.3.2 The Gulf of Mexico

The oil seepage rates in the GoM have been attempted quantified several times by the use of satellite remote sensing to map oil slicks on surface. In the 1990s, estimates ranged between 4,000 and 17,000 t per year. Kvenvolden and Cooper (2003) reviewed different data sets available from synthetic-aperture radar (SAR) and other remote sensing data, and found that a likely estimation for the total GoM seep rate is about 140,000 t per year. In their calculations, they assumed that the average thickness of the oil slicks is 0.1 µm, and that oil persists and is

visible on the surface for 12 h before evaporation. There are some uncertainties in these assumptions, for instance regarding temporal variations and weather patterns, but no one can argue the fact that the GoM is a prolific seep area.

Similar to offshore California, the prolific seepage is made possible by the presence of near-surface faulting. In the GoM, the faulting is mostly associated with salt domes and diapirs, as are some of the largest oil reservoirs in the area. Renewed or continued salt movements cause the formation of efficient pathways for seeping oil and gas (Geyer and Sweet 1972). Salt structures and associated faults are found both onshore (in Texas, Louisiana, Mississippi and Alabama), on the continental shelf and beyond the shelf out to a depth of about 3000 m (Judd and Hovland 2007).

The heavy seepage affects several aspects of the local environment. On the seafloor, pockmarks, tar mounds and asphalt mud volcanoes have all been extensively reported, and floating tar balls are continuously being deposited on the beaches in all of the aforementioned states. In seep areas, seabed piston cores have yielded as much as 15% oil by weight and hold gases with thermogenic isotope values. Tar has been found in sediments in more than 3000 m water depth (National Research Council (U.S.) 2003). In Fig. 2.9, two photographs of weathered oil found on the beach in Port Aransas, Texas, taken by the writer in April 2018, are shown. These samples are believed to originate from either natural oil seeps in the GoM, but could also possibly be residue from the Macondo oil spill in 2010.

Fig. 2.9 Weathered oil found on Port Aransas Beach, Texas, sample ca. 1 cm. Photographs by Tveit (2018).

CHAPTER 3

METHODOLOGY

The aim of this work is to make a quantitative analysis of the fate of leaking oil and gas from permanently abandoned wells. In this chapter, the basis of fate modeling, the two different case studies and the software used for modeling is presented.

3.1 Fate modeling

When doing a fate analysis of a small hydrocarbon leak from a well, the intention is to quantify how the oil and gas fractionates in the environment. Upon release, gas will mainly rise through the water by bubble-mediated transport, being subject to dissolution during its time in the water. Gas bubbles may either dissolve completely or transport gas to the atmosphere, or the fate of gas may constitute a combination of the two. The mass transfer between gas bubbles and seawater is a function of several variables, including bubble size, diffusivity, level of contamination in the liquid, salinity, water depth, ambient temperature and pressure (Olsen et al. 2017).

The fate of released oil is more complex. Released oil will undergo a series of physical and chemical changes, commonly called weathering processes, including the processes of evaporation, dispersion, emulsification, dissolution, oxidation, sedimentation and biodegradation (Lindo-Atichati et al. 2016). These processes can be visualized as in Fig. 3.1, showing the fate of naturally seeping oil and gas.

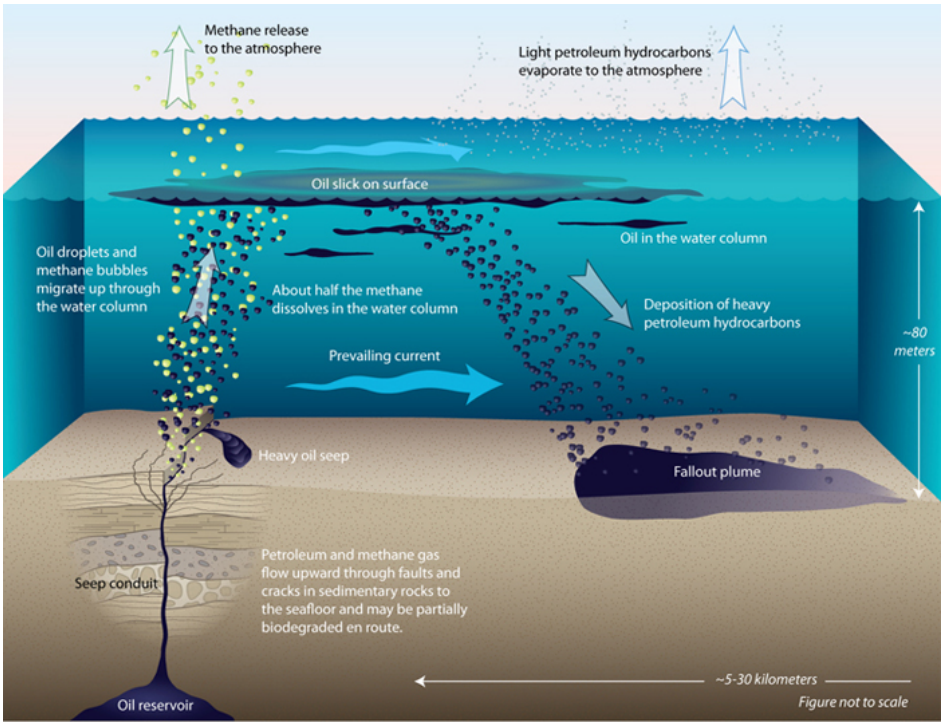

Fig. 3.1 Fate of naturally seeping oil and gas, figure reproduced from WHOI (2014).

Due to buoyancy effects, oil, which is normally lighter than water, will rise vertically through the water column. When the oil reaches the surface, it forms oil slicks floating on the water surface, from where it may evaporate. The fate and extent of the slicks are dependent on wind and wave activity, and thus the fraction of oil on surface will be larger in calm weather than in windy conditions, where breaking waves will crash down and oil deeper down into the water column (Nissanka and Yapa 2017). Evaporation rates from the oil on surface are mainly dependent on the composition of the oil, as lighter compounds are more willing to enter gaseous phase than heavier compounds. The evaporation rate is also dependent on ambient temperature, resulting in higher evaporation rates in summer than in winter (Fingas 2011). After the light components have evaporated, the remaining, weathered oil floating on surface will be enriched in heavier compounds until the point where the bulk density of the oil is likely to exceed ambient seawater density. This causes the residual oil on surface to sink, and ultimately it may settle and be deposited on the seafloor sediments. The settling of the oil on the sediments can increase in

waters with suspended particulate matter. As weathered oil can be quite sticky, it can adhere to the surface of particles in the water, increasing sedimentation rates for the compounds that are still lighter than the surrounding water (Riazi and Roomi 2008, Farwell et al. 2009). In the case of offshore oil seeps, the sediment deposition often occurs some distance away form the source, as oil on surface will be transported by wind and currents before the enrichment and subsequent sinking of heavy compounds take place, this is also shown in Fig. 3.1 (Farwell et al. 2009). The weathered oil on surface may also form what is known as tar balls, and in seep areas near the coast, such as offshore California and the GoM, these isolated tar globules will often drift and be washed ashore, contaminating beaches and shore lines (Hornafius et al. 1999).

When oil is floating on surface or located in the uppermost water layer, it may be subject to emulsification. Due to wave activity or turbulence, water droplets may mix and become trapped in the oil, which is broken down into smaller and smaller droplets. A stable emulsion of oil and water may contain between 60 and 85 % water, thus expanding the volume of the oil by two to five times. Amongst oil spill workers, this type of emulsion is often called "chocolate mousse" or "mousse". In addition to the increased bulk weight due to the absorbed water, dynamic viscosity of the oil mixture increases from typically a few hundred mPa·s to about one hundred thousand mPa·s, an increase with typical factor of 1000, making the emulsion a heavy, almost semi-solid material (Fingas and Fieldhouse 2004). Emulsification has been shown to be dependent on the chemical composition of the oil, specifically on the amount of resins and asphaltenes present in the oil, and the viscosity. For an emulsion to form, the oil must be viscous enough to keep water droplets trapped in place, but not so viscous that water droplets may not enter (National Research Council (U.S.) 2003, Fingas 2011).

Oil submerged in the water column may be subject to dispersion and dissolution processes. Natural dispersion occurs when fine droplets of oil are created by wave action or turbulence and are later transferred into the water. Typically, droplets smaller than 20 μm, or 0.020 mm, are relatively stable in water and will remain so for large periods of time, allowing them to be transported over large distances by currents in the water. In general, heavy oils will not disperse

naturally to any significant extent, whereas light crude or refined oil products can disperse almost completely if the saturate content is high and the asphaltenes and resin contents are low. Dispersion is dependent on significant wave action and energetic seas, making dispersion more likely in winter than in summer.

The dissolution process is the chemical stabilization of oil components in water. It is considered to be an important process, as the most soluble compounds of crude oil, light aromatic compounds, are also commonly the most toxic compounds. Solubility decreases rapidly with increasing molecule size, and a few examples of the solubility of different aromatics compounds and oil types have been presented in Table 3.1, with numbers adapted from National Research Council (U.S.) (2003). The sizes of the oil droplets in water may also affect dissolution rates.

Table 3.1 Solubility of selected aromatics and oils.

Name	Weight	Solubility [mg/l]	Test conditions
Benzene	78.11 g/mol	1700	Distilled water at 25°C
Toluene	92.14 g/mol	530	Distilled water at 25°C
Ethylbenzene	106.17 g/mol	170	Distilled water at 25°C
Naphthalene	128.17 g/mol	30	Distilled water at 25°C
Fluorene	166.22 g/mol	2	Distilled water at 25°C
Chrysene	228.29 g/mol	0.002	Distilled water at 25°C
Gasoline	0.734 g/cm^3	98	Distilled water at 22°C
Bunker C oil	0.925 g/cm^3	6	Distilled water at 22°C
Diesel fuel	0.862 g/cm^3	3	Distilled water at 20°C

When oil is dissolved in the water, it becomes more prone to oxidation effects. Oxidation of oil is the process of altering the chemical composition of the oil, either executed by light-catalyzed reactions (photooxidation) or microorganisms in the seawater (microbial oxidation). The ultimate fate of oxidation, given unrestricted time and oxygen supply, is conversion of oil compounds into carbon dioxide and water:

$$CH_2O + O_2 \rightarrow CO_2 + H_2O$$

where CH_2O is a symbol for all organic compounds. Photooxidation occurs when sunlight acts on oil in the surface layers, but it is not well understood how photooxidation specifically affects oil, neither is it considered an important part of the weathering processes (Fingas 2011). Microbial oxidation is of much more importance, and is also referred to as biodegradation. Different species of bacteria, fungi and yeast are capable of metabolizing different hydrocarbons as a food energy source. These organisms are prolific in seep areas, but are present everywhere in the environment. The rate of biodegradation depends primarily on the nature of the hydrocarbons. The saturated alkanes, particularly those with 12 to 20 carbon atoms, are often consumed first, together with smaller aromatics. More resistant to biodegradation are branched alkanes and multi-ring aromatics, and most resistant are the polar petroleum compounds such as sulfur- and nitrogen-containing compounds (National Research Council (U.S.) 2003). The rate of biodegradation also depends on ambient temperature and the supply of oxygen, and in general, biodegradations rates tend to increase with increasing temperature. However, biodegradation is a very slow process for some oils, and oil can be persistent in the environment after release for years. Therefore, biodegradation is not considered an important weathering process in the short term (Fingas 2011).

To summarize, fate modeling is a multi-faceted process, as the fate of oil and/or gas releases will vary according to the oil/gas composition, characteristics of the release, the environmental parameters, the marine organisms present in the area, the season and the weather.

3.2 Case studies

Two case studies have been performed for the current work. The first case presented is a tale of a real, historic gas release case of leaking wells after PP&A on the NCS. The second case is a theoretical oil release case at a Norwegian oil field. Both fields have been anonymized for this work.

3.2.1 Field A

For the first case study of this thesis, an operator on the NCS has provided data from an undisclosed gas and condensate field, that after roughly 20 years of production was plugged and abandoned some years ago. As all data are confidential, the field has been anonymized and hereafter it will be referred to as Field A. The platform wells were located in 70 m water depth, and produced natural gas with specific gravity of 0.69. After the P&A campaign, gas leaks developed outside the casing strings and were discovered in a large number of wells. After performing a geological and petrophysical study, the main source of the leaks was found to be thermogenic gas in a limestone bed at 2050 m [6,700 ft] depth. The gas was migrating through the original casing cement between the 13-3/8" and the 20" casing, and it is likely that the leak paths were made up by channels in the cement, due to gas cut cement during the primary cementing in production drilling. In order to remediate the leaks, new cement plugs in open hole were required, as the operator pursues a zero leak philosophy. Extensive repairs and section milling were executed, and the re-abandonment added an extra 10 months to the project. The extra work more than doubled the total costs of the P&A campaign from 221 million NOK to 506 million NOK, not including the costs of conductor removal. It was decided to leave the conductors in place for observation for some time, and depending on the type of vessel hired to do the conductor removal operations, the price was calculated to be in the range of 50 – 170 million NOK. It is important to note that these costs would be much higher with today's price ranges, and after the latest revision of NORSOK D-010 (Eshraghi 2012). The case study at Field A will try to answer the question of what the consequences would be if the operator did not adhere to the zero leak acceptance criteria of NORSOK D-010 (2013), and how leaving the leaks in place would affect the environment. We return to the question from the introduction, and investigate whether doing zero harm to the environment necessarily means having to allow zero leak. To answer this, three examples of leak rates have been chosen for modeling.

The leak rates from the leaking wells at Field A was continuously monitored throughout the process, and an overview is given in Fig. 3.2 and Fig. 3.3. Confidential information has been censored out of the graphs, which are copied from internal reports. In Fig. 3.2, well number 16 (W-16) shows interesting behavior; throughout a period of approximately five months, the leak

rate is almost constant at 7 l/hr. In Fig. 3.3, well number 4 (W-04) shows similar behavior, with an almost constant leak rate at 45 l/hr for a three-month period. These two leak rates have been chosen for the case study, as one might hypothesize that if re-abandonment was not performed, this steady-state behavior might have continued. The third chosen case is well number 8 (W-08), which peaked at 120 l/hr. This is chosen as a worst-case scenario.

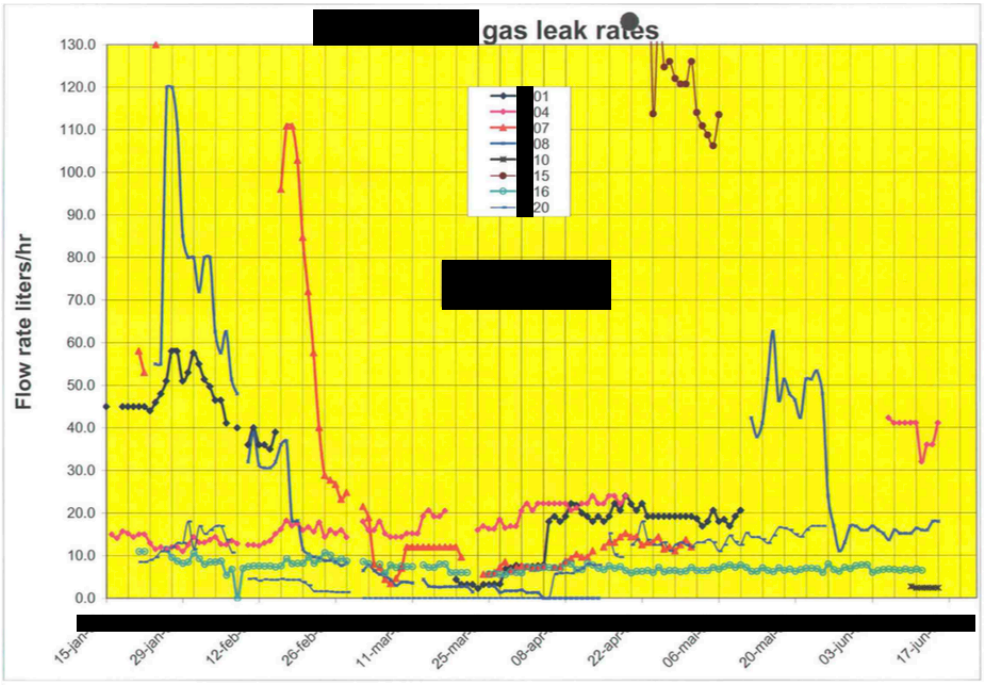

Fig. 3.2 Monitoring of leaking gas wells at Field A, January to June.

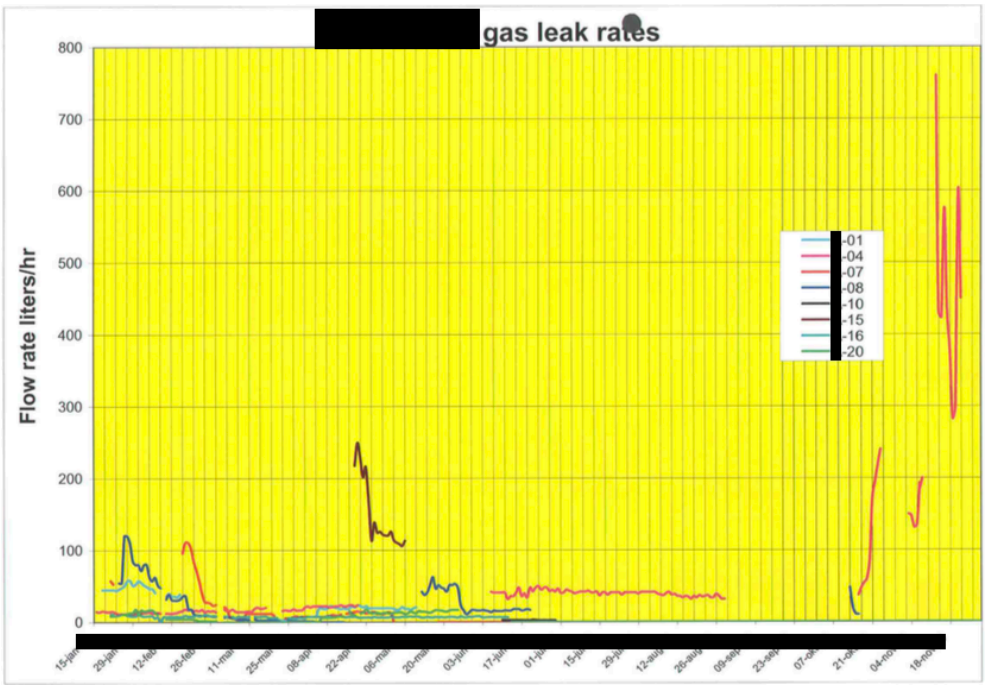

Fig. 3.3 Monitoring of leaking gas wells at Field A, January to November.

When entering the leak rates in the Gastrack model, the required unit is Sm^3/day, so leak rates must be converted by the following formula, as shown in Table 2.2:

$$\frac{\text{l}}{\text{hr}} * 24 \frac{\text{hr}}{\text{day}} * 0.001 \frac{\text{Sm}^3}{\text{l}} = \frac{\text{Sm}^3}{\text{day}}$$

Table 2.2 Leak rate conversion.

Well	Leak rate [l/hr]	Leak rate [Sm^3/day]
W-04	45	1.080
W-08	120	2.880
W-16	7	0.168

The initial sizes of the bubbles must also be entered in the software, so assumptions must be made. This is further described in chapter 3.5.4.1.

3.2.2 Field B

The second case study is a theoretical oil leak at Field B. Field B is an oil field located in the southern part of the Norwegian sector of the North Sea at approximately 70 m water depth. It was discovered in the 1970s, as the first indication of oil and gas in carbonate rocks on the NCS. Production started in the 1980s from the Upper Cretaceous Hod and Tor Formations at 2400 m (NPD 2018b). Due to the porous and soft chalk matrix, depletion during production has led to reservoir compaction and subsidence, which again has led to failure in the overburden. As one of the platforms started sinking, the clearance between deck and sea became too small, and it was decided to plug all 30 platform wells. One of the main challenges in executing the plugging and abandonment of these wells is the deformation and collapse of wells, which may restrict access to the well, making it difficult to place the barriers at the required depth. Also, primary cement is degraded and often not suitable as part of the permanent barriers. Pulling tubing through kinks in the casings also poses a challenge, and furthermore, the overburden contains nine distinct permeable zones (DPZ), which all needs to be isolated by barriers according to regulations (Straume 2012).

Operator at Field B has been positive to use the field as a test spot for new technology and new PP&A solutions. There is an on-going project aiming to verify the PWC method and include a specific verification process for PWC in the new version of NORSOK D-010, which is being drafted in 2018 / 2019 (Delabroy et al. 2017, Gundersen 2017). In 2017, American company BiSN ran its first North Sea project on Field B, using metal alloy bismuth to create metal-to-metal seals and successfully eliminating surface liner pressure in multiple wells (OE Staff 2017). Norwegian company Interwell P&A also executed the first trial on the NCS in the first quarter of 2018, after previous successful runs in Canada, deploying their tools to establish a cross-sectional, everlasting thermite barrier plug (Skjold 2017).

The combination of the challenging conditions and the deployment of new, experimental technology may induce an increased well integrity risk. As the PP&A work is ongoing at Field B, it was considered interesting to use the field as subject for leak simulations. It is important to underline that the objective of this thesis is not to evaluate leakage risk or quality of new technology, and that the reason for choosing this particular field as a test case is purely due to the interesting conditions present. But still, it is not entirely unlikely that these kinds of evaluations may come in handy in the future, in case a leak should be detected at some point.

3.3 Software

The software used for the modeling part of this thesis is provided by SINTEF. Their Marine Environment Modeling Workbench (MEMW) is a framework for analyzing releases to the marine environment by performing various modeling, simulation and presentation tasks. A number of different scenarios can be modeled, and the user can to a large extent choose which output is of interest for the relevant case. MEMW provides a set of unified and consistent environmental analysis tools, and can provide the user with extensive databases, including geographical locations, an ocean depth database, a chemical database and an oil database. In the current work, a location database of Northern Europe has been provided, along with a database containing properties of more than 130 oils and petroleum products, including all North Sea oils. The oil database provides information such as chemical composition, viscosity and API gravity (SINTEF 2017). In this thesis, the MEMW models OSCAR and Gastrack are used.

3.3.1 The OSCAR model

The Oil Spill Contingency And Response model is a numerical model made for quantifying environmental consequences of oil spills and effectiveness of various response strategies. OSCAR computes the fate and weathering of oil after a release at surface or at a given depth, and investigates potential biological effects. As described in the MEMW User's Manual (SINTEF 2017), OSCAR is a tool for:

- Oil spill response support and analysis
- Oil spill contingency planning

- Analysis of biological impacts resulting from oil and chemical spills
- Stochastic risk analysis

A release scenario is set up by entering relevant site information, such as geographical area, exact coordinates and a chosen grid for the simulation. The included depth database provides bathymetric data. A release profile, usually an oil or chemical from the database, is chosen, and chemical composition may be adjusted if necessary. The duration of the release and the total volume or rate must also be entered. After running the simulation, the output can be read directly from netCDF files, text files or by interactive mapping possibilities and animations in the MEMW interface. Examples of output can be mass balance, mean and maximum concentrations, viscosity of oil slick, biodegradation rates and affected area or shoreline.

3.3.2 The Gastrack model

MEMW has a near-field model included, Plume3D, which is used with OSCAR for plume computations. According to Johansen (2000), the model is one of the most advanced and complete models available today for deep-water well blowouts. Initially, Plume3D was not capable of simulating pure gas blowouts or releases, and lacked the ability to track gas bubbles and dissolved gas in the water column. However, after input from Total E&P Norge on behalf of the Norwegian Deepwater Program (NDP), this functionality has been developed and included by implementing a gas-tracking module, Gastrack. Now the model can create gas bubbles at the release locations and track their fate through the water column, where some may rise due to buoyancy and be transported by the ambient current to surface, and others may dissolve completely into the seawater.

When applying Gastrack, the MEMW interface can show the bubbles in planar and cross-sectional views and provide maps of surfacing gas mass flux (mass per area per time), surface void fraction (%) and mass balance logs (SINTEF 2017).

3.3.3 Model conventions and concepts

When setting up a release scenario, MEMW defines depth in meters, positive down from mean water level, and horizontal distances are given in meters and kilometers. Amount of released

substance can be entered by the user in a variety of units, defining either mass, volume or rate; such as tonnes, kilograms, barrels, gallons, liters per hour, tonnes per day etc.

The MEMW models use particles to compute transport, behavior and effects of pollutants released to the environment. Particles can be strictly Lagrangian or "pseudo-Lagrangian". The first indicates that particles are passively transported with the surrounding water, and may represent dissolved substances or drifting plankton. The latter represents droplets in water, which in addition to being affected by the advection and turbulence of the surrounding water, are also subject to vertical rising or settling velocity. The number of particles chosen to represent the released substance affects the resolution and accuracy of the results.

3.3.4 Scientific background of model

In April 1977, a blowout at the Ekofisk Bravo platform occurred. In seven days, approximately 13,000 t of oil was released to the sea. Luckily, the blowout caused less damage than feared. Due to the lightness of the oil, a large portion evaporated in the days following the blowout. The rest of the surface oil was dispersed naturally in the sea, and the oil never reached land (Audunson 1980). After this event, new focus was placed on oil spill research and development (R&D) on the NCS, and since 1978, approximately 40 experimental oil spills have been conducted in Norwegian waters, including small and large releases in both open and ice covered waters. By releasing crude oil into the environment and tracking it, for instance by ship and/or from air, valuable information about how it spreads, disperses and fractionates can be obtained and theories verified. Combined with theoretical modeling, laboratory testing and basin studies, this forms a strong basis for the MEMW state-of-the-art 3D models describing the fate and effect of oil releases.

3.4 Model parameters

The model parameters greatly affect the output of the simulations, in terms of accuracy, resolution in time and space, size of output files and computational speed. An increase in the number of particles or smaller grid cells will provide better spatial resolution, and a smaller time

step produces better temporal resolution. Both will result in more calculations being performed by the machine, decrease speed of computation and thereby increase simulation times. Increasing the number of particles or grid dimensions will decrease speed of computation by a power between 1 and 2, while decrease in time step will give a linear increase in simulation time (SINTEF 2017).

3.4.1 Number of particles

The user must enter the number of liquid/solid particles, dissolved particles and gas particles that are to be used to represent the release. In the MEMW User's manual, 1000 particles are recommended as a starting point, and 30,000 are the maximum number of particles recommended. To achieve as accurate results as possible, 30,000 particles are used in the simulations performed for this work.

3.4.2 Concentration grid dimensions (xyz)

A three dimensional grid must be chosen for the simulation, where the xy plane is the horizontal plane and z direction is the vertical. The x and y values are given in meters and represent east-west direction and north-south direction, respectively. The maximum number of horizontal grid cells used for the current work is 100 × 100, and the size of the individual cells is therefore dependent on the grid size. For instance, a grid size of 1 km × 1 km will give individual cells of 10 m × 10 m. The smallest grid that will be applied is 100 m × 100 m, made up by cells sized 1 m × 1 m, and this will provide the best horizontal resolution possible in the software.

The z value specifies the number of layers in the water column, a number limited to 10 by the software. The user can choose which intervals are relevant for the specific simulation and enter the start and end depth value, which is then divided into 10 vertical sections. If the user wants to view the results of a simulation from a seabed release, and track the oil or gas all the way to surface, the thickness of the layers will be set to one tenth of the depth entered by the user. For deep-sea releases, the vertical resolution will therefore be limited.

The various outputs from the simulations, such as mean and maximum concentration, are averaged over and given per cell. If the size of the cell is large compared to the characteristics of the release, the results will be subject to a false numerical dilution, and consequently, local concentrations may be underestimated (SINTEF 2017). Due to these effects, grid sizes for the simulations must be chosen according to the desired output. For simulations investigating long time mass balance for oil releases, a large grid must be used, as oil persists in the environment for quite a long time, and is thus transported with the currents and the seawater over large areas. For simulations investigating maximum concentrations of potentially harmful substances near the release site, a smaller grid should be chosen to improve spatial resolution.

3.4.3 Time step

The user must determine the computational time step to use in the simulation, that is to say how often the machine will perform new calculations during the duration of the simulation. Smaller time steps give better temporal resolution, but will result in longer simulation times. Excessively large time steps may result in unrealistic results. Output interval must also be entered. For the simulations on gas release described in this thesis, a computational time step of 6 seconds have been chosen, with output intervals of 30 seconds. Consequently, every fifth data point will be stored in the output files. A larger output interval will decrease the size of output files and make it easier to navigate in the interactive user interface of the software. The time steps must also be seen in relation to the duration of the simulations. For the five day simulations on mean and maximum concentrations following an oil release, a computational time step of 1 minute have been chosen, with output intervals of 5 minutes. In this case, both high spatial and temporal resolution are desirable. For the 90 day simulations on mass balance following an oil release, a computational time step of 20 minutes have been chosen, with output intervals of 3 hours. In this case, the overall fractions of the oil are the most important, and both spatial and temporal resolution may be poorer without affecting the results.

3.5 Input parameters

In addition to the aforementioned model parameters, some input parameters must be entered. Shown in Fig. 3.4 is the start page in the OSCAR interface for creating new release scenarios. A new scenario is created by clicking on the map and selecting the coordinates for a release site.

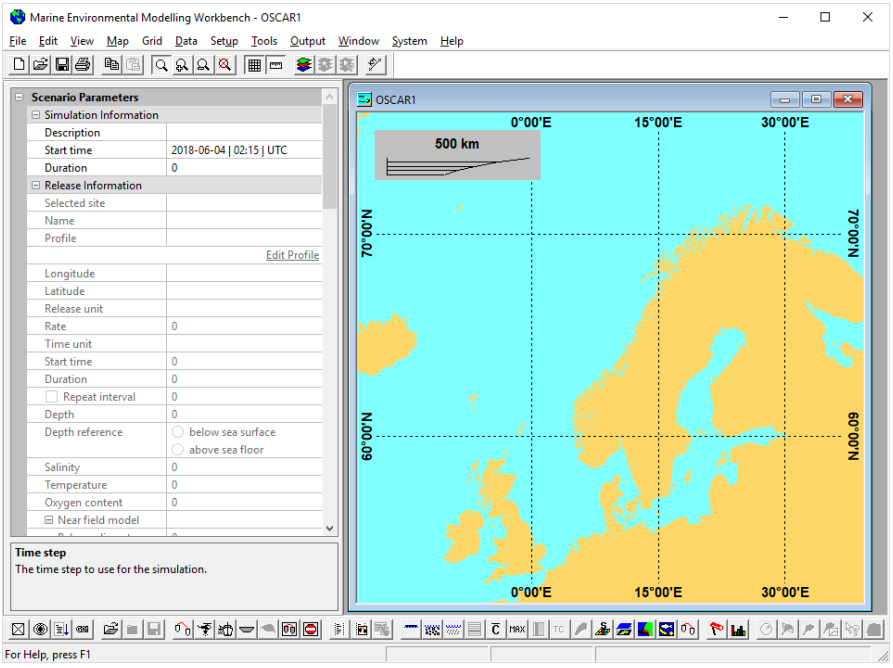

Fig. 3.4 OSCAR start page interface for new release scenario.

3.5.1 Release site

The exact geographical location of the release scenario must be entered in degrees of longitude and latitude. In the current work, the simulations have been executed on specific wells, and the exact co-ordinates for each well have been retrieved from NPD Factpages and entered in the software. Bathymetry data are automatically downloaded from the depth database in the software when a grid is chosen. Different grids have been chosen for the different scenarios to fit the respective purposes. The depth of the release has been set to 0 m above the seafloor for all cases, as all releases are emerging from the subsurface and escaping through the seabed.

3.5.2 Time and duration of simulation and release

Start time of the simulation must be entered with exact date and time, together with the number of days for the simulation to run. Within the simulation window, a start time and duration of a release must also be entered. The duration of a release can be entered in various units, such as hours, days and weeks, and several releases can be set up within the same simulation. For the work in this thesis, releases from a single point representing a well and constant release rates representing steady state leaks have been chosen.

To check for seasonal variations in the fate of the leaks, all simulations have been run for both winter and summer cases. There are strong seasonal variations in the hydrographic conditions in the entire central and northern offshore areas of the North Sea. In spring, warming of the atmosphere and decreasing storm activity reduce the extent of vertical mixing in the water column, which results in the formation of a strong thermocline. A thermocline is defined as a thin and distinct layer of water in which the temperature changes more rapidly with depth than it does in the layers above or below, as illustrated in Fig. 3.5. In the ocean, the thermocline divides the upper mixed layers and the deeper, calmer water below. As the spring and summer progresses, the depth and the gradient of the thermocline both increase, gradually suppressing vertical exchange between the deep and shallow water. During this time, gas bubbles and oil droplets may be trapped beneath the thermocline, as vertical transport will be limited (Schneider von Deimling et al. 2011). When cooling starts in October, paired with increasing wind speed, the water column will destabilize and the thermocline will fade and eventually disappear. By February, the water column will be near homogenous and vertical mixing will be at maximum level (Pohlmann 1996).

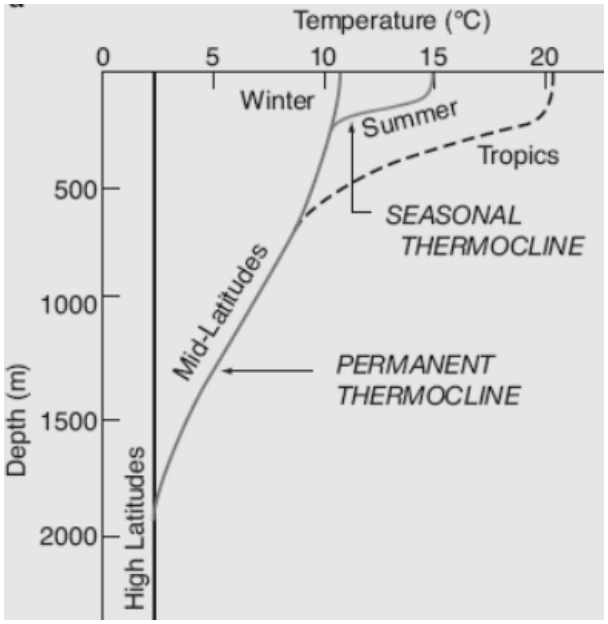

Fig. 3.5 Seasonal variations in sea temperature by the formation of a thermocline in Mid-Latitudes. Figure reproduced from Wikimedia Commons (2014).

3.5.3 Release profile

Rates for the gas releases are chosen based on the leaking wells at Field A, as previously shown. Release rates for the oil case at Field B are based upon data from natural seepages and some assumptions. There are not too many studies conducted on the rate of individual oil seeps, as the focus of most research is the seepage from an area and the consequences in a larger picture. But Johansen et al. (2017) did a specific seabed video survey of two oil seep spots in the GoM at 1200 m water depth. The two vents emitted oil droplets with an average diameter of 5 mm at rates of 1.11 and 0.31 l/h, respectively. This is equivalent to 4.7 and 1.3 droplets per second. Another study at the Mississippi canyon in the GoM used SAR surveys to evaluate the thickness and extent of oil slicks, dividing into a grid of surface blocks representing clusters of seeps. The most active cluster of seeps was estimated to leak 0.14 m^3/d, or 140 l/d = 5.83 l/h (Garcia-Pineda et al. 2016). As the initial objective of the simulations is to evaluate the consequences of a small leak, this latter leak rate is considered too high to model as a leak from a single well. A worst-case scenario of 1.0 l/h is chosen, followed by two scenarios of 0.1 and 0.01 l/h. With a presumed

characteristic droplet size of 5 mm diameter, these leak rates are equivalent to maximum 4.24 droplets per second or minimum 1 droplet every 24 seconds.

3.5.4 Bubble / droplet size

The size of the gas bubbles or oil droplets entering the water column is an important parameter for the fate of the leak (MacDonald et al. 2002, Leifer et al. 2004, Wang and Socolofsky 2015, Lindo-Atichati et al. 2016). However, predicting bubble and droplet sizes is a complicated process, as they depend on a number of variables. The variables include, but are not limited to, rheology of the fluid(s), mass flux, horizontal water velocity, surfactant contamination such as oiliness in gas bubbles, sizes of the grains and the pore channels in the sediments, size and geometry of the defect if the fluid escapes through rock, ambient temperature and pressure (Leifer and Culling 2010, MacDonald et al. 2002). Temporal variation also occurs, Leifer and Boles (2005) describe how increased water flow across a vent mouth may reduce the size of gas bubbles, Johansen et al. (2017) argues that tidal fluctuations will affect release rates, due to the succeeding changes in the hydrostatic pressure at sea floor, and Leifer et al. (2004) performed seabed surveys that showed how seabed morphology varies with time, ultimately changing the seepage characteristics of an area.

Due to the difficulty in predicting bubble and droplet sizes for a leaking well, the simulations for the current work will include sensitivity analyses on bubble and droplet sizes, which will be compared with the standard values and size distributions built in to the software. The basis for the chosen bubble and droplet sizes is a review of common size distributions found at natural seep sites.

There are also challenges present when trying to determine the exact size of the gas bubbles and oil droplets during investigations of natural seepage. Different methods of measuring are used, such as visual detection by divers, use of seismic, cameras mounted on sea floor and ROVs (Johansen et al. 2017, Mikolaj et al. 1972). In video and ROV analysis, the size of the bubbles or droplets is often compared with an object of known size, such as a ruler or funnel mounted near the seep. However, if the distance from the rising bubble or droplets and the measuring

equipment is unknown, this can make it tricky to accurately predict their size. In addition, the shape of the seeping bubbles and droplets is often ellipsoidal or uneven, and bubbles may oscillate when rising through the water. Large and/or clean bubbles will oscillate more than small and/or oily bubbles (Leifer and MacDonald 2003). In general, oily bubbles are larger and released at slower rates than clean bubbles, making them more stable in the water and less likely to oscillate (Johansen et al. 2017). Oil and gas are often seeping from the same source and the same vents, and therefore, oil and gas are often subject to mixing. Gas bubbles can have an oily coating and oil droplets may contain gas. As reliable data on size distributions from natural seeps on pure gas bubble sizes and oil droplet sizes are limited, a range of different sizes will be subject for modeling.

3.5.4.1 Gas bubbles

The standard initial bubble size in the software is set to 10 mm. In 2010, Leifer and Culling (2010) examined the formation of seep bubble plumes in the Coal Oil Point seep field, based on the fact that little had previously been published on the size distribution of seep bubble-emission. By utilizing a video bubble measurement system at seafloor and a laboratory set up to produce gas bubbles from a sediment bed in a tank, the bubble size distribution and its relation to mass flux rate and the characteristics of the sediment were analyzed. Results showed that where lower emission flux was experienced, the bubble size distributions were best described by a narrow, peaked graph in the shape of a Gaussian function, while higher emission flux rates produced a broad spectrum of bubble sizes, best described by a power law, ranging from very small to very large bubbles. Field observations were consistent with laboratory observations, and typical bubble sizes were in the range of 500 to 5,200 μm radius. The results are also consistent with field observations made by Leifer and Boles (2005) at the Shane Seep in COP, where two minor vents exhibited narrow, sharply peaked size distributions with peaks at 3,500 and 2,200 μm radius, while a larger vent exhibited a broader size distribution including bubbles ranging from 200 μm to 1 cm radius.

The size of the sediments and the pore throat the gas travels through is one of the key factors in determining bubble sizes. Fluid escaping from a small orifice is emitted in smaller bubbles than

fluid escaping from larger orifices or cracks. For small flow rates, gas bubbles will be of uniform size even if the flow rate is changed. Increased flow rate will only increase the number of bubbles, not their size. In the case of larger flow rates, as mentioned, the size distribution of the emitted bubbles will be broader. Thus, sediment properties are more important for bubble size distribution in small leak rates (Leifer and Culling 2010). In the Tommeliten seep area, gas bubbles show a more or less uniform size at 4.5 mm diameter, consistent with the theory on a low rate mass flux (Schneider von Deimling et al. 2011). As Field A is very comparable to the Tommeliten seep area, the bubble size of 4.5 mm is chosen to be the characteristic size for the modeling process. To perform a bubble size sensitivity analyses, minimum and maximum size of bubbles are set to 1 and 10 mm, as this is descriptive of the ranges of bubble sizes reported in various studies of natural seepages around the world.

3.5.4.2 Oil droplets

The OSCAR software computes the oil droplet size by using the Rosin-Rammler distribution function, which is the most commonly used equation for describing particle size distribution (González-Tello et al. 2008). Two parameters are used, m representing the mean diameter and η, giving an indication of the particle-size range. The Rosin-Rammler equation is given by:

$$F_M(D) = e^{-(\frac{D}{m})^{\eta}}$$

where F_M predicts the mass fraction of particles having size greater than the diameter D, m denotes the characteristic droplet size D_c and η is the size-spread parameter. A cumulative distribution function is given by:

$$F_{M,C}(D) = 1 - e^{-(\frac{D}{m})^{\eta}}$$

Both distribution functions are presented in Fig. 3.6, together with a probability density function of droplet sizes, given by the derivative of the Rosin-Rammler equation:

$$f_M(D) = \frac{\eta}{m}\left(\frac{D}{m}\right)^{\eta-1} e^{-(\frac{D}{m})^{\eta}}$$

Fig. 3.6 is based on the default settings in OSCAR, where the characteristic droplet size D_c is set to 3,000 µm diameter and the size-spread parameter η is set to 1.7999. Minimum and maximum droplet size to be included in the simulation, D_{min} and D_{max}, must also be entered, and as a default they are set to 0 µm and 6,000 µm, respectively (SINTEF 2017). With the given distribution, 63.21 % of the particles will be smaller than the characteristic particle size.

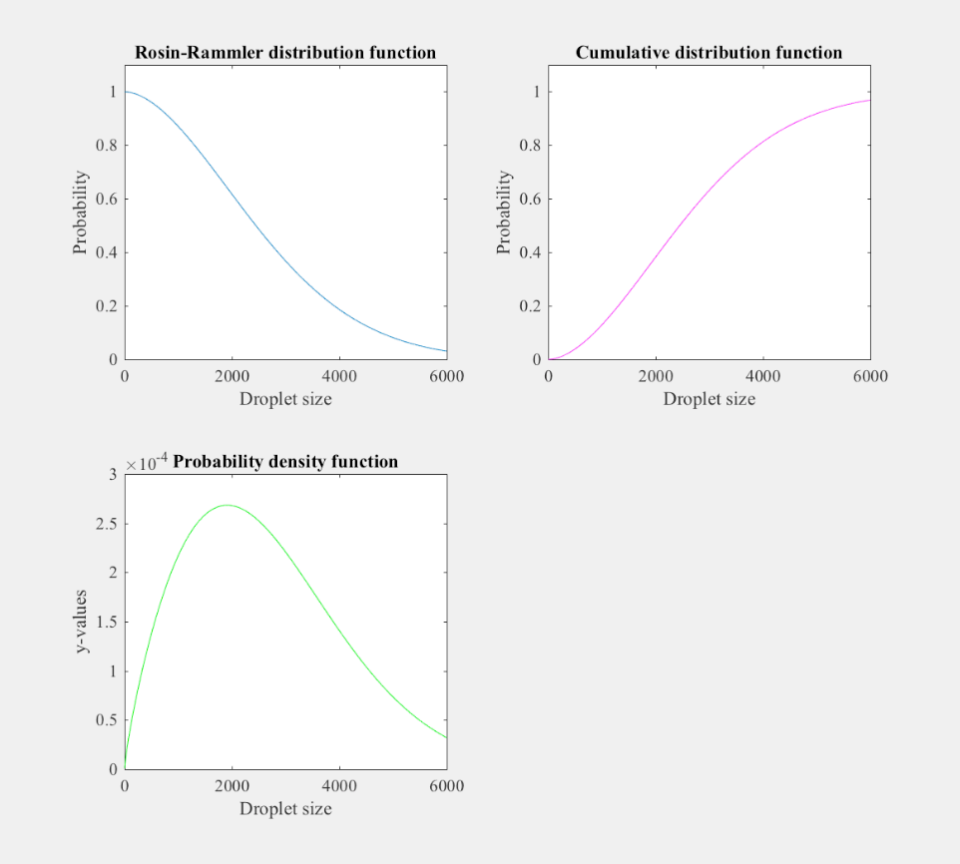

Fig. 3.6 Oil droplet size distribution, OSCAR default settings. Graphs made in MatLab.

As the fate of the oil is closely related to the size of the droplets being expelled from the source, sensitivity analysis is included in the current work to evaluate the effects of different droplet sizes. As mentioned in chapter 3.5.4, there is limited information available on droplet size distributions amongst natural hydrocarbon seeps, and accurately predicting this for a theoretical

case would be very challenging, providing unreliable results. Therefore, four different, theoretical scenarios on droplet size distribution have been applied in the current work. The first scenario is using the built-in, standard values of the software, as described in this chapter. To choose which other values to use in the sensitivity analysis, a literature review on natural oil seepages has been performed.

In a study conducted by divers at near-shore seeps in the Santa Barbara Channel, more specifically in the Coal Oil Point region, oil seeps were identified by small, black oil globules breaking through the uppermost layer of sand with a typical diameter of 5 mm. (Mikolaj et al. 1972). The water depth in the area is 13 m. The same study also reports on large variations, where some observations tell of oil globule formation and release taking place in as little as a few seconds, with small, spherical globules popping from the bottom, while in other observations, larger, elongated globules of 1.5 cm diameter could take up to 5 minutes to form. The larger, unevenly shaped globules would occasionally rise with umbilical stringers, reaching as much as one or two meters of length before breaking off. The same typical diameter of 5 mm. was also encountered in a study in the Northern Gulf of Mexico. Size distribution of oily bubbles from vents in two different locations at 1200 m depth was investigated by video analysis, and results averaged at 5 mm diameter with a standard deviation of 1.30 (Johansen et al. 2017).

Garcia-Pineda et al. (2016) defined natural seepages of oil and gas to normally be in the range of 1 – 10 mm diameter in size, and in 2002, MacDonald et al. (2002) used an oil droplet size of 1 cm diameter in a study to calculate oil slick trajectories. This is consistent with observations on oil seepage from shallow gas hydrate deposits in the Northern Gulf of Mexico, where oil trapped under gas hydrate deposits at 525 – 550 m depth would be expelled in 1 cm drops (Leifer and MacDonald 2003).

Based on these different studies and observations, uniform oil droplet sizes of 1, 5 and 10 mm are chosen for the sensitivity analysis in the current work. For simplicity, the built-in size distribution in the software is from now on referred to as a droplet size of 3 mm.

3.5.5 Environmental parameters

Currents will transport oil slicks, bubbles, droplets and dissolved oil and gas in the water column, and thereby affect the fate of the release. Wind will help transport oil slicks in lateral direction, and in addition induce wave activity. When subjected to waves, the fraction of oil at surface being mixed into the upper water column will increase, and thereby evaporation rates will decrease. Current and wind data are therefore vital for oil trajectory modeling.

Current and wind data are provided as a courtesy of SINTEF and was produced by using the SINMOD hydrodynamic model. A data set for 2014 is used in the simulations, which covers the southern half of the NCS. The spatial resolution is 1⅓ km, and the dataset has a temporal resolution of 2 hours.

Temperature and salinity profiles for the water column, which can be visualized as in Fig. 3.7, have been downloaded from Meteorologisk Institutt (2018a). These data are not measured directly, but calculated at different depths. As the fate of oil and gas is influenced by the ambient temperature and salinity, it is desirable to have the software utilize these gradients, comparing to choosing fixed values for the whole water column. In Fig. 3.7 we can see temperature and salinity profiles valid for Field B during winter (left) and summer (right). As the water depth in Field B is less than 75 m, a spot approximately 60 km away from Field B with 80 m water depth was chosen to retrieve these data, as the data files calculate values at 50 and 75 m. In both cases, salinity varies only slightly throughout the water column, with values increasing with depth. The variation is larger in summer than in winter, probably due to the effect of more mixing in winter. When evaluating the temperature data, they clearly show that during winter, the mixed layer extends all the way to seafloor, giving small temperature changes with depth. In summer, the heating of the upper layers cause a thermocline to form at appx. 20 - 30 m depth. However, due to few data points making up these graphs, the exact location of the thermocline is uncertain. In both cases, winter and summer, the temperature at seafloor approaches 8°C, and as leaking oil and gas will travel slowly upwards through the well, an assumption is made that the temperature of the released oil and gas will be equal to the water temperature at the release point.

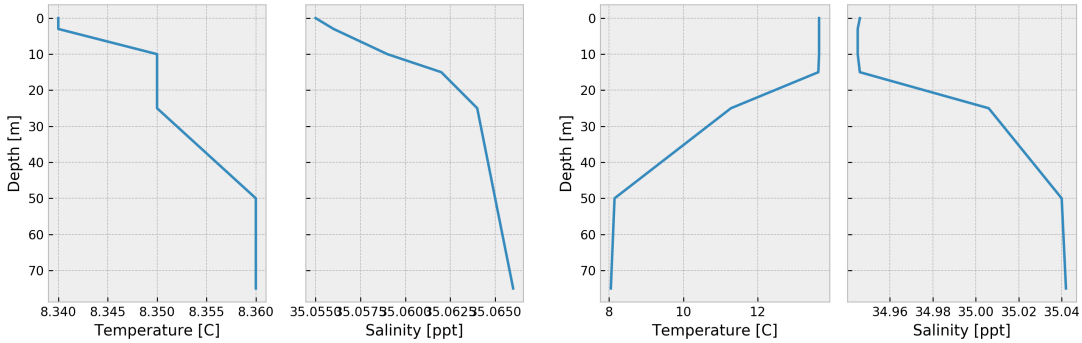

Fig. 3.7 Temperature and salinity profiles for the water column, winter data on the left, summer data on the right. Data applicable for Field B. Graphs made with data from Meteorologisk Institutt (2018a).

Similar data have been downloaded and analyzed for Field A to use in simulations.

Atmospheric temperature is very significant when modeling the evaporation rates of surface oil. Atmospheric temperature data has been downloaded from eKlima, the Norwegian Meteorologisk Institutts klimadatabase, which is an open access database providing the users with data and analytical tools (Meteorologisk Institutt 2018b). For the current work, weather reports from offshore weather stations, often installed on platforms, has been downloaded and used. In Appendix A, an example of such data is provided that is valid for Field A. Similar data has been downloaded for Field B, but are not included in the appendices. The atmospheric temperature data have been used as basis for determining the dates of the different simulations. Winter and summer simulations have been executed during the coldest and warmest months, respectively. For short simulations, February and August represent the coldest and warmest months. For the simulations of 90 days duration, they have been run for January until March and July until September, as these are the collection of coldest and warmest months. Average temperatures have been applied for the various time intervals.

CHAPTER 4

RESULTS AND DISCUSSION

4.1 Simulation process

The results presented in this section are products of a large number of simulations. Much trial and error have been needed in order to understand the software and to determine which parameters should be optimized and sensitivity tested. Generally, the simulation process has followed the order represented in Fig. 4.1. The relevant output results have been presented in tables, graphs and some screen shots from the dynamic software interface to ease the understanding for the reader. Some of the graphs have been made using Python programming, and these scripts are included in Appendix B. The rest of the graphs are made using Excel.

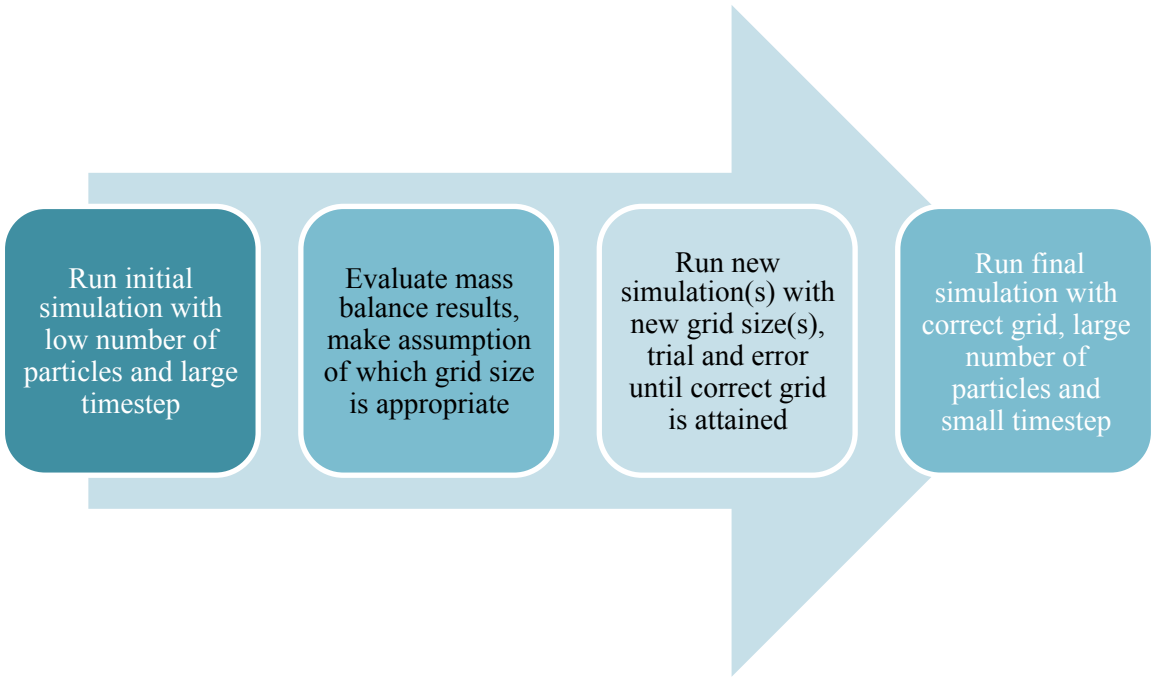

Fig. 4.1 Simulation process.

4.2 Case A – Field A

4.2.1 Determining grid size for simulation

Released gas bubbles will have a density substantially lower than the surrounding seawater, and will therefore be subject to buoyancy forces, driving the bubbles upwards with a rise velocity v. The rise velocity can be expressed by the following expression, derived from Stoke's law:

$$v = \frac{2}{9}\frac{(\rho_p - \rho_f)}{\mu} g R^2$$

where R is the radius of a spherical bubble, μ is the dynamic viscosity of the rising fluid, ρ_p and ρ_f are the density of the gas particles and the seawater fluid, respectively, and g is the gravitational acceleration. Thus, the rise velocity is a function of bubble size, fluid density and viscosity. In a release scenario, we assume the fluid density and viscosity to be constant variables, as the seeping gas comes from one specific source, and hence only the size of the bubbles will affect the rise velocity. The gas bubbles will also move in horizontal direction, as they are affected by local currents, and one can safely assume that the bubbles will reach surface some distance from the release point. If three different bubble sizes are modeled under the same scenario with equal current data, the distance from release point to surface will therefore also be a function of bubble size.

When determining a grid size for the simulations on Field A, it is important to make sure that the grid is large enough to cover all the locations where the gas may reach surface. If the gas is transported horizontally beyond the grid at any time during the simulation, the gas gets released to the atmosphere outside the grid, and thus the mean surface gas mass flux from the released fluid will be underestimated. Well W-16 and W-08 were chosen to determine a grid size, as they had the smallest and largest release rates of 7 l/hr and 120 l/hr, respectively. Simulations were run for 24 hours for each well, for both winter and summer scenarios. To achieve the best spatial resolution possible, the smallest cell size of 1 m × 1 m was chosen for the initial simulations, making the grid 100 m × 100 m in total. The output from the software is the surface gas mass flux as a function of time, namely how much gas is released from the sea to the atmosphere per

area per time. Graphs of the mean gas mass fluxes were created using python programming, and the results are presented in Fig. 4.2.

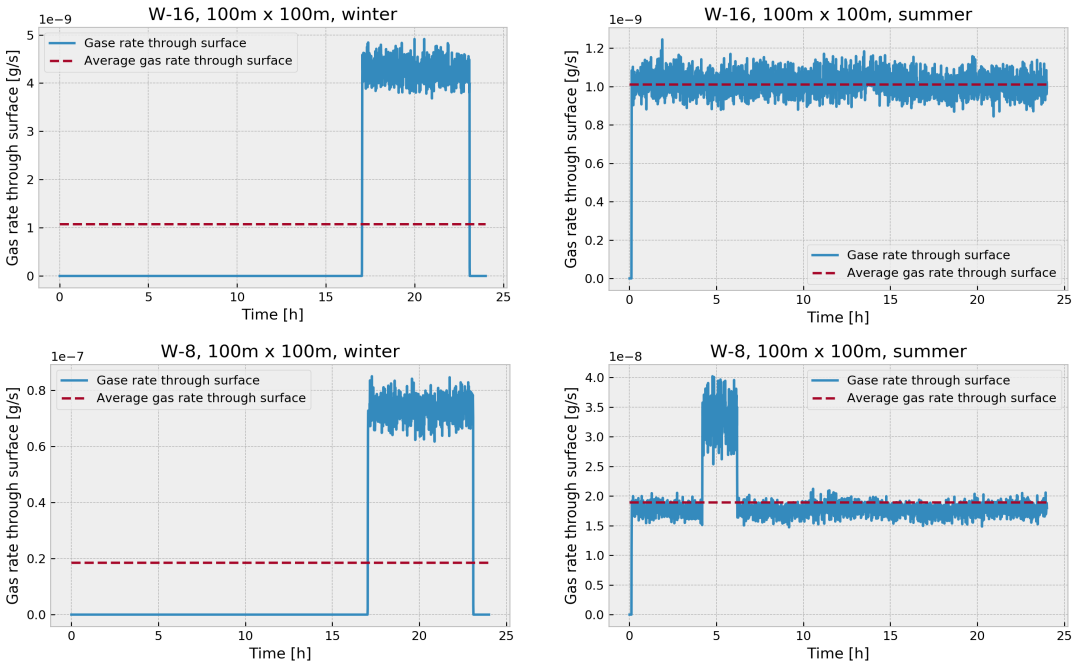

Fig. 4.2 Surface gas mass fluxes for 100m x 100m grid, W-08 and W-16.

As shown, the gas bubbles are in some periods transported outside the grid during winter, probably due to the stronger winter currents, and this is visible as a gas rate through surface equal to zero in the graphs on the left. This leads to an underestimation of the total gas mass flux, represented by the red, dotted line. In the summer simulations, the currents are a bit milder, and the gas does not escape the grid. However, as one wants to use the same grid size for all simulations that will be compared to each other, a larger grid must be chosen to include all gas. A new grid size of 200 m × 200 m, with cell sizes 2 m × 2 m was chosen for further modeling. The results from the different grid sizes for well W-16 and W-08 are presented in Fig. 4.3 and Fig. 4.4, and as one can see, the new grid size includes more of the gas.

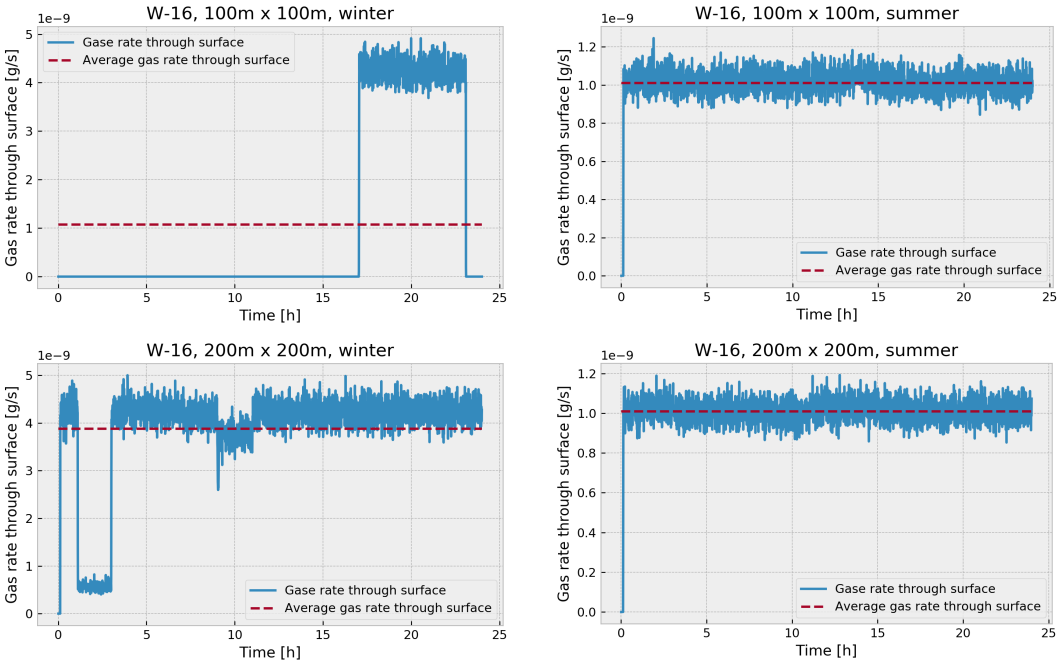

Fig. 4.3 Surface gas mass fluxes for different grid sizes, W-16.

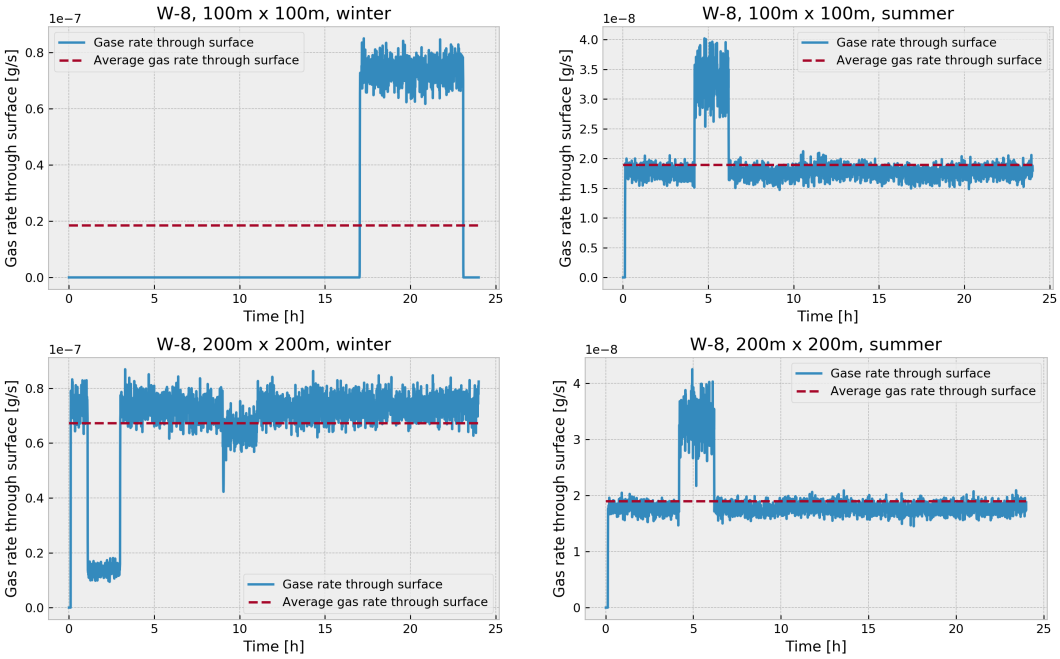

Fig. 4.4 Surface gas mass fluxes for different grid sizes, W-08.

The simulations show that there is a drop in the gas rate through surface in the 200 m × 200 m grid in winter simulations in the time interval of approximately 1 to 3 hours. If we assume that the gas rate through surface should be more or less constant, as in the summer simulations, one might think that some of the gas has escaped through the grid in this period. This is investigated in the software interface, and a cross sectional view of the bubble stream at different times t for W-08 is presented in Fig. 4.5.

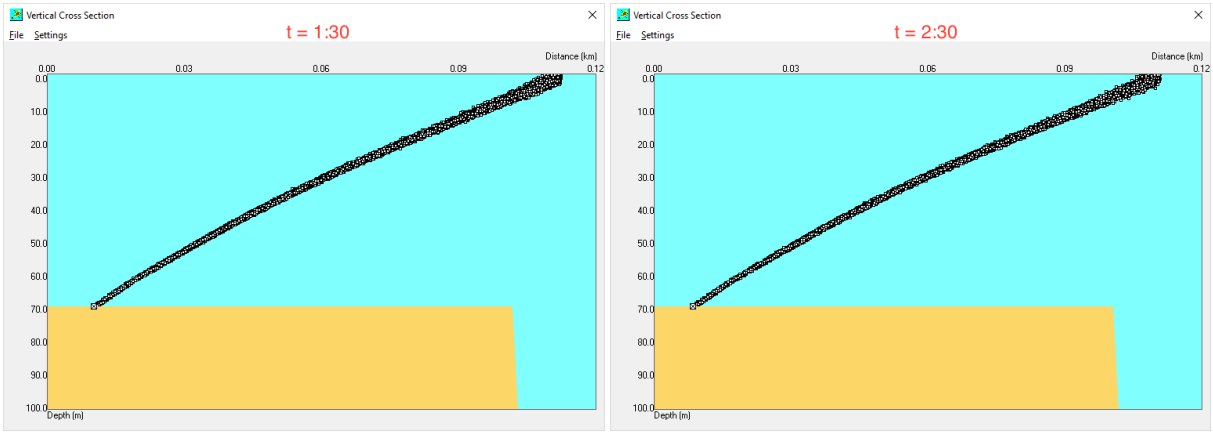

Fig. 4.5 Cross sectional views to evaluate escaping gas at times t.

The boundary of the grid is seen as the end of the yellow seabed, and as is evident, some gas indeed escapes the grid before reaching surface. Even though some gas is seen to escape over the boundary of the grid, the grid size of 200 m × 200 m was chosen for use in the further simulations due to resolution and the short time period of escape from the grid.

4.2.2 Determining duration of simulation

To achieve satisfactory temporal resolution, the correct duration of simulation must be chosen. This can be evaluated by considering Fig. 4.3 and Fig. 4.4 and reviewing the results. According to the graphs, the gas rate through surface, or gas mass flux, quickly establishes a more or less constant rate after t = 0 hours, and remain in the same interval throughout the simulation time of 24 hours. An exception is the summer simulation results for W-08, where the gas mass flux rises in the time interval of 4 to 6 hours. As the leaks from the wells are steady state leaks with constant rate and gas bubbles of uniform size, the rise velocity is assumed to be more or less the

same for all bubbles, and the only cause for temporal variation should therefore be the currents. From the graph, where the gas mass flux shows nearly steady state behavior, it is assumed that simulation times of 24 hours is adequate to include temporal variations.

4.2.3 Mass balance results and its dependence on bubble size

As previously stated, bubble size is an important parameter for the fate of the gas. Therefore, a bubble sensitivity analysis was performed on well W-16 to evaluate the effects of bubble size on transport of gas to atmosphere. Gas mass flux from sea to atmosphere as function of time for different bubble sizes is graphically presented in Fig. 4.6.

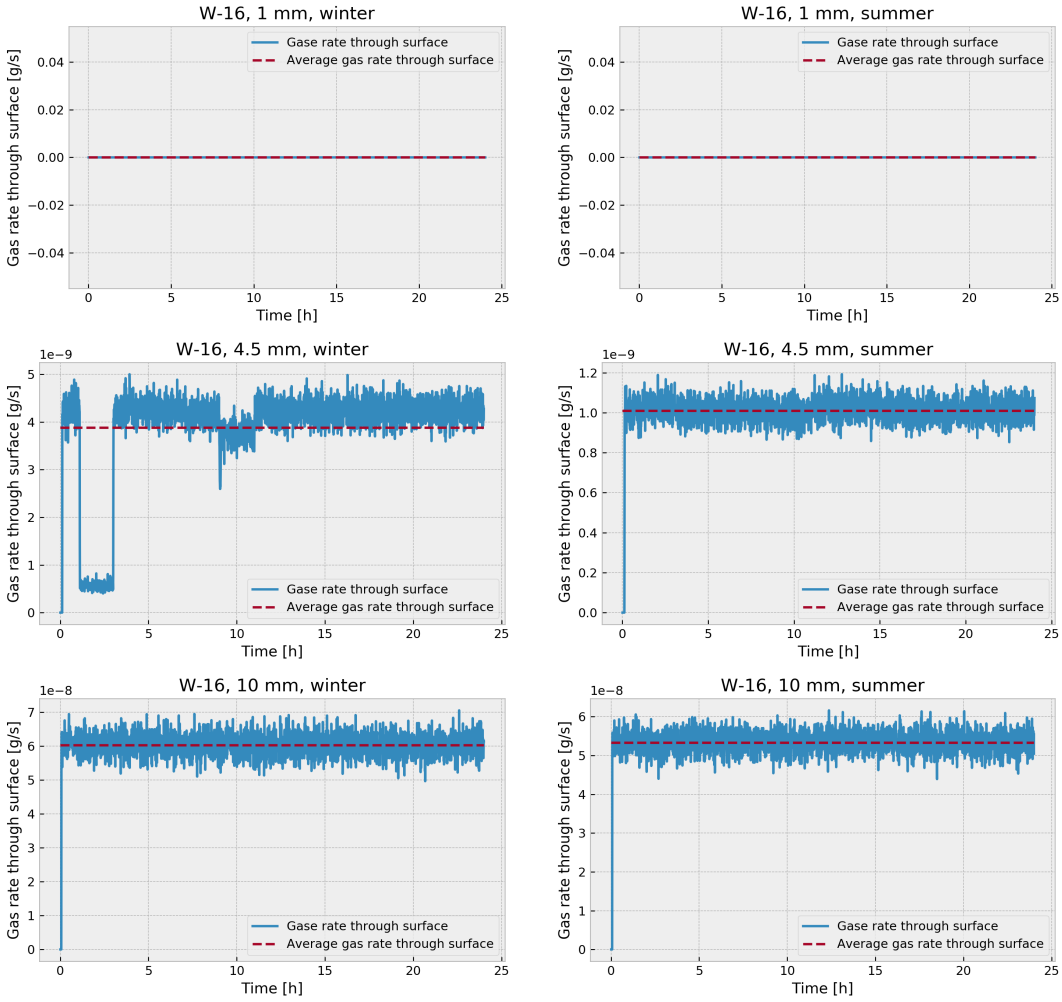

Fig. 4.6 Gas mass flux variation according to different bubble sizes.

The average values of gas rate through surface are presented in Table 4.1, along with the percentage of gas dissolved and percentage of gas reaching the atmosphere. With the expected bubble size range between 1 and 10 mm, the results show that a maximum of ~ 4.5 % of the released gas will reach the atmosphere from direct bubble transport. As shown, there is a clear pattern between increased bubble size and increased transport to atmosphere, and seasonal variations are present with increased atmospheric transport in the winter months. This is a result of the oceanographic conditions and the increased vertical mixing in winter.

Table 4.1 Mean gas mass flux rate and fractions of gas released to atmosphere and gas dissolved, as function of bubble sizes.

Well W-16	**Leak rate**	**Winter (01.02.2014)**			**Summer (01.08.2014)**		
Initial bubble size		% of gas dissolved	% of gas to atmosphere	Mean gas mass flux rate [g/s]	% of gas dissolved	% of gas to atmosphere	Mean gas mass flux rate [g/s]
1 mm	7 l/hr 0.168 Sm^3/d	100 %	0.000 %	0.0	100 %	0.000 %	0.0
4.5 mm	7 l/hr 0.168 Sm^3/d	97.108 %	0.289 %	3.880×10^{-9}	99.925 %	0.075 %	1.009×10^{-9}
10 mm	7 l/hr 0.168 Sm^3/d	95.510 %	4.490 %	6.023×10^{-8}	96.029 %	3.971 %	5.328×10^{-8}

As previously shown, the distance from the release point to the point on surface where the bubbles appear can be expressed as a function of the bubble sizes. This can be presented visually in the software, and a cross-sectional view of W-16 in winter is shown in Fig. 4.7. Here it becomes visible how smaller bubbles with lower vertical rise velocity will be overcome by currents and dissolve in the lower water layer, while larger bubbles may reach the surface at different distances according to bubble size.

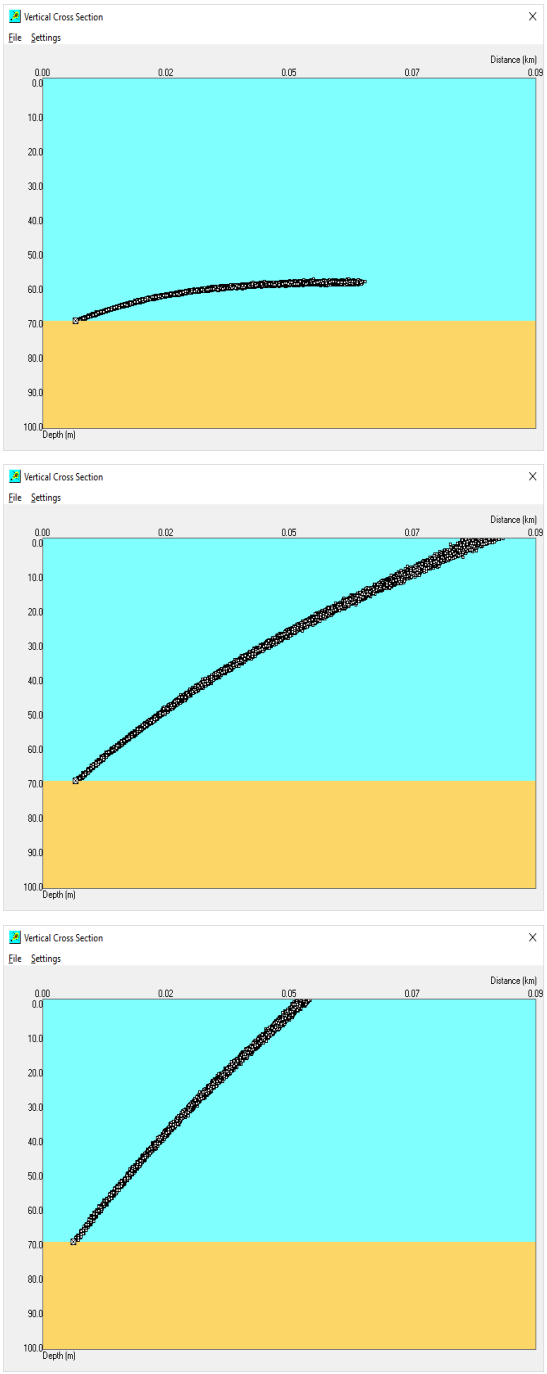

Fig. 4.7 Cross sectional view of gas releases with different bubble sizes. Top: bubble size = 1 mm. Middle: bubble size = 4.5 mm, gas bubbles reaches surface ~80 m from the well. Bottom: bubble size = 10 mm, gas bubbles reaches surface ~50 m from the well.

4.2.4 Leak rate sensitivity analysis

When it is established that the atmospheric transport of gas to surface is dependent on bubble size, it is desired to test is there are any differences with leak rate. Three new simulations are run, one for each well with corresponding leak rate, and a uniform bubble size of 4.5 mm has been chosen. The mass balance results from the simulations are presented in Table 4.2.

Table 4.2 Fractions of gas released to atmosphere and gas dissolved, as function of leak rates.

Well	Leak rate	Bubble size	Winter (01.02.2014)		Summer (01.08.2014)	
			% of gas dissolved	% of gas to atmosphere	% of gas dissolved	% of gas to atmosphere
W-04	45 l/h 1.080 Sm^3/d	4.5 mm	99.709 %	0.291 %	99.924 %	0.076 %
W-08	120 l/h 2.880 Sm^3/d	4.5 mm	99.708 %	0.292 %	99.918 %	0.082 %
W-16	7 l/hr 0.168 Sm^3/d	4.5 mm	99.711 %	0.289 %	99.925 %	0.075 %

The obtained result shows that the percentage distribution is almost exactly similar, with no tendency to change with increasing or decreasing flow rate. Even though the factor separating the leak rates in W-08 and W-16 is more than 17, the difference in atmospheric transport is no more than 0.003 %. The fraction of gas that enters the atmosphere is therefore thought to be independent of flow rate, at least for the flow rates presented in this case.

4.2.5 Comparing the results with natural seeps at Tommeliten

Field A is at a very similar water depth as the Tommeliten natural seeps, and the seabed and the temperature profiles in the areas are quite similar. Therefore, the results from Field A simulations and the investigations of the fate of natural seeps at Tommeliten are well suited for comparison.

At the Tommeliten seep area, Schneider von Deimling et al. (2011) estimated that less than 4 % of the methane reaches the upper mixed layer during the summer months, from where it can escape to the atmosphere. As the research cruises in mid-latitude areas tend to take place during the calmer summer season, no estimation for the winter months was made. However, as the thermocline breaks down and the entire water column starts to mix, some gas trapped under the thermocline may also enter the atmosphere, and it is therefore suggested that the methane flux to atmosphere may be underestimated. The results are consistent with the Field A results from Gastrack, which shows seasonal variations and a maximum of ~4.5 % of the gas being transported to the atmosphere. Both the current work and the Tommeliten study did modeling on different bubble sizes, and in Fig. 4.8, the fate of different sized bubbles are presented. As is expected, the atmospheric transport of methane increases with increasing initial bubble size. The changes in size of bubbles are (simplified) due to two effects; methane loss to the surrounding water causes the bubble to shrink, while the decreased hydrostatic pressure as the bubble rises causes the bubble to expand.

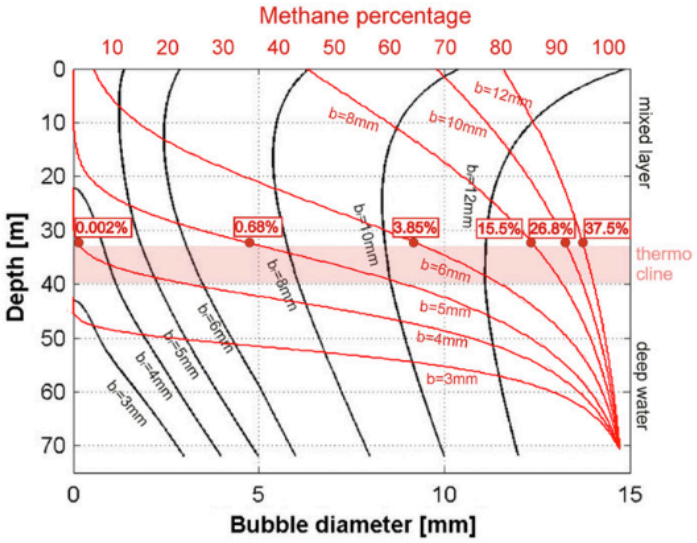

Fig. 4.8 Changes in methane percentage and bubble diameter as functions of initial bubble sizes. Figure reproduced from Schneider von Deimling et al. (2011). Each line represents a bubble with initial diameter b.

It is interesting that the atmospheric transportation from the three different leak rates at Field A is similar with the greater leak rate at Tommeliten. Tommeliten's leak rate of 26.3 t/yr equals:

$$\frac{26.3\,\frac{\mathrm{t}}{\mathrm{yr}} * 1000\,\frac{\mathrm{kg}}{\mathrm{t}}}{0.671\,\frac{\mathrm{kg}}{\mathrm{m}^3} * 365\,\frac{\mathrm{d}}{\mathrm{yr}} * 24\,\frac{\mathrm{h}}{\mathrm{d}} * 0.001\,\frac{\mathrm{m}^3}{\mathrm{l}}} = 4474.3\,\frac{\mathrm{l}}{\mathrm{h}} = 107.4\,\frac{\mathrm{Sm}^3}{\mathrm{d}}$$

which is substantially more than our case study of 7, 45 and 120 l/h. In fact, the worst-case leak scenario only constitutes ~2.7 % of the daily seepage rate at Tommeliten. This shows that effective methane transfer in the water column depends on initial bubble size, and that the initial bubble size will determine the fate of the bubble. However, there are some other factors that may affect these numbers as well.

4.2.6 Factors affecting atmospheric transport of methane

When a gas bubble rises from the seafloor through the water column, an exchange of gases will take place. As seawater is highly undersaturated in methane, methane will easily dissolve in the water column, while other gases present in the seawater, such as nitrogen (N_2) and oxygen (O_2), will enter the bubble (McGinnis et al. 2006). A simplified version of this process is presented in Fig. 4.9.

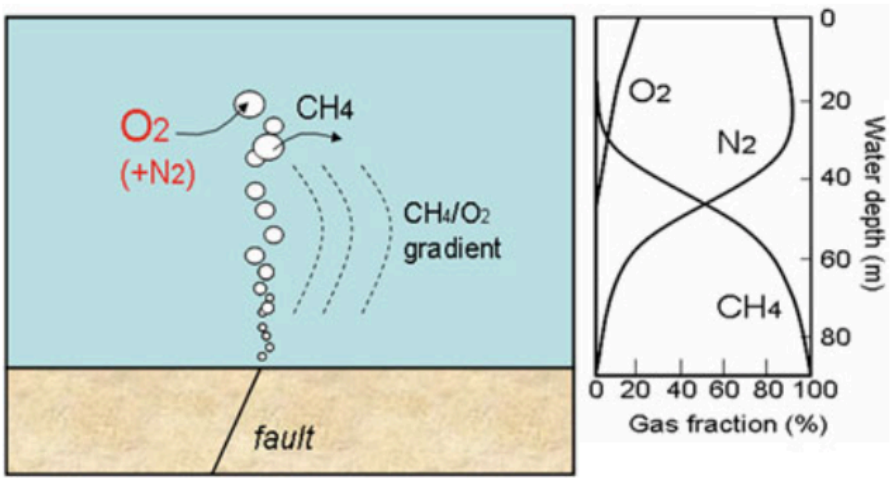

Fig. 4.9 Gas exchange in seep bubble, figure reproduced from Etiope (2015).

As one can see, the rising bubbles will be enriched in O_2 and N_2, while being depleted of methane. The diagram in Fig. 4.9 was derived from McGinnis et al. (2006), who modeled gas exchange in 5 mm diameter bubbles released at 100 m depth. After rising 70 – 80 m, the bubble would no longer contain methane. This case is very comparable to our case of 4.5 mm bubbles in 70 m water depth, releasing only ~0.3 % of initial gas content to the atmosphere in the winter months when water is well mixed. The most important factors that influence the rate of this gas exchange are partial pressure, initial bubble size and bubble-water contact time (McGinnis et al. 2006). The effects of bubble sizes are already shown by the simulations, and intuitively, bubble-water contact time depends on water depth and rise velocity, and increased contact time will increase gas exchange. Thus, bubbles released at shallow water have a higher potential of releasing natural gas to the atmosphere than bubbles released in deep water.

The gas exchange will reach maximum level for clean gas bubbles, but there are some factors that may reduce the gas exchange rate, and thus protect the natural gas inside the bubble. A surface coating of gas hydrate or oil, or presence of surface contaminants, will increase atmospheric transport. During a survey in the GoM, Solomon et al. (2009) found significant methane fluxes to the atmosphere originating from deepwater hydrocarbon seeps at 550 - 600 m depth. The combination of oil coated bubbles and a large flow rate from the seeps resulted in very efficient transport to surface. It is shown that a large mass flux of natural gas can reduce the hydrostatic pressure in the water column, causing an upwelling of flow of both water and gas in a natural gas bubble plume (Clark et al. 2003). This will increase the vertical rise velocity of the bubbles inside the plume and decrease water-bubble contact time, even for heavier, oil-coated bubbles (Leifer and MacDonald 2003). Also, the dissolved methane levels in the plume will rise, further decreasing the flux over the bubble surface. Eventually, the plume water may become supersaturated with methane, and methane loss from the bubbles may stop completely (Washburn et al. 2005). The combination of these effects may result in very efficient bubble-mediated transport of methane to surface, even from deep releases. The same effects can be seen with gas hydrate coatings on bubbles. However, these often form in water depths below ~ 500 m, in the gas hydrate stability zone (GHSZ), and are not relevant for the scope of this thesis that focuses on

the NCS with relatively shallow water depth (Hovland et al. 2012, MacDonald et al. 2002). A third effect reducing gas exchange in bubbles is surface contamination or surfactants. Bubbles may "pick up" hitchhikers on their ascent through the water, such as flakes from bacterial mats or floating microorganisms. These hitchhikers can slow down the gas exchange, but may also increase the mass of the bubble, slowing it down and increasing water-bubble contact time, and thus the effect of surfactants may vary both ways in terms of efficient, vertical methane transport (Judd and Hovland 2007).

From the different studies published on natural hydrocarbon seepages, it appears that the atmospheric transport of methane is largest in seeps occurring at shallow water depth or in locations with high mass flux. As the aim of the current work is to evaluate small leaks from abandoned wells, plume dynamics will not be further discussed, though it is important to clarify that in the case of a substantially increased leak rate, one cannot expect the same, high dissolution rate as presented in these results.

In addition to being transported directly to the atmosphere by bubbles, dissolved natural gas can also reach the atmosphere by diffusion from the mixed layer or by turbulent air-sea gas exchange (Leifer and Patro 2002). This is not addressed by the software or models presented. On a larger time scale, this dissolved gas may eventually reach surface, and increase the percentages presented in the results. Indeed, in the first study on the leaking exploration wells by Vielstädte et al. (2015), it was concluded that less than 2 % of the leaking gas would reach the atmosphere by bubble-mediated transport, but in the follow up study by Vielstädte et al. (2017), it was estimated that the percentage of gas reaching the atmosphere from leaking wells could possibly reach 42 %, if one included diffusion. Clearly, there are large differences between these numbers, and they should be more looked into if it is desired to do a thorough and complete fate analysis in the case of a leaking well.

4.2.7 Environmental effects of natural gas in the atmosphere

Reviewing the potential harmful effects of natural gas leaking from a well and reaching the atmosphere is made easy by the vast amount of literature published on natural gas seepages.

Most of it focuses on methane, the lightest and most abundant component of natural gas. As methane is a potent greenhouse gas, with a global warming potential 25 times larger than that of carbon dioxide (CO_2), the interest in studying natural seepages is largely focused on the contribution of methane to the atmosphere (Yvon-Durocher et al. 2014, Reeburgh 2007). This is also the focus of the study by Vielstädte et al. (2017), aiming to calculate the contribution to global warming from possibly leaking wells on the NCS. They concluded that leaking wells might be a significant source of atmospheric methane, with their worst-case scenario of gas leakage amounting to 17,000 t/y. With an estimated atmospheric transport of 42 %, significantly higher than the results from the current work or the study executed at Tommeliten, a maximum of 7,000 t/y was estimated to reach the atmosphere. To put this number into perspective, the global, annual methane flux to the atmosphere is estimated to be 535 Tg per year, or 535 million t/y (Reeburgh 2007). Thus, even the worst-case scenario of leaking wells on the NCS show a small contribution to global emissions.

The other components in natural gas, C_2 until C_6, may also reach the surface. In general, these components may be a source of air pollution and locally reduced air quality (National Research Council (U.S.) 2003). In California, the extensive seepage of natural gas and light hydrocarbons evaporating from oil slicks is a major source of air pollution and reactive organic compounds (ROC) in the atmosphere. In fact, chemical analysis of air grab samples collected by airplanes over the Santa Barbara Channel showed that 86 % of the non-methane hydrocarbons in the atmosphere originated from natural seeps, versus only 14 % originating from anthropogenic sources, such as emissions from cars, etc. (Hornafius et al. 1999). The ROC are volatile organic compounds that are capable of producing radicals upon reaction with sunlight and common atmospheric oxides and radicals. This is a precursor to smog-forming ozone in Santa Barbara County, a major environmental issue and a health threat to its inhabitants. The smog covers the city in a toxic haze, as can be seen in Fig. 4.10. In the case of leaking wells on the NCS, ROC will also be emitted to the atmosphere, but due to the small release rates, the low fraction of ROCs in natural gas and the long distance from shore, resulting air pollution should not pose a problem of equal magnitude. The main focus when assessing the environmental impact of

leaking natural gas might be better directed at the medium where the largest fraction of released gas ends up, namely the ocean.

Fig. 4.10 Los Angeles skyline seen through the smog, photograph by HI (2005).

4.2.8 Environmental effects of natural gas in the sea

Environmental effects of methane in the sea following a leaking well can be reviewed by, once again, diving into the literature on natural seepages. As previously shown, seeping natural gas will to some extent be degraded in the sediments by anaerobic and aerobic microorganisms, with end products such as CO_2, carbonate rocks, pyrite and H_2S. In the water column, aerobic degradation of the seeping gas continues, with bacteria utilizing O_2 to create CO_2 as a typical end product (Reeburgh 2007, Judd and Hovland 2007). In the case of a leaking well, the same processes would be taking place. If we assume that gas from a particular, leaking well is degraded by bacteria in a certain volume of water, this body of water will experience depletion of oxygen and enrichment in CO_2. On a large scale, this may contribute to the ongoing process of ocean acidification. This was also the conclusion of Biastoch et al. (2011), who studied the potential effects of methane being released from dissolving gas hydrates in the arctic. Ocean acidification is a process that has been occurring parallel to the rising atmospheric CO_2 levels, as approximately one third of the anthropogenic CO_2 added to the atmosphere by the burning of

fossil fuels are taken up into the ocean. Besides climate change, ocean acidification is often referred to as the "other CO_2 problem", and it is responsible for lowering the pH and disturbing chemical balances in the ocean. This directly affects a wide range of marine organisms that is dependent on building shells from calcium carbonate, ranging from planktonic organisms and mollusks to corals, coralline algae and organisms such as clams and crabs. As all organisms are linked together in complicated and vulnerable ecosystems, any significant change due to ocean acidification has the potential of far-reaching consequences for the oceans of the future, and for the millions of people and animals dependent on its food and other resources for livelihoods (Doney et al. 2009).

Since the beginning of the industrial era, it is estimated that the ocean has absorbed some 525 billion tons of CO_2 from the atmosphere, with the current rate at around 22 million tons per day (Bennett). It is interesting to put this in the context of the leaking well case. If we go back to the equation for aerobic degradation of methane, we see that the degradation of one CH_4 molecule produces one CO_2 molecule:

$$CH_4 + 2O_2 \rightarrow CO_2 + 2H_2O$$

We know that the molecular weight of CH_4 is 16.04 g mol^{-1}, and that the molecular weight of CO_2 is 44.01 g mol^{-1}. According to the ratio between them, the degradation of one weight unit CH_4 will therefore produce 2.7438 weight units of CO_2. If we return to our leaking well case, and the Tommeliten seep area, and assume that 100 % of the released gas is dissolved in the sea and later degraded, the following production of CO_2 would make up an almost imperceptible contribution to the ocean acidification. The numbers are tabulated in Table 4.3.

Table 4.3 Contribution of leaking gas to ocean acidification.

Well	Leak rate	Weight CH_4 [kg] (0.671 kg / Sm^3)	Weight CO_2 [kg]	Percentage of daily CO_2 uptake
W-04	45 l/h 1.080 Sm^3/d	0.725	1.988	9.04×10^{-9}
W-08	120 l/h 2.880 Sm^3/d	1.932	5.302	2.41×10^{-8}
W-16	7 l/hr 0.168 Sm^3/d	0.113	0.309	1.40×10^{-9}
Tommeliten seep area	4474.3 l/h 107.4 Sm^3/d	72.07	197.7	8.99×10^{-7}

As is clearly visible, the impact from leaking wells on ocean acidifications are not considered to be great. The coupled condition of oxygen depletion however, may have greater impact on the local environment.

In areas of prominent seepage, O_2 levels may drop to a very low concentration and the site may become hypoxic. This is due to the combined effect of gas exchange in seeping natural gas bubbles and microorganisms using oxygen for degradation. Hypoxia is defined as oxygen concentrations below 60 µM (or 2 µg/l), against a normal concentration in air saturated water above 220 µM (or 7 µg/l). The process is accelerated in the case where limited or no input of new oxygenated water exists, for instance in deep water where circulation is slow. Hypoxic waters have been reported in Venezuela, the GoM, offshore Namibia and in Greece (Etiope 2015). The condition can be critical for biodiversity and the local ecosystems, and the upwelling of hypoxic water can have a fatal effect on fish near the surface. In some cases of intense seepage and absent circulation of oxygenated water, O_2 concentrations may drop to zero, making the site anoxic. Large anoxic dead zones were considered a possible scenario in the early phases of the Deepwater Horizon Spill in the GoM in 2010. Fortunately, the worst-case scenario of total anoxia was not achieved, but several studies show that the oil and gas degradation consumed massive amounts of

oxygen and resulted in a persistent oxygen anomaly in deep gulf waters. To this day, the extent of long-term consequences has not yet revealed itself (Beyer et al. 2016).

Oxygen is a vital ingredient in the metabolism of near all living species. Numerous studies show that oxygen deficit in the seawater directly influences the rate of fish metabolism, in addition to decreasing their resistance to many organic and inorganic poisons. Oxygen deficit will increase the rate of blood circulation through the gills and make fish more susceptible to natural gas poisoning. Indeed, in the Sea of Azov, a shallow bay north of the Black Sea, observations after two major, accidental gas blowouts in 1982 and 1985 showed a cause-effect relationship between natural gas release and mass fish mortality (Patin 1999). Methane and other short-chained alkanes are easily dissolved and spread out in the seawater, and will in small concentrations probably be degraded before any negative impact is made on the environment. However, impact is a question of concentration. Patin (1999) suggested that when concentration of methane in seawater exceeded 1 ml/l, a level of acute toxicity would be experienced. Concentrations below 0.01 ml/l would be within ecological tolerance. The results presented in the current work are not able to state something on which concentrations of dissolved gas in the seawater would be experienced, as this is not currently within the functionality of the Gastrack software.

It is known that in areas of high seepage, benthic communities including aforementioned methane-oxidizing and sulfide-oxidizing microorganisms will thrive. This can attract fish and other macro-fauna, providing them with nutrition and enriching the food chain (Hovland 2008, Hovland et al. 2012). In areas where gas bubbles bring spots of bacterial mats with them on their ascent, these are often deposited in the water column, attracting feeding animals (Judd and Hovland 2007). In the Gullfaks seepage area, hermit crabs have been seen fighting over pieces of bacterial mat, and the area is one of Norway's heavily fished areas (Hovland 2007). The biological diversity and the intricate food chains in the ocean is a wide area of research, and to properly assess the environmental effects of dissolved gas in the ocean due to leaking wells is outside the scope of this work. However, the results show that for relatively small leak rates, the fraction of released gas dissolving in the seawater remains approximately constant. This

information could easily be used by marine biologists or toxicologists to help answer the question of environmental impact of different leak rates in abandoned wells.

4.3 Case B

4.3.1 Mass balance results

When investigating and modeling the fate of oil from a leaking well, the first question that arises is where the oil will go, and how it will be divided in the environment into different fractions. The overview over the different fractions is called the mass balance. In the software, the mass balance is represented by a graph with percentages, as the example shown in Fig. 4.11. The different fractions are explained briefly in Table 4.4. Note that percentages in all mass balance results denote weight percent.

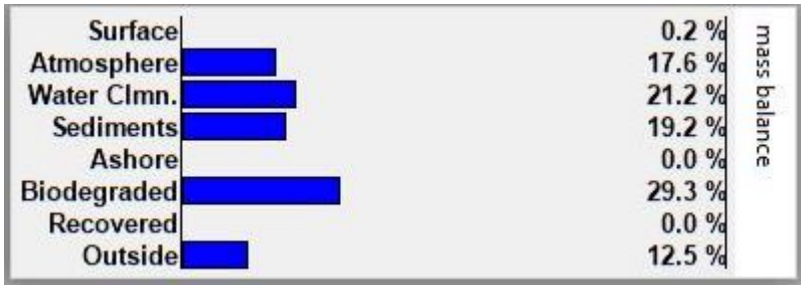

Fig. 4.11 Example of mass balance results from OSCAR.

Table 4.4 Mass balance fractions.

Fraction	Explanation	Relevant for this work
Surface	Oil floating on surface	Yes
Atmosphere	Evaporated oil	Yes
Water column	Oil in water, either as emulsion, droplets, adhered to particulates or dissolved	Yes

Sediments	Oil deposited on seafloor	Yes
Ashore	Oil washed ashore	No
Biodegraded	Oil transformed by marine organisms	Yes
Recovered	Oil collected in oil spill cleanups	No
Outside	Oil transported outside the grid whilst submerged in water	Yes

To investigate the mass balance during a constant release from a well, simulations for the three different leak rates of 0.01, 0.1 and 1.0 l/h were performed. All leak rates were modeled in winter and summer for all four, different droplet size distributions. In total, this makes 24 simulations. Start dates were 01.01.2014 and 01.07.2014, respectively, and duration of the simulation was 90 days each with constant leak rates. Six graphs showing the evolution of the mass balance results during the simulation are included in Appendix C, and a table with all the percentage values for all 24 simulations is included in Appendix D. The resulting graphs for day 1 and day 90 are shown in Fig. 4.12 and Fig. 4.13.

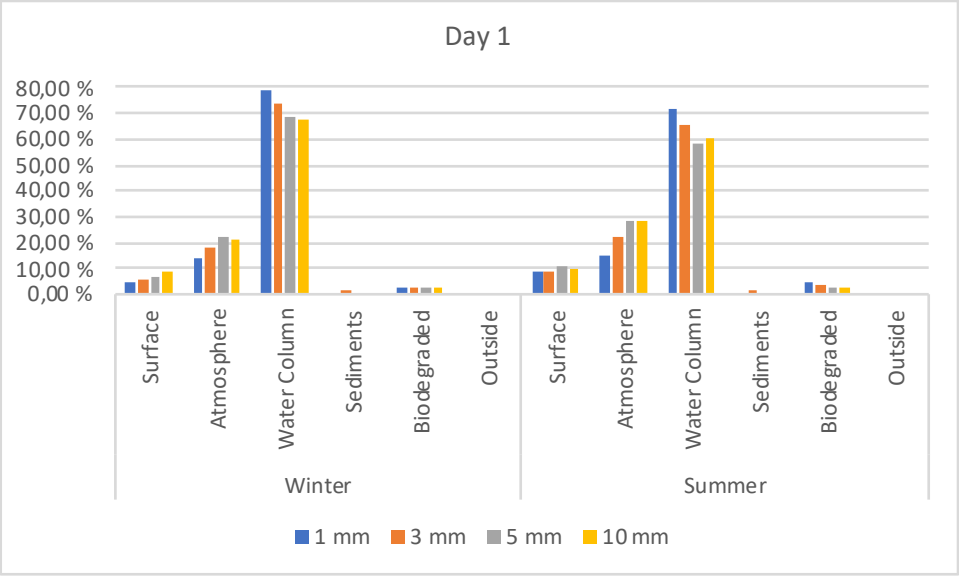

Fig. 4.12 Mass balance results day 1.

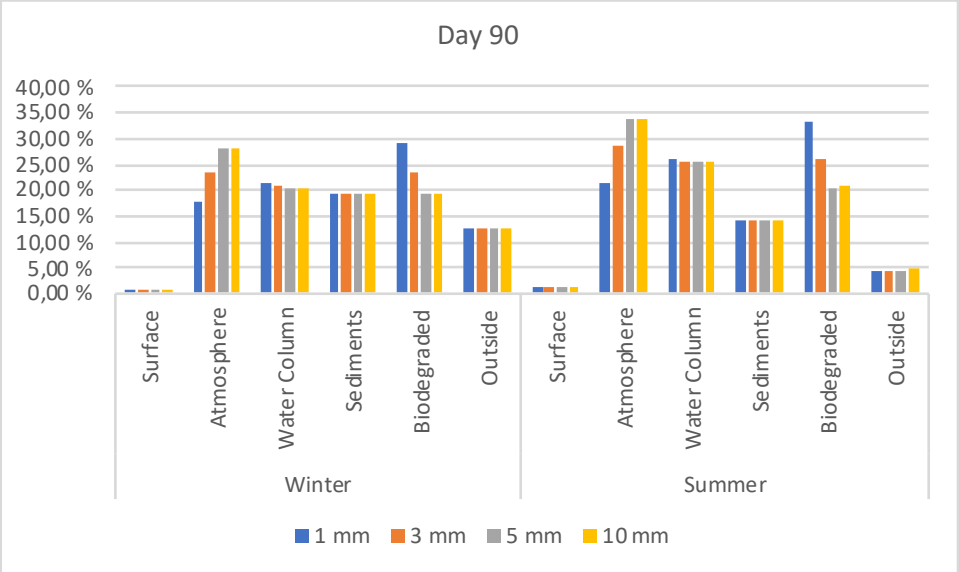

Fig. 4.13 Mass balance results day 90.

The percentages denoting the different fractions are the sums of all oil released up to time t. In the beginning of the simulation, oil will start to rise upwards through the water column, and some will reach surface and evaporate. These will be the dominating fractions in the beginning of the release. As oil on surface is weathered with time, some of the heaviest compounds will start to deposit on the seafloor and biodegradation will start both in water and in the sediments. Consequently, as time passes by, the fraction of oil that has evaporated, been deposited on sediments or biodegraded will rise, as the percentages in the mass balance results are describing the fate of all the released oil for 90 days. Thus, at day 90, the oil still left dissolved in the water column or floating on surface will at some point be biodegraded, released to the atmosphere by evaporation or deposited in the sediments. In a way, these three fractions are the "end stations" of the oil release.

As oil is generally not soluble in water, it will persist in the environment for quite some time. Leaking oil will therefore be able to travel over large distances with currents before reaching an end station, and even though the chosen grid size for mass balance evaluation is 200 km × 200 km, ~4.5% and ~13% of the oil escapes the grid in summer and winter, respectively, as shown in

Fig. 4.13. Even though some oil escapes, a larger grid was considered unpractical in regards to the small leak rates. To depict the size of the grid, a map from the software showing a random point in the North Sea and the outlines of a 200 km × 200 km grid is included in Fig. 4.14. As one can see, a grid this size covers quite a large bit of the North Sea! It could therefore be possible that oil from a leaking well may reach other sectors of the North Sea, thus affecting the environment of other countries as well.

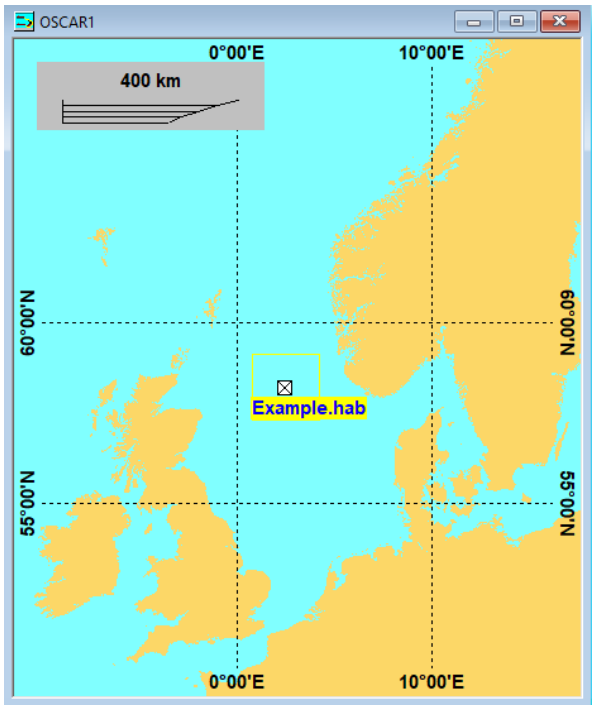

Fig. 4.14 Example of 200km x 200km size grid in the North Sea.

4.3.1.1 Droplet size sensitivity analysis

From Fig. 4.13, it is clear which fractions are dependent on droplet size and which are not. This has been presented graphically in Fig. 4.15 and Fig. 4.16, using the day 90 results from leak rate of 0.01 l/h. Percentage values are retrieved from the table in Appendix D.

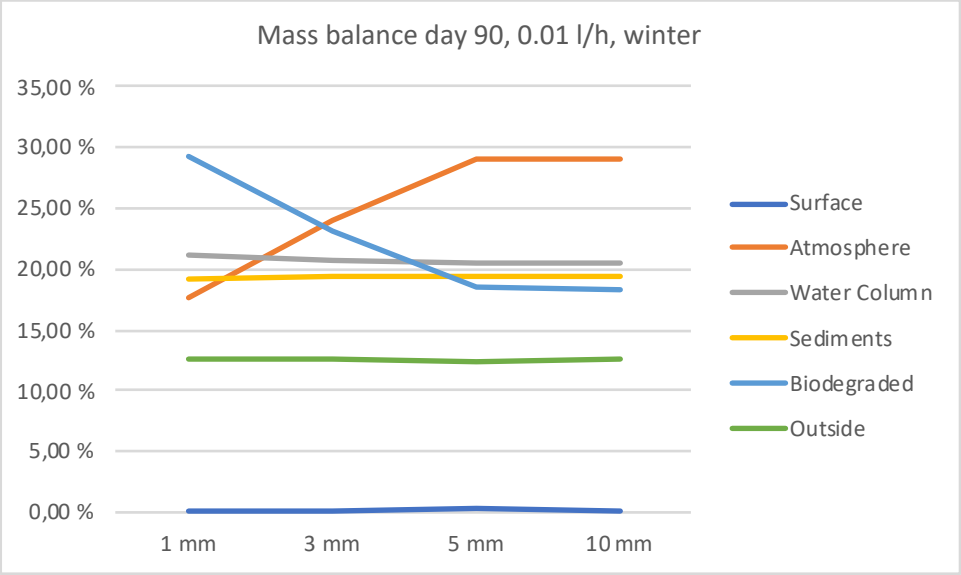

Fig. 4.15 Mass balance results in winter as function of droplet size.

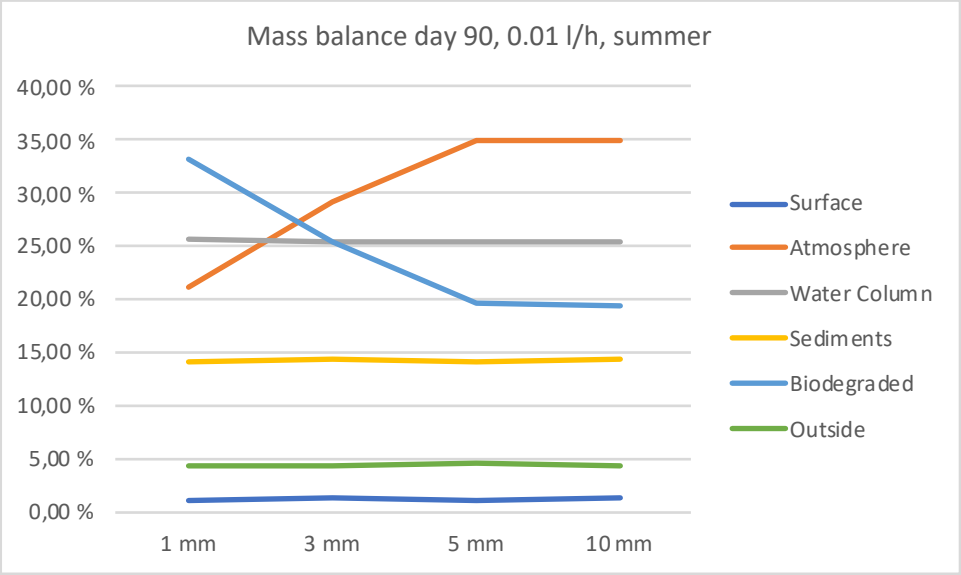

Fig. 4.16 Mass balance results in summer as function of droplet size.

From the figures, it is clear that the two fractions dependent on droplet size are the atmospheric and the biodegraded fractions, and they are inversely dependent of each other. This is consistent with literature on natural seepages and other marine releases. Larger droplets will be more likely to reach surface and form surface slicks, from where evaporation occurs. Smaller droplets will have a lower vertical rise velocity, increasing droplet-water contact time, favoring dissolution. Thus, the fraction of oil reaching surface, and consequently the evaporation rate, is lesser for smaller droplets. In fact, this is the reason why chemical dispersants are often used in accidental oil spill cleanups to decrease droplet sizes in areas where surface oil pose a risk to the environment (Li et al. 2016).

When it comes to biodegradation rates, they increase with decreasing droplet size. Smaller droplets have a higher surface area relative to volume of oil, increasing both the effective area from where the water-soluble components can dissolve into the water and the area available for the attachment of oil-degrading bacteria. The biodegradation also depends on the water-oil contact time, which increases in smaller droplet sizes, as they have lesser vertical velocity. A study by Brakstad et al. (2015), who investigated the biodegradation rates of Macondo oil in Norwegian seawater at low temperature (4 – 5 °C), showed improved biodegradation rates after dispersant treatment of oil, and this is in accordance with a large range of previous laboratory studies and the results of the fate modeling presented here.

It is interesting that the evaporation rate increases and the biodegradation rate decreases with increasing droplet size, but only up to 5 mm droplets. If we compare the results from 5 mm and 10 mm droplets, they are approximately the same. Thus, modeling even greater droplet sizes than 10 mm is considered unnecessary.

4.3.1.2 Leak rate sensitivity analysis

From the obtained results, it is evident that the mass balance results are not dependent on leak rate. The table in Appendix D shows that the different winter and summer results are almost identical to each other, regardless of the leak rate. This is not unintuitive when we consider that leak rates of 0.24 - 24 l/day are spread out over an area of several hundred kilometers. An

example of the mass balance results for the simulations with 3 mm droplet sizes is presented in Fig. 4.17 and Fig. 4.18, and as is shown, mass balance results are independent on leak rate, at least for the cases modeled in the current work.

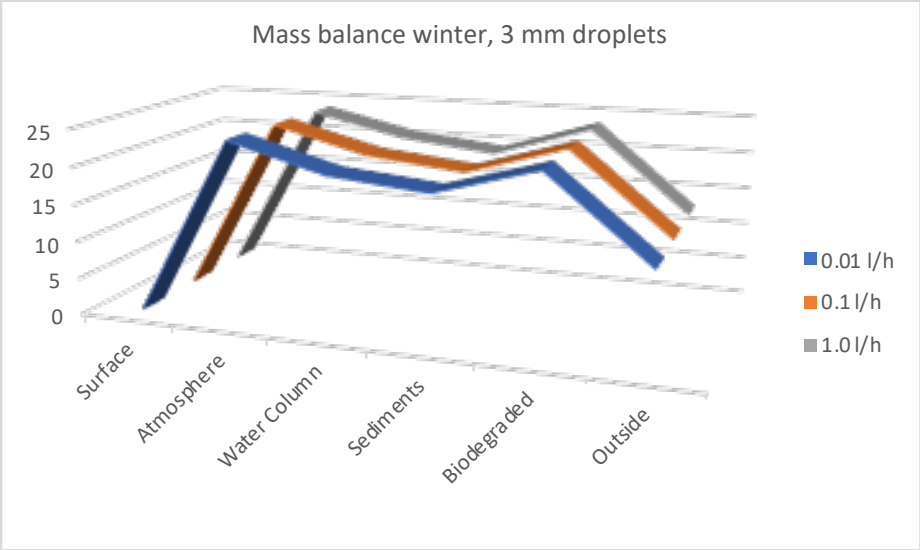

Fig. 4.17 Mass balance as function of leak rate, winter.

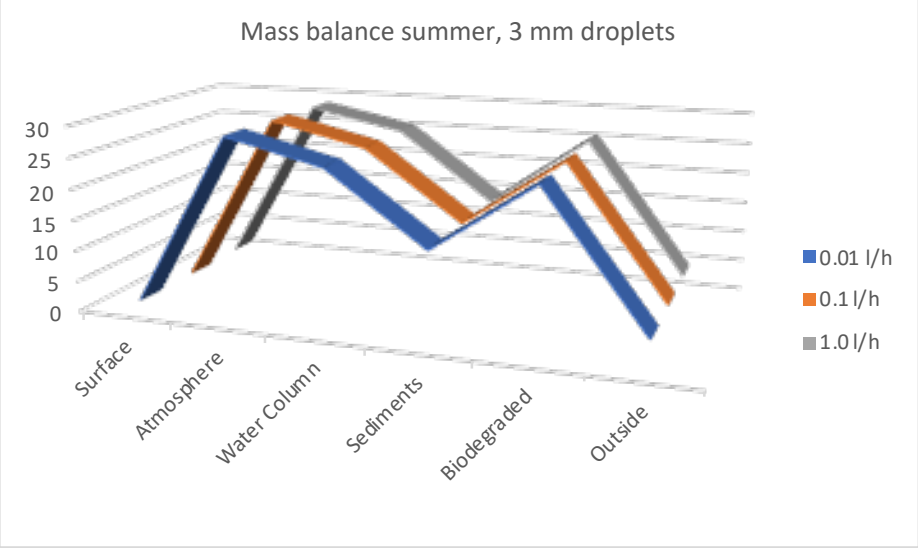

Fig. 4.18 Mass balance as function of leak rate, summer.

4.3.1.3 Seasonal variations

It is already established that the fate of leaking oil and gas is affected by the season. Atmospheric temperature, ocean temperature curves and magnitude of winds and waves are all factors in play. From the mass balance results presented until now, it can be difficult to state something decisive on the differences between winter and summer simulations, as the currents are stronger and a larger portion of the released oil is transported outside the grid in winter. Additionally, it is unknown what will happen to the oil that is transported outside the grid or the oil still dissolved or suspended in the water column. To resolve this, the discussion on seasonal variations is given in the next chapter.

4.3.2 Ultimate fate of oil

It is desirable to understand the ultimate fate of the oil that in the last chapter was still trapped in the water column, on surface or had traveled beyond the grid. To understand the ultimate fractions of oil at the three end stations, atmosphere, sediments and biodegraded, a new set of simulations was set up. As previous results showed that the mass balance results did not depend on leak rate, a single leak rate of 0.1 l/h were chosen for the new simulations. The releases were set to last five days each, starting 01.01.2014 and 01.07.2014 for winter and summer simulations, respectively, and the simulations were set to run for 90 days. Simulations for all, four droplet size distributions were run for both winter and summer, in total 8 simulations. In order to capture all the oil, a large grid size was chosen at 400 km × 400 km. The results are presented in Table 4.5 and Fig. 4.19.

Table 4.5 Mass balance results, for a 5 day release, 90 day simulation.

	Droplet size	Surface	Atmosphere	Water Column	Sediments	Biodegraded	Outside grid
Winter	1 mm	0.0 %	16.7 %	0.0 %	48.7 %	34.4 %	0.3 %
	3 mm	0.0 %	22.2 %	0.0 %	48.9 %	28.7 %	0.2 %
	5 mm	0.0 %	26.6 %	0.0 %	48.9 %	24.2 %	0.2 %
	10 mm	0.0 %	26.9 %	0.0 %	49.0 %	23.8 %	0.2 %

Summer	1 mm	0.0 %	20.3 %	2.5 %	38.7 %	38.4 %	0.0 %
	3 mm	0.0 %	28.4 %	2.5 %	39.0 %	30.1 %	0.0 %
	5 mm	0.0 %	34.4 %	2.5 %	39.0 %	24.1 %	0.0 %
	10 mm	0.0 %	34.2 %	2.6 %	39.0 %	24.2 %	0.0 %

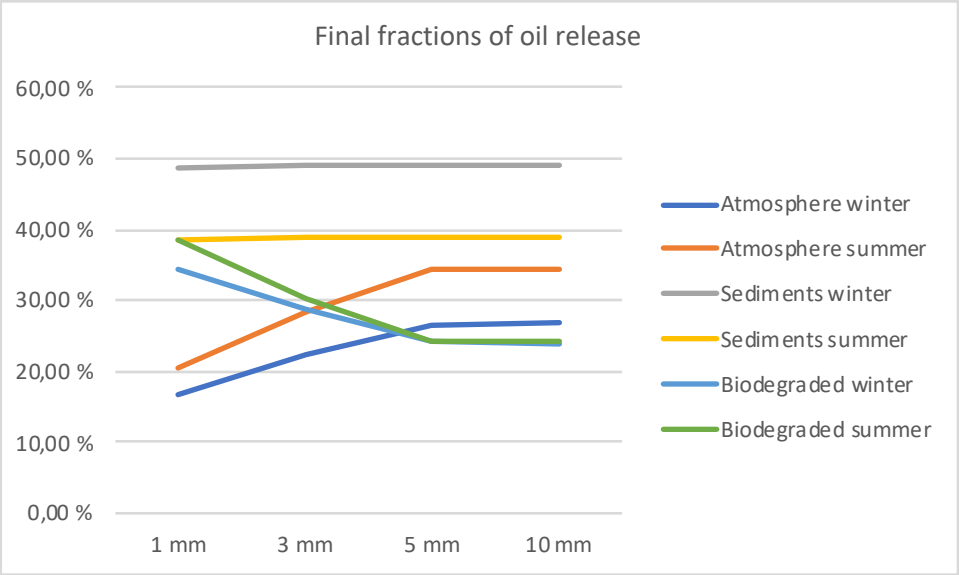

Fig. 4.19 Final mass balance according to season and droplet size.

The same relation between droplet sizes and atmospheric and biodegradation fractions are observed as in the last chapter. When it comes to the sediment fractions, they seem to be independent of droplet size, so it is likely, and consistent with theory, that this fraction depends more on the chemical composition of the oil. The heavier compounds are more likely to be deposited on the seafloor. However, there are some seasonal variations, approximately 10 % more oil will be deposited in the sediments during a leak in winter compared to summer. It is assumed that this is a combined effect of decreased evaporation and biodegradation rates in winter. Also, evaporation of different compounds is dependent on atmospheric temperature, making some compounds evaporate in summer, but perhaps not in winter. It is noted that the sediment fractions are by far the largest, meaning that nearly 40 – 50 % of all released oil will end up deposited on the seabed sediments.

Seasonal variations are present for all fractions. In summer, evaporation rates are higher due to warmer weather. Biodegradation rates are also slightly higher in summer than in winter, especially for small droplet sizes, due to general seasonal fluctuations of microbial activity in the water column. The warmer summer water speeds up the biodegradation rates, consistent with theory (Fingas 2011). A graph of the final fraction distributions is shown in Fig. 4.20.

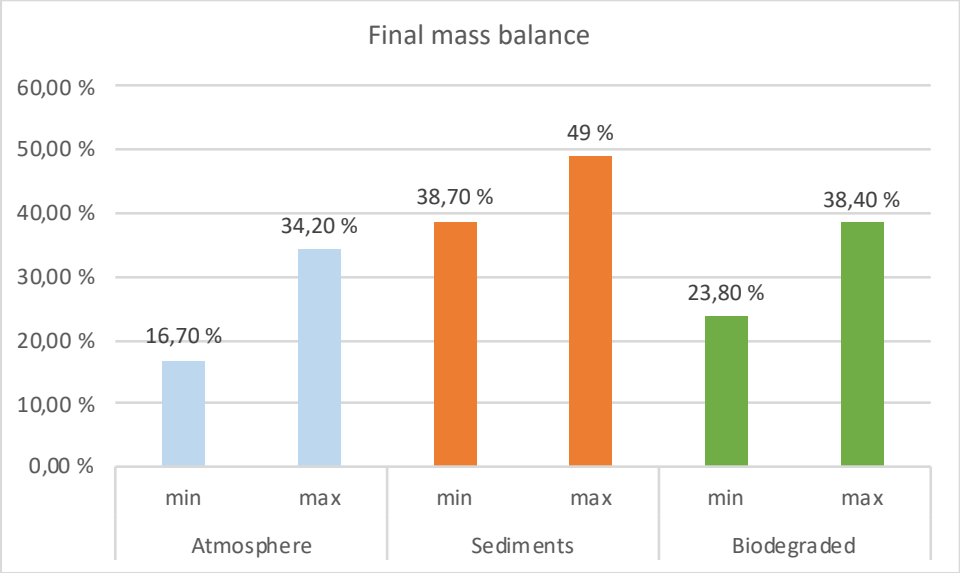

Fig. 4.20 Minimum and maximum values of final mass balance fractions.

In addition to finding the final fractions of the end station, it is also interesting to see how long it takes before all surface or submerged oil reaches an end station. To show this, mass balance plots as function of time for the case of 5 mm droplets are presented in Fig. 4.21 and Fig. 4.22. The results show that the fractions of submerged and surface oil become near unnoticeable at t = 25 days for winter and t = 60+ days for summer. In Fig. 4.22 it is also worth noticing how the fraction of surface oil oscillates. This is due to weather conditions, in calm weather with low wave and wind activity the surface oil fraction increases.

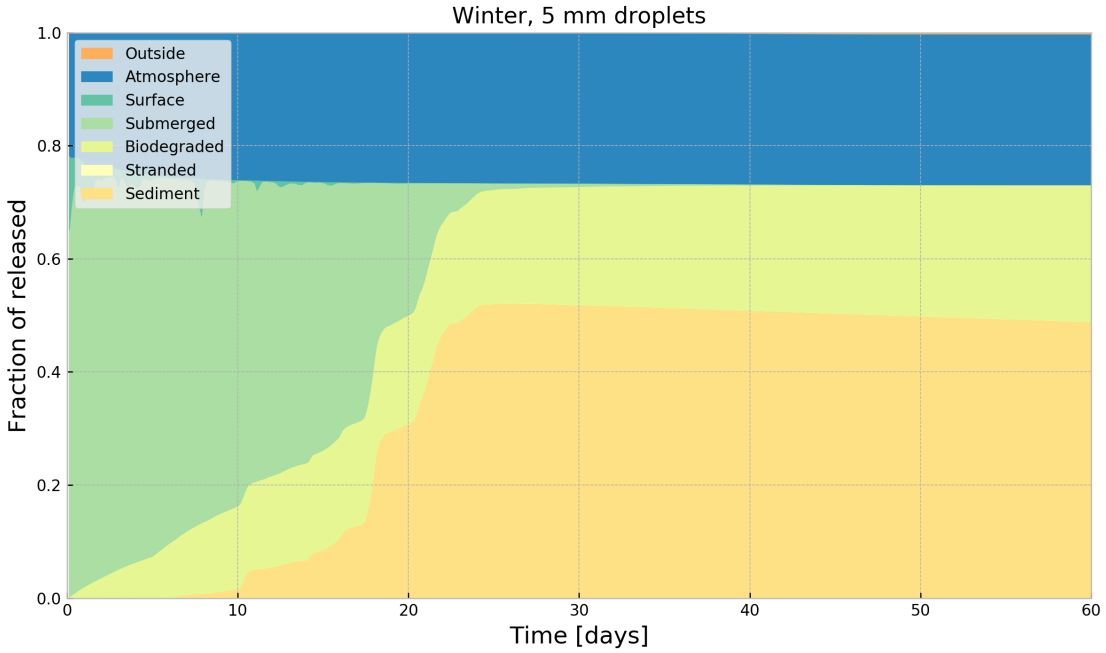

Fig. 4.21 Mass balance as function of time following a five day oil release, winter.

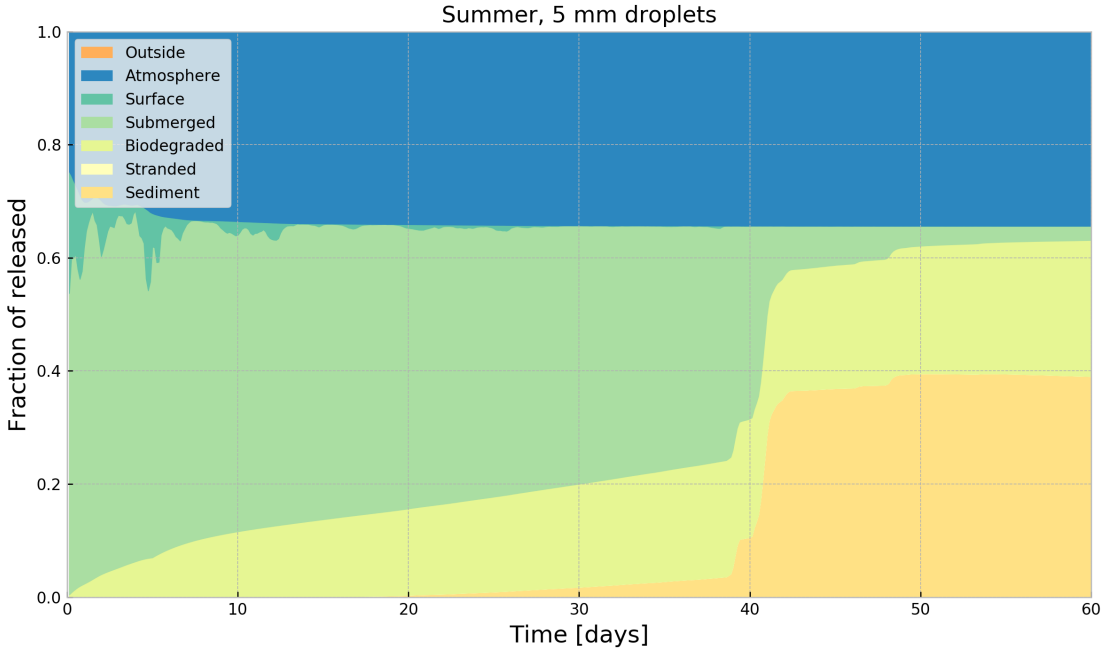

Fig. 4.22 Mass balance as function of time following a five day oil release, summer.

When these relations are established, next it is interesting to evaluate how long it takes before the oil that has settled into the sediments gets biodegraded.

4.3.3 Oil persistence in the sediments

To investigate the biodegradation rates for oil in the sediments, a simulation for a full year was performed, modeling a leak rate of 0.1 l/h for five days duration starting 01.01.2014. The results are presented in Fig. 4.23, where the results for the first 60 days are the same results as Fig. 4.21.

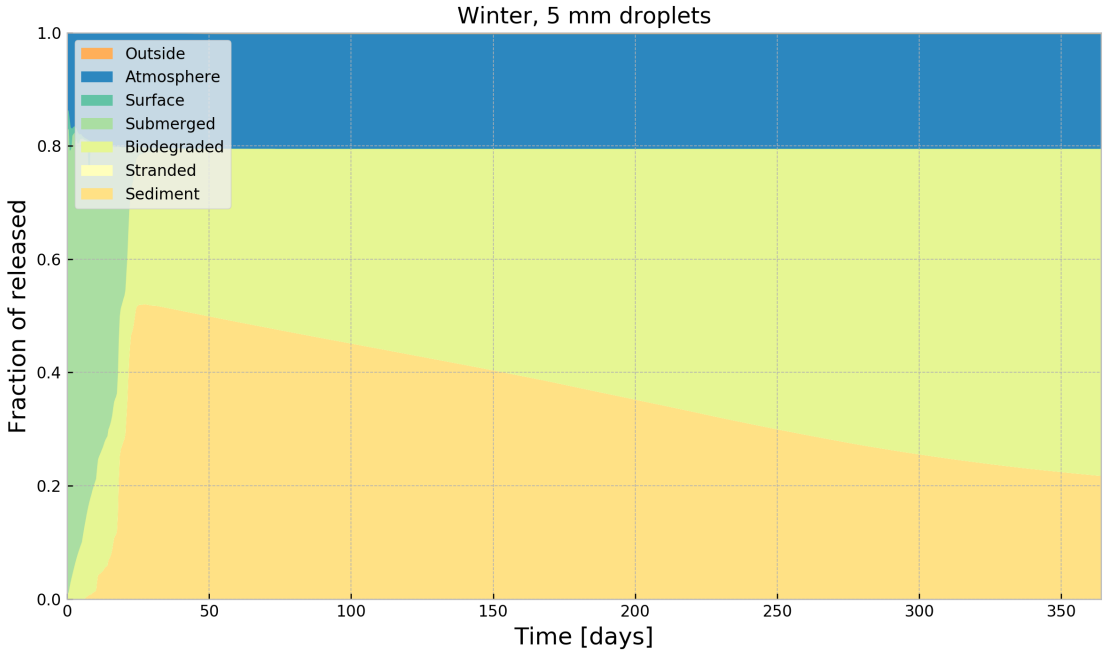

Fig. 4.23 Mass balance for one year following a five day release.

The fraction of oil settled on the seafloor sediments reaches its maximum at approximately 50 % in 25 days, and is reduced to approximately 22 % by the end of the year. A simple estimation of constant biodegradation rates would then give a result of oil persistence in sediments of nearly two years.

4.3.4 Concentration analysis – determining grid size

Finished with the mass balance analysis, the next important aspect of fate modeling of oil is the concentrations analysis. As mentioned in chapter 3.4.2, mean and maximum concentrations of dissolved oil in the water column are averaged over the entire cell, so the sizes of the cells may affect the results. Large cells may cause a false dilution of the concentrations. Choosing the right size grid is therefore essential when investigating which concentrations that will follow the different release rates. After recommendation from SINTEF Ocean, the smallest grid chosen is 500 m × 500 m, with grid cells 5 m × 5 m in xy plane. In z direction, the cell size is 8 m, as the total depth of the simulation is set to 80 m with 10 layers. 80 m was chosen as depth of interrogation, as the water depth in the release site is 70 m, and varies slightly in the area. The argument for choosing 5 m × 5 m grid cells is to let the horizontal and vertical resolution be comparable. In addition, there are some uncertainties in the current and weather data, so running simulations with cells of smaller size would therefore most likely not provide more accurate results.

When running the first simulations investigating concentrations, a constant release rate of 0.1 l/h was chosen, and the duration of the release and the simulation was set to five days. Winter and summer simulations were set up, starting 01.02.2014 at 12:00 pm and 01.08.2014 at 12.00 pm, respectively. The grid was 500 m × 500 m, as best spatial resolution possible close to the release site was desirable. The temporal resolution was also of importance, and simulation time step was set to 1 minute with output interval of 5 minutes. Simulations were run for all four droplet sizes, so in total 8 simulations were executed.

When evaluating the results of these simulations, mass balance showed that more than 95 % of the released oil was transported outside the grid with the currents. To include more of the release, 8 new simulations were set up with a 2 km × 2 km grid with 20 m × 20 m cells. A comparison of the results for the two different grid sizes is presented in Table 4.6, and presented graphically in Fig. 4.24 and Fig. 4.25.

Table 4.6 Mean and maximum concentrations for different grid sizes. (*) denotes an unexpected result, as concentrations are generally higher in winter than in summer, but is assumed to be normal variation due to statistics.

Grid size Cell size	Droplet size (diameter)	Winter		Summer	
		Mean conc.	Max. conc.	Mean conc.	Max. conc.
500 m **5 m x 5m**	1 mm	0.147 ppb	20.07 ppb	0.099 ppb	17.72 ppb
	3 mm	0.057 ppb	10.64 ppb	0.048 ppb	7.512 ppb
	5 mm	0.051 ppb	6.726 ppb	0.039 ppb	4.457 ppb
	10 mm	0.037 ppb	3.346 ppb	0.024 ppb	2.624 ppb
2 km **20 m x 20 m**	1 mm	0.022 ppb	4.355 ppb*	0.013 ppb	6.002 ppb
	3 mm	0.015 ppb	3.527 ppb	0.008 ppb	2.440 ppb
	5 mm	0.011 ppb	1.531 ppb	0.006 ppb	1.280 ppb
	10 mm	0.008 ppb	1.209 ppb	0.004 ppb	0.667 ppb

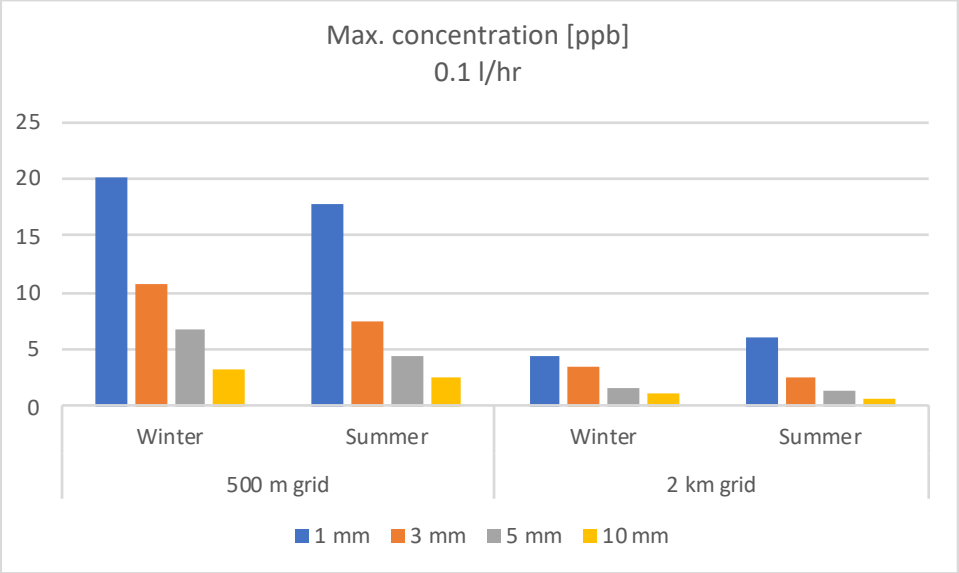

Fig. 4.24 Maximum concentrations for different droplets sizes and grids.

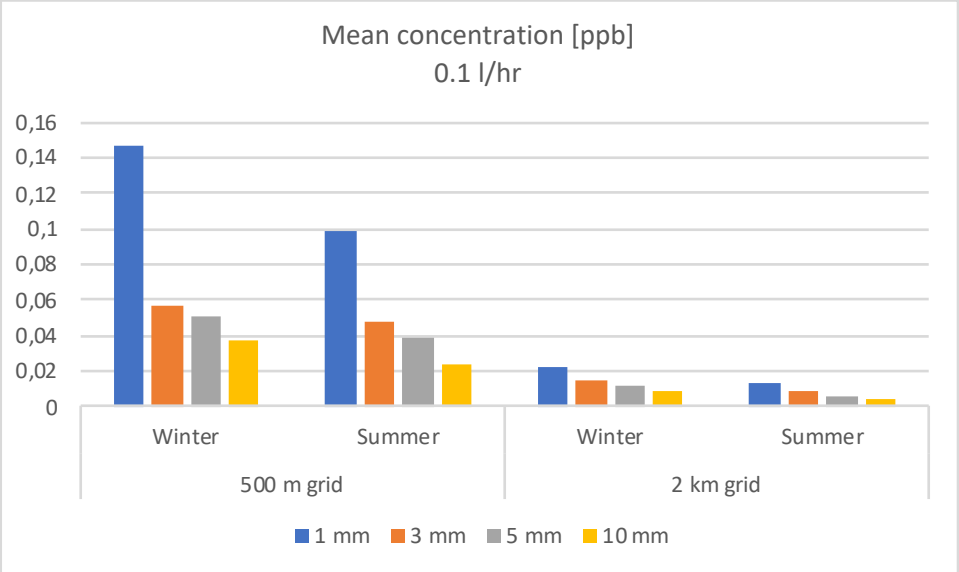

Fig. 4.25 Mean concentrations for different droplet sizes and grids.

As one might expect, the resulting concentrations for the larger grid were considerably diluted, and even though the grid was 16 times larger than the first, approximately 90 % of the released fluid still travelled beyond the grid. However, the maximum concentrations are still expected to occur close to the release site. In addition to being transported away horizontally from the release site with currents, released oil in will also spread out radially and be distributed vertically throughout the water column. Therefore, it will be quickly diluted as it travels away from the release site. As this assumption is supported by the simulation results, the smallest grid will be used to determine maximum concentrations for evaluation of possibly harmful consequences of leaking wells.

4.3.5 Leak rates and resulting concentrations

When running the first simulations investigating concentrations, constant release rates of 0.01, 0.1 and 1.0 l/h were chosen, and the duration of the releases and the simulations was set to five days. Winter and summer simulations were set up, starting 01.02.2014 at 12:00 pm and 01.08.2014 at 12.00 pm, respectively. Simulations were run for all four droplet sizes, so in total 24 simulations were executed. The grid was 500 m × 500 m, as best resolution possible close to the release site

was desirable. The results are presented in Table 4.7, where mean concentration values are average values of all mean concentrations values during the simulation, while the maximum concentration values are denoting the maximum concentration in a single grid cell during any time t of the simulation. In Fig. 4.26 the maximum concentrations as a function of time are presented, and the peak values are what is presented in Table 4.7.

Table 4.7 Mean and maximum concentration following the release scenarios. (*) denotes an unexpected result, as concentrations are generally higher in winter than in summer, but is assumed to be normal variation due to statistics.

Release rate	**Droplet size (diameter)**	**Winter**		**Summer**	
		Mean conc.	Max. conc.	Mean conc.	Max. conc.
0.01 l/h	1 mm	0.017 ppb	1.863 ppb*	0.010 ppb	2.259 ppb
	3 mm	0.007 ppb	0.950 ppb	0.006 ppb	0.779 ppb
	5 mm	0.005 ppb	0.664 ppb	0.004 ppb	0.429 ppb
	10 mm	0.004 ppb	0.377 ppb	0.003 ppb	0.261 ppb
0.1 l/h	1 mm	0.147 ppb	20.07 ppb	0.099 ppb	17.72 ppb
	3 mm	0.057 ppb	10.64 ppb	0.048 ppb	7.512 ppb
	5 mm	0.051 ppb	6.726 ppb	0.039 ppb	4.457 ppb
	10 mm	0.037 ppb	3.346 ppb	0.024 ppb	2.624 ppb
1.0 l/h	1 mm	1.418 ppb	198.09 ppb*	0.993 ppb	255.1 ppb
	3 mm	0.521 ppb	101.6 ppb	0.427 ppb	74.08 ppb
	5 mm	0.482 ppb	53.72 ppb	0.363 ppb	44.15 ppb
	10 mm	0.332 ppb	45.97 ppb	0.225 ppb	23.01 ppb

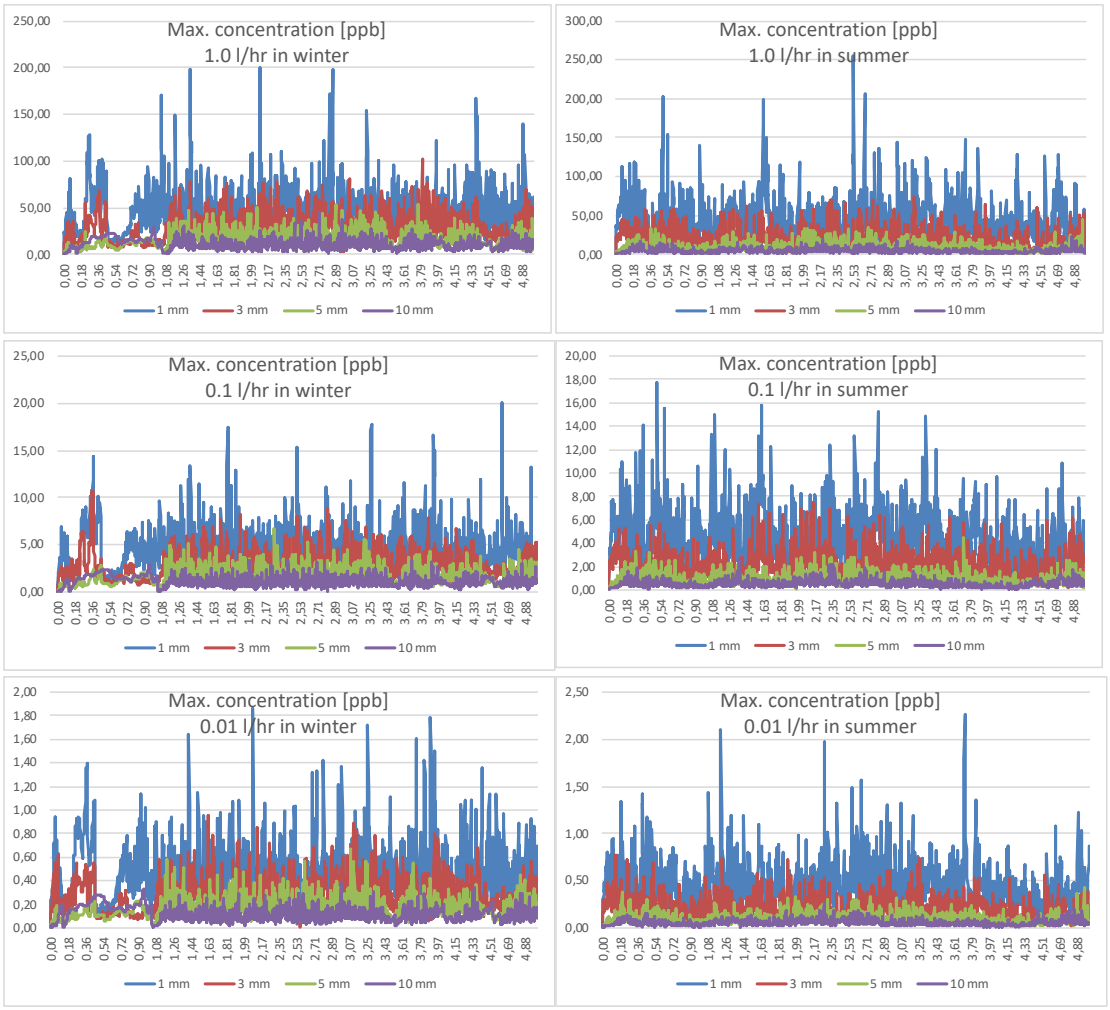

Fig. 4.26 Maximum concentrations following the release scenarios as function of time [days].

From the obtained results, it is seen that increasing the leak rate by factors of 10 also increases the mean and maximum concentrations by a comparable factor. To show this, the results from 0.01 and 0.1 l/h have been multiplied by 100 and 10, respectively, and plotted versus the concentration data from 1.0 l/h leak rate. This is presented graphically in Fig. 4.27 and Fig. 4.28.

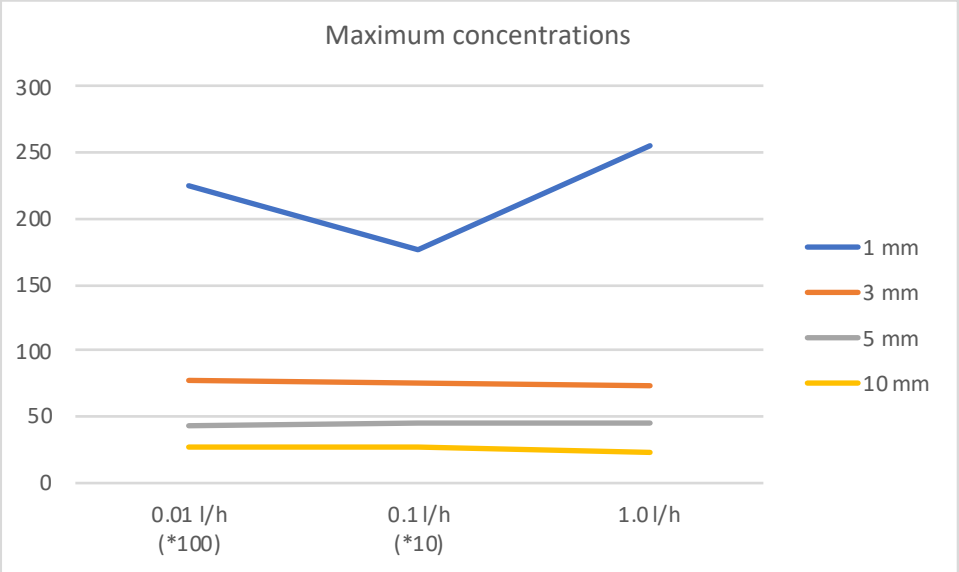

Fig. 4.27 Maximum concentrations, comparison between leak rates.

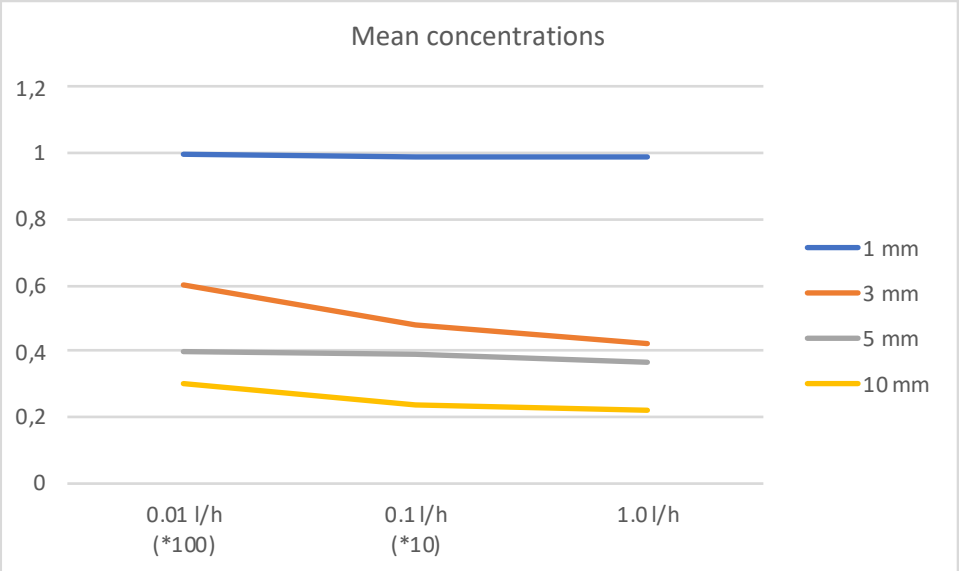

Fig. 4.28 Mean concentrations, comparison between leak rates.

4.3.6 Environmental effects of evaporated oil

As presented in chapter 4.2.7, light hydrocarbons that evaporate to the atmosphere can cause local air pollution. In small amounts in remote locations offshore, this will probably not have the greatest impact on the environment. What could theoretically cause some damage is H_2S, which is highly toxic, but in general, the content of H_2S in Norwegian oil and gas is very low, and it is considered unlikely that a small amount of gas escaping the sea will be inhaled by man or animal and causes great impact.

4.3.7 Environmental effects of oil in the water column

The fraction of oil submerged in water is the combination of dissolved oil, oil droplets and oil in emulsion with water, and its potential for damaging its surroundings is dependent on the concentration. To evaluate the potentially harmful effects from leaking wells, the results from the software will be converted from ppb to mg/l. First, the maximum concentration value from Table 4.7 is chosen, namely the summer value at 255.1 ppb, which is the resulting maximum concentration following the highest leak rate of 1.0 l/h combined with the smallest droplet size at 1 mm. This corresponds to:

$$255.1 \text{ ppb} = 0.2551 \text{ ppm} = 0.0002551 \frac{\text{ml}}{\text{l}} = 2.551 * 10^{-4} \frac{\text{ml}}{\text{l}}$$

The density of oil in Field B is given in the OSCAR software as 841 kg/m^3 = 0.841 kg/l = 841 mg/ml, and this concentration thus corresponds to:

$$2.551 * 10^{-4} \frac{\text{ml}}{\text{l}} * \ 841 \frac{\text{mg}}{\text{ml}} = 0.2145 \frac{\text{mg}}{\text{l}}$$

It is important to realize that this is a single value from a single grid cell at a single time t near the release point. It is not representative for the entire area or duration of the simulation, as is evident from the graphs in Fig. 4.26 on maximum concentration. Therefore, it is perhaps more interesting to look at the mean concentration results, as these are more representative of the general concentrations in the area over time. The maximum mean concentrations occur in the winter simulations for the smallest droplet size of 1 mm. In mg/l, they make:

0.01 l/h:

$$0.017 \text{ ppb} = 1.7 * 10^{-8} \frac{\text{ml}}{\text{l}}$$

$$1.7 * 10^{-8} \frac{\text{ml}}{\text{l}} * \ 841 \frac{\text{mg}}{\text{ml}} = 1.430 * 10^{-5} \frac{\text{mg}}{\text{l}}$$

0.1 l/h:

$$0.147 \text{ ppb} = 0.000147 \text{ ppm} = 1.47 * 10^{-7} \frac{\text{ml}}{\text{l}}$$

$$1.47 * 10^{-7} \frac{\text{ml}}{\text{l}} * \ 841 \frac{\text{mg}}{\text{ml}} = 1.236 * 10^{-4} \frac{\text{mg}}{\text{l}}$$

1.0 l/h:

$$1.418 \text{ ppb} = 0.001418 \text{ ppm} = 1.418 * 10^{-6} \frac{\text{ml}}{\text{l}}$$

$$1.418 * 10^{-6} \frac{\text{ml}}{\text{l}} * \ 841 \frac{\text{mg}}{\text{ml}} = 1.192 * 10^{-3} \frac{\text{mg}}{\text{l}}$$

To attempt to quantify the environmental effects following oil releases, the relation between concentration and effect can be divided into sectors. Patin (1999) reviewed available experimental data to distinguish oil pollution in the sea by four different toxicological zones:

- No effect concentrations (zone 1)
- Primary threshold responses (zone 2)
- Sublethal effects (zone 3)
- Acute toxicity (zone 4)

When applying the experimental data to actual levels of pollution found in different areas of the world's oceans, the results suggested that no biological effect is detectable when the concentrations of the sum of hydrocarbons are below 10^{-3} mg/l in seawater, and this is therefore set as the maximum value for zone 1. When marine organisms are exposed to zone 2 concentrations, which is the zone of primary threshold responses, the damage they experience is often reversible or compensated at a cellular level, and it does not lead to any obvious biological

consequences in the sea. Patin (1999) therefore suggests that when trying to establish a maximum permissible concentration (MPC) of oil hydrocarbons in the seawater, it should be within the range of zone 2 at 0.001 – 0.01 mg/l. The MPC is a level chosen between the no effect and the sublethal effect zones, and is thereby a useful standard to set. The sublethal effects of zone 3 at 0.01 – 1.0 mg/l will not cause immediate death of any marine organisms, but can cause clear physiological, biochemical and behavioral effects, including disturbance of reproductive functions. When subjected to the acute toxicity of zone 4 with concentrations exceeding 0.1 mg/l, lethal effects occur within a short period of time. Zone 3 and zone 4 concentrations levels are often found in areas such as gulfs, ports, harbors, bays and estuaries, and in other shallow water environments where water circulation is slow and a chronic source of oil pollution exists, such as natural seepage, releases from ships and tankers or accidental spills. An overview of the different toxicological zones is given in Fig. 4.29. Zone 0 denotes the background level in pristine areas (Patin 1999).

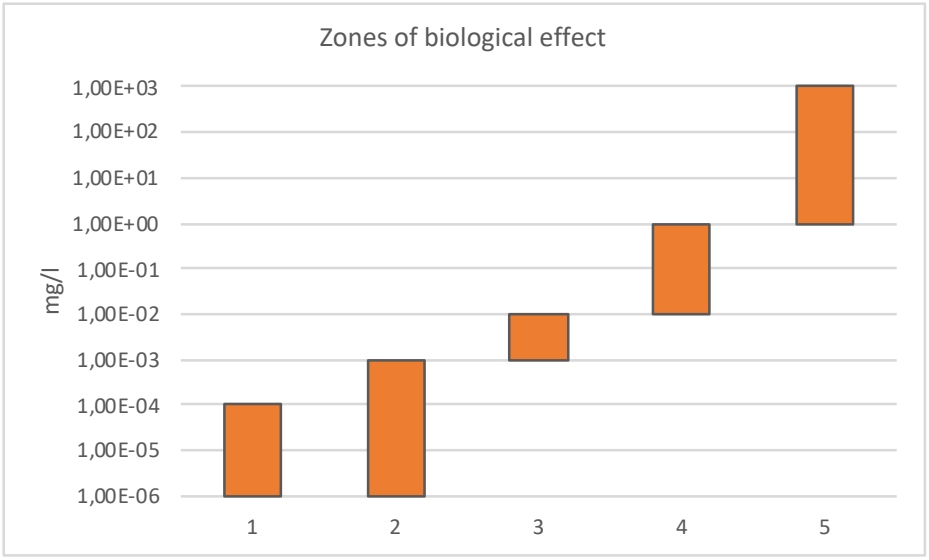

Fig. 4.29 Zones of biological effect as a function of dissolved oil in mg/l. Adapted by numbers from Figure 42 in Patin (1999).

By the method described above for converting the ppb data to mg/l for Field B, the biological effects for the concentration data of Table 4.7 can be color coded according to potential toxicity, as shown in Table 4.8.

Table 4.8 Resulting zones of biological effects following the different oil release scenarios.

Release rate	Droplet size (diameter)	Winter		Summer	
		Mean conc.	Max. conc.	Mean conc.	Max. conc.
0.01 l/h	1 mm	Zone 1	Zone 2	Zone 1	Zone 2
	3 mm	Zone 1	Zone 1	Zone 1	Zone 1
	5 mm	Zone 1	Zone 1	Zone 1	Zone 1
	10 mm	Zone 1	Zone 1	Zone 1	Zone 1
0.1 l/h	1 mm	Zone 1	Zone 3	Zone 1	Zone 3
	3 mm	Zone 1	Zone 2	Zone 1	Zone 2
	5 mm	Zone 1	Zone 2	Zone 1	Zone 2
	10 mm	Zone 1	Zone 2	Zone 1	Zone 2
1.0 l/h	1 mm	Zone 2	Zone 3	Zone 1	Zone 3
	3 mm	Zone 1	Zone 3	Zone 1	Zone 3
	5 mm	Zone 1	Zone 3	Zone 1	Zone 3
	10 mm	Zone 1	Zone 3	Zone 1	Zone 3

As is shown, none of the simulated results regarding mean or maximum concentration reaches the zone 4 of acute toxicity. Some of the values of the maximum concentrations reaches zone 3, but as previously stated, these values are not representative for the overall concentrations in the area of the leak.

This sort of cause-effect analysis based on concentration of dissolved oil is a very simplified approach. As is known, the term "oil" does not denote a uniform substance, but rather a collection of several thousand possible components consisting of mainly carbon and hydrogen atoms. Oils also contain varying amounts of other substances, such as nitrogen, sulfur and oxygen, in addition to trace metals such as nickel, vanadium and chromium. When analysts have

found over 17,500 different components of crude oil, it is natural to deduce that the specific behavior and fate of individual oils in the environment differ from each other (Fingas 2011).

Knowing these facts, there are two, obvious weaknesses in evaluating the environmental effects by the method of the last section. First, the zones of concentration values are set without regards to the chemical composition of the oil in question. It is just a general pinpoint for crude oil based on different datasets from the author's literature review, and does not take into account that some oils have higher toxic potential than others, due to varying toxicity of the different compounds constituting the oil. Second, using the concentration data from the OSCAR software, the concentrations are given in ppb, which is a simple volume fraction denoting a certain amount of oil in a certain amount of water. It fails to take into account, which oil components end up in the different fractions – light components for instance, are more likely to evaporate to the atmosphere, while heavier components are more likely to be deposited on the seabed in the sediments. Benthic societies on the seabed are therefore more likely to interact with the heavier compounds, while phytoplankton in the upper water levels are more likely to interact with the lighter compounds. Fish and other marine organisms swimming in the water column may have increased exposure to lighter, volatile compounds with high solubility potentials, and thus the interactions between marine life forms and released oil in all of these different segments will vary greatly. To complicate matters even further, different species might react differently to each oil compound as well. To summarize, the toxicity of a release is dependent not only on the concentration data, but also on the chemical composition of oil, the fate of the different components, the variety of marine organism affected by the release and other, in situ environmental parameters.

Even though a complete analysis is beyond the capacity of this work, there are some interesting aspects that can be further examined. The OSCAR dynamic user interface offers the option of viewing concentration maps in the dynamic user interface for different, selected oil compounds. This way, one can isolate and investigate the fate of the most toxic compounds. In general, the aromatic compounds are the most toxic, as these contain benzene rings. Benzene rings consist of six carbon atoms in a cyclic structure. These ring structures are very stable, making benzene very

persistent in the environment, increasing toxicity. The most common, smaller aromatic compounds are referred to as BTEX (Benzene, Toluene, Ethyl-benzene and Xylenes), while the aromatic compounds containing two or more benzene rings are referred to as polycyclic aromatic hydrocarbons, or PAHs (Fingas 2011). By selecting these compounds, concentration maps can be generated in the software for each compounds, or a selected group of compounds, as shown in Fig. 4.30. A complete analysis of the concentrations per compound or compound group has not been executed for the current work.

a) b)

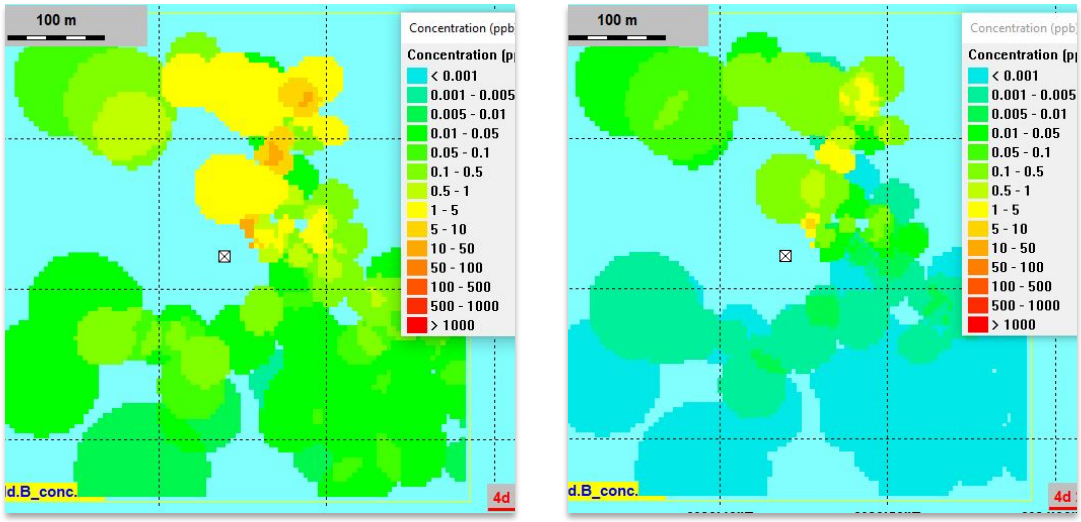

Fig. 4.30 Maximum concentration maps for a) all compounds, b) naphtalenes at a random time t. Maps show an aerial view, color codes represent the vertical layer with highest concentrations.

The aromatic hydrocarbons range from the monocyclic benzene with molecular weight of 78 to the nine ring compounds, with molecular weight up to 478. Paired with this, the different compounds' physical and chemical properties varies, such as aqueous solubility, vapor pressure, boiling point etc. Toxicity also varies from compound to compound, and may increase or decrease when mixed with other components. The simulation results are therefore a simplification if used to evaluate toxicity based on concentration data. In research, lots have been

published on these subjects, including the annual review of Mearns et al. (2017) summarizing more than 2000 journal articles and studies on the effects of pollution on marine organisms. These articles are often concerned with the specific effect on one marine organism in relation to a specific PAHs exposure, and to give an overview of benchmark concentrations would be impossible in the current work. Even though lots of work is being conducted in this area of research, there are still knowledge gaps regarding the toxic effects and long term consequences of PAH contamination (Pampanin and Sydnes 2017).

In other words, evaluating the specific consequences oil pollution pose for the environment, with all the associated biological responses, is beyond the scope of the current work. No simple answer to the initial question exists – of whether doing zero harm on our environment has to equal zero leaks. However, as this is an important question to provide answers for, it would be interesting if other, competent people of other disciplines would look into these types of simulations and analyses, such as marine biologists, toxicologists and other researchers interested in the ocean and the modeling of oil releases.

4.3.8 Environmental effects of oil in the sediments

As previously suggested by analysis of simulation results, oil may be persistent in the sediments for up to two years following even a short release, and in the case of leaking wells, a more or less constant deposition of oil hydrocarbons would be taking place on the seafloor sediments. Bioturbation, the turning and mixing of the sediments by marine life forms such as worms, mussels or bottom feeding fish, may cause the deposited oil components to mix further down into the sediment layers (Durgut et al. 2015). As described in the previous section, the potentially harmful effect on the environment is a function of the concentration in the sediments, and there are different estimates of the zones of biological effect. Patin (1999) suggested that no biological effect is detectable when the concentrations of the sum of hydrocarbons are below 10 mg/kg in bottom sediments in a dry sample, but for the same reasons mentioned in the last section, this benchmark value is not an accurate description of individual release scenarios. The composition on the oil and the fraction of the most toxic compounds are essential, but not addressed. Neither does it take into account the sensitivity of specific ecosystems or the variety of marine organisms.

The OSCAR model provides sediment concentration in the dynamic interface, where an "interrogate output" function is available. By clicking the map of the affected area, the concentration at that specific point can be found. One can also get the concentration along a line as a graph. Examples are given in Fig. 4.31.

a)

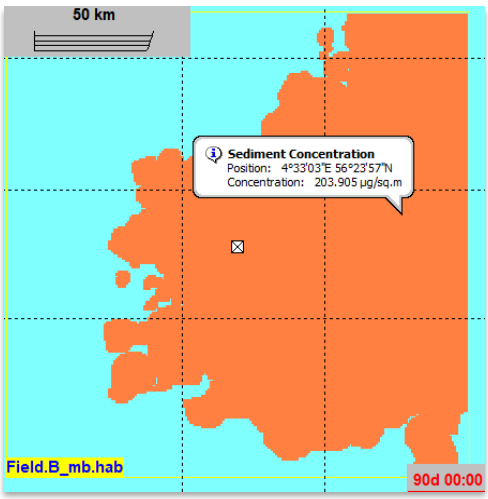

b)

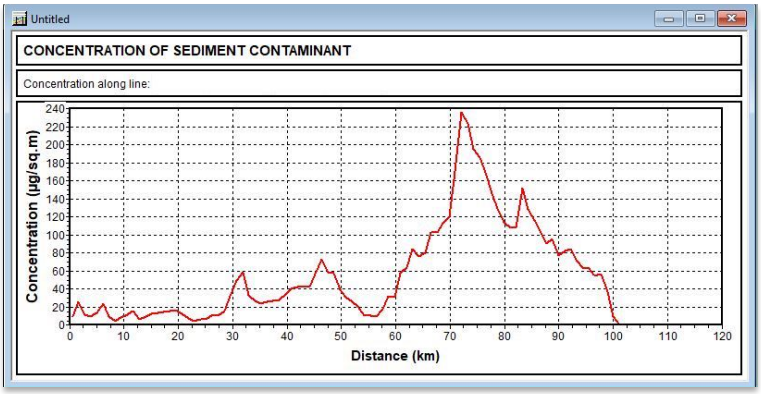

Fig. 4.31 Sediment concentrations. a) Concentration at random point. b) Concentration eastwards from the well.

The 90-day simulations in winter gave maximum concentrations of oil deposited on sediments at nearly 240 μg/m^2, as depicted in Fig. 4.31b. The maximum concentration was found at a point 72 km eastwards from the release point. To convert this to mg/kg of dry sediment, information about specific weight of both the sediments and the deposited oil is needed, in addition to the mixing depth of the deposited oil in the sediments, and these calculations have not been executed for the current work. Ideally, concentrations and depth of oil in the sediments should be confirmed by sediment samples to evaluate environmental effects (Durgut et al. 2015). The concentration data presented are just the results from simulations spanning over 90 days, and thus the ultimate concentrations can be expected to increase with time in the case of constant leaking wells. In a long-time perspective, equilibrium between the deposition of oil on the sediments and the biodegradations rates may form, giving some constant concentration values, but this has not been further investigated for the current work.

The software can also provide maps of sediment deposition by different components. Examples are given in Fig. 4.32, and as is visible, and consistent with theory, the heavier oil compounds are more likely to be deposited on the seafloor sediments. Note that in these figures, oil compounds are grouped by their carbon number, and thus includes both saturates and aromatics. The grid size is 200 km × 200 km, and it is evident that the boundaries of sediment deposition will extend even further in North and East directions, which thus appear to be the directions of the strongest currents in the area.

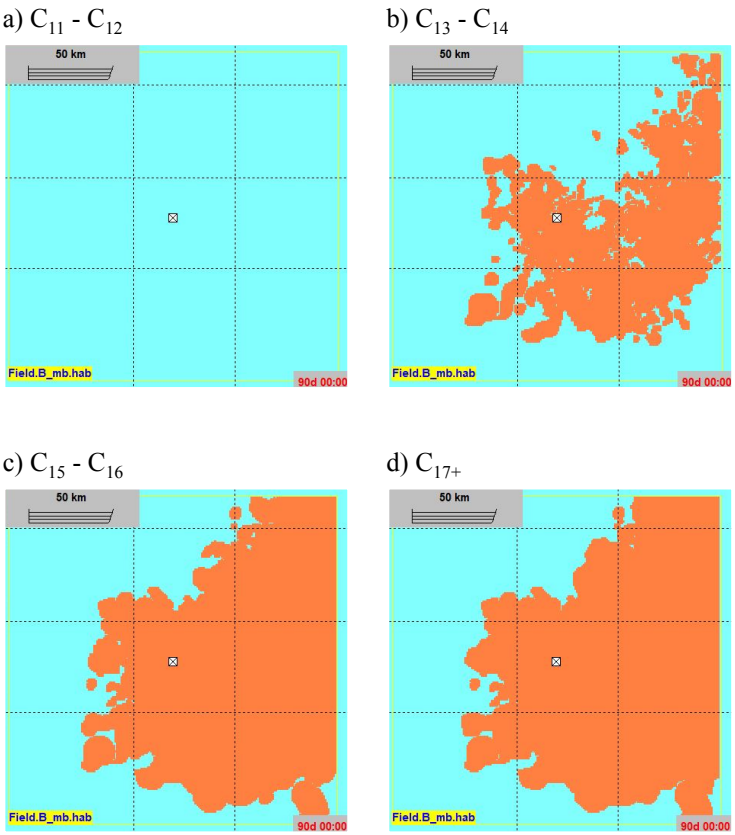

Fig. 4.32 Sediment deposition of different oil compounds grouped by carbon numbers. The solid, orange color representing the deposition shows that the concentrations are kept below 0.0001 kg/m^2, or 10^5 µg/m^2, as defined by the software.

Even though all of the oil in the sediments might eventually be biodegraded, the threat of the toxic compounds is not necessarily removed from the environment. PAHs and other hydrocarbons degraded or consumed by microorganisms might accumulate in these organisms, and as these are part of a larger scale food chain in the ocean, the toxins might affect other species as well (Patin 1999). Hydrocarbons in general are not soluble in water, and therefore they tend to be stored in lipid rich tissue, thus being able to accumulate in the food chain (Pampanin and Sydnes 2017). As some of these substances can be toxic to humans, regulators such as the European Union (EU) have created regulations on maximum permissible levels of PAHs and

other hydrocarbons in for instance shell fish and fish meat, to eliminate the risk to human health from the consumption of contaminated foods (European Commission (EC) 2016).

There are large uncertainties concerning the long-term toxic effect of oil in the sediments. However, in their extensive report on inputs, fates and effects of oil in the sea, National Research Council (U.S.) (2003) summarizes some of the research done in heavy seep areas offshore California and in the Gulf of Mexico, and suggests that even though the input from seeps are really large in these areas, ecological impacts appear to be limited. Even though one would expect significant impact to marine organisms, several studies claim that due to the slow and steady rate of release, marine organisms are able to acclimate to PAHs and other toxic compounds in the releases, specifically by the growth of benthic communities able to utilize some of the hydrocarbons. Again, this shows that it is not possible to provide simple answers to the question of quantifying potentially harmful effects following a leaking well, and that these issues should be further researched by competent people within other disciplines than petroleum engineering.

4.4 Acceptable leak rates?

Currently, there are permanently abandoned wells on the NCS with proven, active gas leakage, which might not be surprising due to the tricky nature of permanent plugging and abandonment of wells (Vielstädte et al. 2015). It is also very likely that there could be a number of wells leaking that are going under our radar (Vielstädte et al. 2017). Even so, the Norwegian recommended well integrity standard requires zero leak acceptance criteria, and does not provide any guidance or mentioning of risk analysis in the case of a leaking well. Neither does it require monitoring or additional verification after PP&A (NORSOK D-010 2013). It could therefore be possible that the standard is describing an ideal, and may not be in accordance with the real-life challenges the industry is facing in regards to PP&A. On one hand, the question arises of whether it could be possible to establish an acceptable leak rate for abandoned wells, in order to address the actual risk of leaks. On the other hand, there are a lot of foreign countries and companies looking to the Norwegian well integrity standard for guidance, as it is considered to be amongst the best, and

establishing an acceptable leak rate might be sending the wrong message about the goals and philosophy of PP&A.

The goal of PP&A is to maintain well integrity in an eternal perspective. Therefore, establishing an acceptable leak rate that could be applied to every single well subject to PP&A, eventually more than 11,000 wells in the North Sea, could be practically irresponsible. The results presented in the current work are the results of single wells leaking, and the bigger picture would look a lot different if there were 11,000 wells leaking at once. Still, how to proceed in the case of a leaking well is still unclear. As the tendency in society is to move towards risk-based approaches, one might think that the risks involved with leaks should be addressed in a well integrity standard.

Based on the results presented in the current work, the case of oil and gas leaks should be distinguished from each other. The fate of leaking natural gas is easier to model than oil releases. Even though the fate of gas depends on the same, numerous factors as oil, the ultimate fate and possible consequences are easier to estimate. Also, gas leakage is already present on the NCS, both at natural seeps and in some, abandoned wells, so there exists data that can be used to estimate the impact. The fate of oil is more complex, and oil itself more toxic, and to introduce an acceptance for new, long-term pollution from leaking wells may affect the environment in ways not yet fully understood. Due to this unknown, and the fact that there is no proven oil seepage in the environment already, one should be more careful in the case of oil leaks.

Based on the results and discussion presented, it is evident that the possibly harmful consequences a gas or oil leak may pose for the environment are dependent on numerous factors. Toxicity in water and sediments are mainly controlled by the concentration data. As is shown, fate of leaking oil and gas is a multi-faceted problem, and depends on variables including, but not limited to, fluid composition, water depth, salinity and oxygen content, sensitivity of local release environment, marine life in the area, seasonal variations, size of emerging bubbles and droplets and leak rates. The establishment of an acceptable leak rate measured in volume per time, would not be able to take into account all of these factors, and it is therefore unlikely that establishment of such a leak rate will or could be done. However, by using the methodology presented in the

current work, is should be possible to evaluate the leak rate and associated consequences for individual cases, if the method and numbers presented are further investigated by competent people of relevant disciplines. This could again serve as a source of information in decision analysis, should a leak occur.

4.5 Implications of the work for PP&A

To execute PP&A, operators depend on well integrity standards to guide them, but the current situation provides them with little guidance in the case of leaking wells. It is believable that both operators and regulators would benefit from more research conducted on leaking wells. A strict, zero leak philosophy may hinder research and open discussion, and could be thought pointless unless there are defined measures to follow up this requirement. A well integrity standard should be able to guide the operators in all stages of a well's life, and in the current form, NORSOK D-010 (2013) does not reflect the challenges of the industry or provide proper knowledge and guidance in the case of leaking wells after PP&A. Perhaps the new edition of the standard could provide a methodology for assessing consequences of leaks, without actually opening for defining acceptable leak rates. Increased levels of monitoring after PP&A might provide more, useful data. It is believed that the fate analysis methodology presented in the current work could be an important tool in the case of a leak, and help with the ultimate goal of establishing known procedures and tools for decision making in the case of leaks from permanently abandoned wells.

CHAPTER 5

CONCLUSION

5.1 Gas leakage

In the case of a gas leak from a permanently abandoned well on the NCS:

- Simulations show that a very small amount of gas will reach the surface by bubble-mediated transport. For the modeled cases, ~95 – 99% of the gas released will be dissolved in the sea. This is consistent with data from natural gas seepages at the Tommeliten seepage area.
- The fraction of gas reaching the atmosphere increases with increasing bubble size, and it is larger in winter than in summer due to the formation of a strong thermocline in summer. The fraction of gas reaching the atmosphere is independent of leak rate for the modeled cases.
- Even though the fraction of gas reaching the atmosphere by bubble-mediated transport is low, the ultimate atmospheric transport might be higher due to methane being able to reach the atmosphere by diffusion from seawater on a long-term scale.
- Natural gas that reaches the atmosphere may contribute to local air pollution and global warming. Natural gas dissolved in the sea serve as a nutrient for marine life and may enrich the food chain. The degradation of natural gas by marine organisms may contribute to ocean acidification and oxygen depletion, as O_2 is utilized and CO_2 produced.
- Calculations show that the contribution from leaking wells compared to natural seepages is low.

5.2 Oil leakage

In the case of an oil leak from a permanently abandoned well on the NCS:

- The oil will be affected by the environment and fractionate. Ultimately, the released oil will either evaporate to the atmosphere, be biodegraded or be deposited on the seafloor

sediments. During constant leakage from a well, some oil may also be floating on surface or be suspended in the water as either emulsion, drops or dissolved oil.

- A typical mass balance result from the modeled cases shows that in short time after a release, approximately 17 – 34 % of oil evaporates, 39 – 49 % of oil is deposited in the sediments and 24 – 38 % of oil is biodegraded, mostly in the water column. Oil in the sediments will be subject to biodegradation on a longer time scale.
- Oil is very persistent in the environment. Oil in water may be carried over several hundred km by currents before being biodegraded or deposited on the seafloor.
- Biodegradation rates in the sediments are low, making oil persistent in the environment for up to several years after a release. Oil degraded by marine organisms may accumulate in the food chain. As there are no reported oil seeps on the NCS to compare to a leaking well, possible long-term effects of oil in the environment are not yet well understood.
- Toxicity of oil in water or the sediments is dependent on the concentrations of oil, and also the chemical composition and the relative concentration of the different compounds in either water or sediments.

5.3 Well integrity in permanently abandoned wells

On the NCS, the current revision of the well integrity standard NORSOK D-010 does not address the case of leaking wells. However, operators need guidelines and tools to use when dealing with possible leaks. Even if establishing acceptable leakage rates is not desired or possible, due to the numerous variables included in each analysis, defining a set procedure and methodology to evaluate the risk and possible effects of leaks could be useful. These sorts of evaluations could be based on the methods presented in the current work. This is also in line with the ongoing trend in the industry of moving towards risk-based approaches.

CHAPTER 6

SUGGESTIONS FOR FUTURE WORK

During the process of writing this thesis, several ideas for possible applications and further investigations have revealed themselves, some of which are listed here. They are listed with a hope that these will inspire others to continue the work in the future.

6.1 Calculate diffusion rates

As discussed, the software used for the current work calculates atmospheric transport of natural gas by bubble-mediated transport, and does not take into account the process of diffusion from the sea to the atmosphere. It is suggested to map the important variables and quantify the diffusion rates following leaking wells, in order to make a more complete fate analysis of gas leaks.

6.2 Well integrity in all life phases of a well

Well integrity is not only important in PP&A, but in all stages of a well's life. It is concluded that establishing acceptable leak rates in an eternal perspective is perhaps out of reach, but maybe leaks could be acceptable for shorter time periods. To evaluate leak rate and possible consequences during temporary abandonment or the production phase for instance, one could use the same methodology as presented in the current work.

6.3 Evaluate size of defect

In the case of a defect in a barrier, for instance a microannulus in a cement sheath, the size of defect will result in a certain effective permeability, as described by Nelson and Guillot (2006). If an acceptable leak rate could be established for a well in a particular phase, using Darcy's flow equations and solving for effective permeability, one might estimate the leak's correlating size of defect in the barrier. The size of defect will also be a factor in determining bubble sizes, and consequently the fate of the leak.

6.4 Design a new type of barrier to protect environment

The results presented in this thesis show that the fate of an oil or gas release depends greatly on bubble or droplet size. By evaluating the possible harmful effects of a release, and making an assumption of where the release will cause the least harm, a manipulation of the release could possibly help with minimizing the harmful effects. So – would it then be possible to create a new type of barrier or mechanical device to control the nature of the release, and thus protect the environment? Imagine a coastal area near a particularly populated beach, where rare birds or mammals reside. If an oil leak would occur and reach surface in such an area, it could cause severe impact on the local wildlife. In this case, the oil would perhaps cause less damage if dissolved and dispersed in the sea. The results of the simulations in this thesis show that smaller oil drops are less likely to emerge at surface and form oil slicks, and theory from natural seepages state that the size of the droplets are controlled by many factors, amongst them the nature of the sediment it passes through, its grain size and pore throat sizes. Therefore, it is suggested for future work to look into the possibilities of manipulating a leak, should a leak occur and be detected, perhaps by deploying some sort of dispersant medium or barrier, not in the form of possibly harmful chemicals.

6.5 Downhole Safety Valve

As of today, the Downhole Safety Valve (DHSV) is the only component with an acceptable leak rate defined in NORSOK D-010 (2013). In chapter 15 – "Well barrier elements acceptance tables", the recommended standard states that *"Acceptance of downhole safety valve tests shall meet the following ANSI/API RP 14B requirements:*

a) 0.42 Sm^3/min [900 scf/h] for gas;

b) 0.4 l/min [6.3 gal/hr] for liquid."

These values are considerable larger than the "worst case" scenarios presented in this work. An oil leak of 0.4 l/min, or 24 l/hr, equals 24 times our maximum leak rate of 1 l/hr. A gas leak of 0.42 Sm^3/min, or 25,200 l/hr is 210 times larger than the "worst case" scenario at Field A for 120 l/hr. So, it is suggested to comprehensively study the leak criteria for DHSVs as basis for studying possible leaks of permanently abandoned wells.

6.6 Run simulations at different fields

Field A and Field B are both located in areas with approximately 70 m water depth. As fate analysis of both oil and gas is dependent on their respective contact time with water, it would be interesting to do some simulations at deep-water fields. By comparing simulation results, environmental effects from leaks can be evaluated as function of water depth.

A suggestion for an interesting field to model is the oil field Njord, located in the Norwegian Sea at 330 m water depth. In 2016, production from the Njord field and its satellite field Hyme was temporarily shut down due to structural integrity issues in the floating steel platform unit, Njord A. Operator Equinor decided to launch an upgrading project called "Njord Future", and both the rig and storage vessel, Njord B, have been towed to land for restructuring. Production is expected to resume in late 2020, with ten new wells to be drilled and additional tiebacks from subsea satellite fields Bauge and Fenja to be connected. The remaining resources should be sufficient for maintaining production in the Njord area until 2032 (Offshore Technology 2017).

A total of 54 wells have been drilled since the discovery, including exploration wells (NPD 2018a). While the field is waiting for the work on the rig and ship to be finished, all wells have been temporarily abandoned. If we look back at the PSA's chart over integrity issues in temporary abandoned wells in Fig. 1.5, it could be interesting to hypothesize over and investigate the fate of a leak in this field.

REFERENCES

Aguilar, P., Johnson, C.R., Salazar, J. et al. 2016. Plug and Abandonment Solution for Oilfield Decommissioning in the North Sea. Presented at the SPE Bergen One Day Seminar, Bergen, Norway, 20 April. SPE-180040-MS. https://doi.org/10.2118/180040-MS.

Audunson, T. 1980. The fate and weathering of surface oil from the bravo blowout. *Marine Environmental Research* **3** (1): 35-61. https://doi.org/10.1016/0141-1136(80)90034-3.

Barclay, I., Pellenberg, J., Tettero, F. et al. 2001. The beginning of the end: A review of abandonment and decommissioning practices. *Oilfield Review* **13** (4): 28-41.

Bennett, J. 2018. Ocean Acidification. The Ocean Portal Team, http://ocean.si.edu/ocean-acidification (downloaded 12 May 2018)

Bernard, B.B., Brooks, J.M., and Sackett, W.M. 1978. Light hydrocarbons in recent Texas continental shelf and slope sediments. *Journal of Geophysical Research: Oceans* **83** (C8): 4053-4061. https://doi.org/10.1029/JC083iC08p04053.

Beyer, J., Trannum, H.C., Bakke, T. et al. 2016. Environmental effects of the Deepwater Horizon oil spill: A review. *Marine Pollution Bulletin* **110** (1): 28-51. https://doi.org/10.1016/j.marpolbul.2016.06.027.

Biastoch, A., Treude, T., Rüpke, L.H. et al. 2011. Rising Arctic Ocean temperatures cause gas hydrate destabilization and ocean acidification. *Geophysical Research Letters* **38** (8): 1-5. https://doi.org/10.1029/2011GL047222.

Brakstad, O.G., Nordtug, T., and Throne-Holst, M. 2015. Biodegradation of dispersed Macondo oil in seawater at low temperature and different oil droplet sizes. *Marine Pollution Bulletin* **93** (1): 144-152. https://doi.org/10.1016/j.marpolbul.2015.02.006.

Brooks, J.M., Bernard, B.B., Sackett, W.M. et al. 1979. Natural Gas Seepage On The South Texas Shelf. Presented at the Offshore Technology Conference, Houston, Texas, April 30 - May 3. OTC-3411-MS. https://doi.org/10.4043/3411-MS.

Bünz, S., Polyanov, S., Vadakkepuliyambatta, S. et al. 2012. Active gas venting through hydrate-bearing sediments on the Vestnesa Ridge, offshore W-Svalbard. *Marine Geology* **332-334**: 189-197. https://doi.org/10.1016/j.margeo.2012.09.012.

Campbell, K. and Smith, R. 2013. Permanent Well Abandonment. *The Way Ahead* **9** (3): 25-27. SPE-0313-025-TWA. https://doi.org/10.2118/0313-025-TWA.

Carragher, P.J. and Fulks, J. 2018. Well Abandonment Solutions Utilizing Bismuth and Thermite. Presented at the Offshore Technology Conference, Houston, Texas, USA, 30 April - 3 May. OTC-28897-MS. https://doi.org/10.4043/28897-MS.

CGG Geoconsulting. 2015. Figure: Combined coverage of GLOGOS, FFD and FRogi Seeps, adding verification data to the Global Offshore Seepage Database, Seep-Explorer-and-GLOGOS

Chand, S., Rise, L., Dolan, M. et al. 2008. Active Venting System Offshore Northern Norway. *Eos, Transactions American Geophysical Union* **89** (29): 261-262. https://doi.org/10.1029/2008EO290001.

Clark, J.F., Leifer, I., Washburn, L. et al. 2003. Compositional changes in natural gas bubble plumes: observations from the Coal Oil Point marine hydrocarbon seep field. *Geo-Marine Letters* **23** (3): 187-193. https://doi.org/10.1007/s00367-003-0137-y.

DECOM North Sea. 2014. Decommissioning in the North Sea, Review of Decommissioning Capacity (October 2014).

Delabroy, L., Rodrigues, D., Norum, E. et al. 2017. Perforate, Wash and Cement PWC Verification Process and an Industry Standard for Barrier Acceptance Criteria. Presented at the SPE Bergen One Day Seminar, Bergen, Norway, 5 April. SPE-185938-MS. https://dx.doi.org/10.2118/185938-MS.

Diaz, M. 2017. Requirements for plug and abandonment of oil and gas wells - legislation and job design. Wellcem blog, job-design2 (downloaded 5 January 2018)

Doney, S.C., Fabry, V.J., Feely, R.A. et al. 2009. Ocean Acidification: The Other CO2 Problem. *Annual Review of Marine Science* **1** (1): 169-192. https://doi.org/10.1146/annurev.marine.010908.163834.

Durgut, İ., Rye, H., Reed, M. et al. 2015. Dynamic modeling of environmental risk associated with drilling discharges to marine sediments. *Marine Pollution Bulletin* **99** (1): 240-249. https://doi.org/10.1016/j.marpolbul.2015.07.019.

Eshraghi, D. 2012. Master thesis: P&A - status on regulations and technology, and identification of potential improvements. Retrieved from Brage.; http://hdl.handle.net/11250/183512.

Etiope, G. 2015. *Natural Gas Seepage*, 1. Switzerland: Springer International Publishing (Reprint).

European Commission (EC). 2016. Legislation on Polycyclic Aromatic Hydrocarbons (PAHs). EU Science Hub, https://ec.europa.eu/jrc/en/eurl/pahs/legislation (downloaded 01 June 2018)

Evans, G.W. and Carter, L.G. 1962. Bounding Studies of Cementing Compositions to Pipe and Formations. Presented at the Drilling and Production Practice, New York, New York, 1 January. API-62-072.

Farwell, C., Reddy, C.M., Peacock, E. et al. 2009. Weathering and the Fallout Plume of Heavy Oil from Strong Petroleum Seeps Near Coal Oil Point, CA. *Environmental Science & Technology* **43** (10): 3542-3548. https://doi.org/10.1021/es802586g.

Fingas, M. 2011. *Oil spill science and technology : prevention, response, and cleanup*. Burlington, Mass: Gulf Professional Publishing (Reprint).

Fingas, M. and Fieldhouse, B. 2004. Formation of water-in-oil emulsions and application to oil spill modelling. *Journal of Hazardous Materials* **107** (1): 37-50. https://doi.org/10.1016/j.jhazmat.2003.11.008.

Fronks, R.C. 2002. International Regulations - Meeting the Challenge. Presented at the SPE International Conference on Health, Safety and Environment in Oil and Gas Exploration and Production, Kuala Lumpur, Malaysia, 20-22 March. SPE-73879-MS. https://dx.doi.org/10.2118/73879-MS.

Garcia-Pineda, O., MacDonald, I., Silva, M. et al. 2016. Transience and persistence of natural hydrocarbon seepage in Mississippi Canyon, Gulf of Mexico. *Deep Sea Research Part II: Topical Studies in Oceanography* **129**: 119-129. https://doi.org/10.1016/j.dsr2.2015.05.011.

Geyer, R.A. and Sweet, W.E., Jr. 1972. Natural Hydrocarbon Seepage in the Gulf of Mexico. Presented at the SPE Symposium on Environmental Conservation, Lafayette, Louisiana, 13-14 November. SPE-4199-MS. https://doi.org/10.2118/4199-MS.

González-Tello, P., Camacho, F., Vicaria, J.M. et al. 2008. A modified Nukiyama–Tanasawa distribution function and a Rosin–Rammler model for the particle-size-distribution analysis. *Powder Technology* **186** (3): 278-281. https://doi.org/10.1016/j.powtec.2007.12.011.

Gundersen, J. 2016. Regulatory Updates - 2016. Presented at the Plug and Abandonment Forum (PAF) seminar, Sola, Norway, 19 October. https://norskoljeoggass.no/globalassets/dokumenter/drift/presentasjonerarrangementer/plug--abandonment-seminar-2016/02-regulatory-updates-psa.pdf.

Gundersen, J. 2017. Regulatory «Updates». Presented at the Plug and Abandonment Forum (PAF) seminar, Sola, Norway, 18 October. https://norskoljeoggass.no/globalassets/dokumenter/drift/presentasjonerarrangementer/plug--abandonment-seminar-2017/04-regulatory-updates---johnny-gundersen-psa-20171022192327.pdf.

HI. 2005. Photograph: Los Angeles skyline seen through smog on I-10 westbound near the I-5 interchange, taken 3 July 2005, https://commons.wikimedia.org/wiki/File:Img0253Los_Angeles_Smog.JPG

Hill, C. 2006. Photograph: Eternal Fire of Baba Gurgur, Kirkuk, Iraq, taken March 2006, https://commons.wikimedia.org/wiki/File:Eternal_Fire_of_Baba_Gurgur,_Kirkuk,_Iraq_-_P3110004.jpg - /media/File:P3110004.jpg

Hornafius, J.S., Quigley, D., and Luyendyk, B.P. 1999. The world's most spectacular marine hydrocarbon seeps (Coal Oil Point, Santa Barbara Channel, California): Quantification of emissions. *Journal of Geophysical Research: Oceans* **104** (C9): 20703-20711. https://doi.org/10.1029/1999JC900148.

Hovland, M. 1988. *Seabed pockmarks and seepages : impact on geology, biology and the marine environment*. London: Graham & Trotman (Reprint).

Hovland, M. 2007. Discovery of prolific natural methane seeps at Gullfaks, northern North Sea. *Geo-Marine Letters* **27** (2): 197-201. https://doi.org/10.1007/s00367-007-0070-6.

Hovland, M. 2008. Deep-water Coral Reefs : Unique Biodiversity Hot-Spots. In. Chichester, UK: Springer Netherlands.

Hovland, M., Jensen, S., and Fichler, C. 2012. Methane and minor oil macro-seep systems — Their complexity and environmental significance. *Marine Geology* **332-334**: 163-173. https://doi.org/10.1016/j.margeo.2012.02.014.

Hovland, M. and Sommerville, J.H. 1985. Characteristics of two natural gas seepages in the North Sea. *Marine and Petroleum Geology* **2** (4): 319-326. https://doi.org/10.1016/0264-8172(85)90027-3.

IEA GHG. 2009. IEA Greenhouse Gas R&D Programme, Long Term Integrity of CO2 Storage – Well Abandonment. Report No. 2009/08, Ch. 5 - Well abandonment regulations (July 2009).

Johansen, C., Todd, A.C., and MacDonald, I.R. 2017. Time series video analysis of bubble release processes at natural hydrocarbon seeps in the Northern Gulf of Mexico. *Marine and Petroleum Geology* **82**: 21-34. https://doi.org/10.1016/j.marpetgeo.2017.01.014.

Johansen, Ø. 2000. DeepBlow – a Lagrangian Plume Model for Deep Water Blowouts. *Spill Science and Technology Bulletin* **6** (2): 103-111. https://dx.doi.org/10.1016/S1353-2561(00)00042-6.

Judd, A. 2004. Natural seabed gas seeps as sources of atmospheric methane. *Environmental Geology* **46** (8): 988-996. https://doi.org/10.1007/s00254-004-1083-3.

Judd, A. and Hovland, M. 2007. *Seabed fluid flow: the impact on geology, biology, and the marine environment*. Cambridge: Cambridge University Press (Reprint).

Khalifeh, M. 2017. Lecture for course in Plug and Abandonment [powerpoint presentation].

Khalifeh, M., Gardner, D., and Haddad, M.Y. 2017. Technology Trends in Cement Job Evaluation Using Logging Tools. Presented at the Abu Dhabi International Petroleum Exhibition & Conference, Abu Dhabi, UAE, 13-16 November. SPE-188274-MS. https://doi.org/10.2118/188274-MS.

Khalifeh, M., Hodne, H., Saasen, A. et al. 2018. Bond Strength Between Different Casing Materials and Cement. Presented at the SPE Norway One Day Seminar, Bergen, Norway, 18 April. SPE-191322-MS. https://doi.org/10.2118/191322-MS.

Khalifeh, M., Hodne, H., Saasen, A. et al. 2013. Techniques and Materials for North Sea Plug and Abandonment Operations. Presented at the Offshore Technology Conference, Houston, Texas, USA, 6-9 May. OTC-23915-MS. https://doi.org/10.4043/23915-MS.

Kvenvolden, K.A. and Cooper, C.K. 2003. Natural seepage of crude oil into the marine environment. *Geo-Marine Letters* **23** (3-4): 140-146. https://doi.org/10.1007/s00367-003-0135-0.

Leifer, I. and Boles, J. 2005. Measurement of marine hydrocarbon seep flow through fractured rock and unconsolidated sediment. *Marine and Petroleum Geology* **22** (4): 551-568. https://doi.org/10.1016/j.marpetgeo.2004.10.026.

Leifer, I., Boles, J.R., Luyendyk, B.P. et al. 2004. Transient discharges from marine hydrocarbon seeps: spatial and temporal variability. *Environmental Geology* **46** (8): 1038-1052. https://doi.org/10.1007/s00254-004-1091-3.

Leifer, I. and Culling, D. 2010. Formation of seep bubble plumes in the Coal Oil Point seep field. *Geo-Marine Letters* **30** (3): 339-353. https://doi.org/10.1007/s00367-010-0187-x.

Leifer, I. and MacDonald, I. 2003. Dynamics of the gas flux from shallow gas hydrate deposits: interaction between oily hydrate bubbles and the oceanic environment. *Earth and Planetary Science Letters* **210** (3): 411-424. https://doi.org/10.1016/S0012-821X(03)00173-0.

Leifer, I. and Patro, R.K. 2002. The bubble mechanism for methane transport from the shallow sea bed to the surface: A review and sensitivity study. *Continental Shelf Research* **22** (16): 2409-2428. https://doi.org/10.1016/S0278-4343(02)00065-1.

Lende, G. 2012. Advances in cementing technology for permanent P&A, Halliburton. Presented at the Plug and Abandonment Forum (PAF) seminar, Sola, Norway, 14. June. https://www.norskoljeoggass.no/drift/presentasjonerarrangementer/plug--abandonment-seminar-2012/.

Li, P., Cai, Q., Lin, W. et al. 2016. Offshore oil spill response practices and emerging challenges. *Marine Pollution Bulletin* **110** (1): 6-27. https://doi.org/10.1016/j.marpolbul.2016.06.020.

Lindo-Atichati, D., Paris, C.B., Le Hénaff, M. et al. 2016. Simulating the effects of droplet size, high-pressure biodegradation, and variable flow rate on the subsea evolution of deep plumes from the Macondo blowout. *Deep Sea Research Part II: Topical Studies in Oceanography* **129**: 301-310. https://doi.org/10.1016/j.dsr2.2014.01.011.

Link, W.K. 1952. Significance of Oil and Gas Seeps in World Oil Exploration. *AAPG Bulletin* **36** (8): 1505-1540.

Liversidge, D., Taoutaou, S., and Agarwal, S. 2006. Permanent Plug and Abandonment Solution for the North Sea. Presented at the SPE Asia Pacific Oil & Gas Conference and Exhibition, Adelaide, Australia, 11-13 September. SPE-100771-MS. https://doi.org/10.2118/100771-MS.

Lldenke. 2000. Photograph: McKittrick tar seep north of Highway 58, taken 1 May 2000, https://commons.wikimedia.org/wiki/File:McKittrick_Tar_Seep_North_of_Highway_58.jpg

Logan, G.A., Jones, A.T., Kennard, J.M. et al. 2010. Australian offshore natural hydrocarbon seepage studies, a review and re-evaluation. *Marine and Petroleum Geology* **27** (1): 26-45. https://doi.org/10.1016/j.marpetgeo.2009.07.002.

MacDonald, I.R., Leifer, I., Sassen, R. et al. 2002. Transfer of hydrocarbons from natural seeps to the water column and atmosphere. *Geofluids* **2** (2): 95-107. https://doi.org/10.1046/j.1468-8123.2002.00023.x.

Mainguy, M., Longuemare, P., Audibert, A. et al. 2007. Analyzing the Risk of Well Plug Failure after Abandonment. *Oil & Gas Science and Technology - Rev. IFP* **62** (3): 311-324. https://doi.org/10.2516/ogst:2007026.

McGinnis, D.F., Greinert, J., Artemov, Y. et al. 2006. Fate of rising methane bubbles in stratified waters: How much methane reaches the atmosphere? *Journal of Geophysical Research: Oceans* **111** (9): 1-15. https://doi.org/10.1029/2005JC003183.

Mearns, A.J., Reish, D.J., Oshida, P.S. et al. 2017. Effects of Pollution on Marine Organisms. *Water Environment Research* **89** (10): 1704-1798. https://doi.org/10.2175/106143017X15023776270647.

Meteorologisk Institutt. 2018a. Catalog http://thredds.met.no/thredds/catalog.html

Meteorologisk Institutt. 2018b. eKlima Gratis tilgang til Meteorologisk institutts vær- og klimadata fra historiske data til sanntidsobservasjoner, http://sharki.oslo.dnmi.no/portal/page?_pageid=73,39035,73_39049&_dad=portal&_schema=PORTAL

Mikolaj, P.G., Allen, A.A., and Schlueter, R.S. 1972. Investigation of the Nature, Extent and Fate of Natural Oil Seepage Off Southern California. Presented at the Offshore Technology Conference, Houston, Texas, May 1-3. OTC-1549-MS. https://doi.org/10.4043/1549-MS.

Ministry of Petroleum and Energy. 2013. Norway's oil history in 5 minutes. Regjeringen, https://www.regjeringen.no/en/topics/energy/oil-and-gas/norways-oil-history-in-5-minutes/id440538/ (downloaded 22 January 2018)

Mohammedyasin, S.M., Lippard, S.J., Omosanya, K.O. et al. 2016. Deep-seated faults and hydrocarbon leakage in the Snøhvit Gas Field, Hammerfest Basin, Southwestern Barents Sea. *Marine and Petroleum Geology* **77**: 160-178. https://doi.org/10.1016/j.marpetgeo.2016.06.011.

Musat, F. 2015. The anaerobic degradation of gaseous, nonmethane alkanes — From in situ processes to microorganisms. *Computational and Structural Biotechnology Journal* **13** (2015): 222-228. https://doi.org/10.1016/j.csbj.2015.03.002.

Myrseth, V., Perez-Valdes, G.A., Bakker, S.J. et al. 2017. Development of a Norwegian Open-Source Plug-and-Abandonment Database With Applications. *SPE Economics and Management* **9** (1): 27-31. SPE-180027-PA. https://doi.org/10.2118/180027-PA.

National Research Council (U.S.). 2003. *Oil in the sea III : inputs, fates, and effects*. Washington, D.C: National Academy Press (Reprint).

Nelson, E.B. and Guillot, D. 2006. *Well cementing*, 2nd edition. Sugar Land, Texas, USA: Schlumberger (Reprint).

Newcomb Jr., W.W. 2002. *The Indians of Texas: From Prehistoric to Modern Times*. Austin, Texas: University of Texas Press (Reprint).

Niemann, H., Elvert, M., Hovland, M. et al. 2005. Methane emission and consumption at a North Sea gas seep (Tommeliten area). *Biogeosciences* **2** (4): 335-351. https://doi.org/10.5194/bg-2-335-2005.

Nissanka, I.D. and Yapa, P.D. 2017. Oil slicks on water surface: Breakup, coalescence, and droplet formation under breaking waves. *Marine Pollution Bulletin* **114** (1): 480-493.

https://doi.org/10.1016/j.marpolbul.2016.10.006.
Nordsøfonden. 2018. Danish oil and gas history, http://www.nordsoefonden.dk/en/danish-oil-and-gas-history (downloaded 22 January 2018)
NORSOK Standard D-010, Well integrity in drilling and well operations. Rev. 4. 2013. Lysaker, Norway: Standards Norway.
NOAA Okeanos Explorer Program. 2012. Photo album: Deep Sea - Cold Seep Communities, Methane Seeps, and Oil Seeps. Photos from NOAA Okeanos Explorer Program, Gulf of Mexico 2012., https://www.flickr.com/photos/noaaphotolib/albums/72157638854547964
NOAA Okeanos Explorer Program. 2013. Photo album: Deep Sea - Cold Seep Communities, Methane Seeps, and Oil Seeps. Photo from NOAA Okeanos Explorer Program, 2013 ROV Shakedown and Field Trials, https://www.flickr.com/photos/noaaphotolib/albums/72157638854547964
NPD. 2018a. Factpages - Njord. Norwegian Petroleum Directorate, http://factpages.npd.no/factpages/Default.aspx?culture=no (downloaded 9 April 2018)
NPD. 2018b. Factpages - Valhall. Norwegian Petroleum Directorate, http://factpages.npd.no/factpages/Default.aspx?culture=no (downloaded 10 April 2018)
OE Staff. 2017. BiSN completes Valhall P&A. Offshore Engineer, http://www.oedigital.com/subsea/item/16174-bisn-completes-valhall-p-a (downloaded 13 April 2018)
Offshore Technology. 2017. Njord Future Project, Norwegian Sea. Offshore Technology, https://www.offshore-technology.com/projects/njord-future-project-norwegian-sea/ (downloaded 8 April 2018)
Oil & Gas UK, Guidelines for the suspension and abandonment of wells. Issue 4. 2012a. Great Britain: The UK Offshore Oil and Gas Industry Association Limited.
Oil & Gas UK, Guidelines on qualification of materials for the suspension and abandonment of wells. Issue 1. 2012b. Great Britain: The UK Offshore Oil and Gas Industry Association Limited.
Olsen, J.E., Dunnebier, D., Davies, E. et al. 2017. Mass transfer between bubbles and seawater. *Chemical Engineering Science* **161**: 308-315. https://doi.org/10.1016/j.ces.2016.12.047.
Ottøy, M.H. 2017. Cost effective P&A - Technology needs. Presented at the Plug and Abandonment Forum (PAF) seminar, Sola, Norway, 12 October. https://norskoljeoggass.no/globalassets/dokumenter/drift/presentasjonerarrangementer/plug--abandonment-seminar-2017/03-cost-effective-p-and-a--technology-needs---mette-halvorsen-ottoy-statoil.pdf.
Pampanin, D.M. and Sydnes, M.O. 2017. *Petrogenic polycyclic aromatic hydrocarbons in the aquatic environment : analysis, synthesis, toxicity and environmental impact*. Sharjah, U.A.E: Bentham Science Publishers (Reprint).
Patin, S. 1999. *Environmental impact of the offshore oil and gas industry*. New York: EcoMonitor Publishing (Reprint).
Pohlmann, T. 1996. Calculating the annual cycle of the vertical eddy viscosity in the North Sea with a three-dimensional baroclinic shelf sea circulation model. *Continental Shelf Research* **16** (2): 147-161. https://doi.org/10.1016/0278-4343(94)E0037-M.
Reeburgh, W.S. 2007. Oceanic Methane Biogeochemistry. *Chemical Reviews* **107** (2): 486-513. https://doi.org/10.1021/cr050362v.
Riazi, M.R. and Roomi, Y.A. 2008. A Model to Predict Rate of Dissolution of Toxic Compounds into Seawater from an Oil Spill. *International Journal of Toxicology* **27** (5): 379-386. https://doi.org/10.1080/10915810802503578.
Salehi, S., Khattak, M.J., Ali, N. et al. 2016. Development of Geopolymer-based Cement Slurries with Enhanced Thickening Time, Compressive and Shear Bond Strength and Durability. Presented at the IADC/SPE Drilling Conference and Exhibition, Fort Worth, Texas, USA, 1-3 March. SPE-178793-MS.

https://doi.org/10.2118/178793-MS.
Schlumberger. 2017. Figure: Potential leak paths, including channeling, microannuli, and mudcake occur due to poorly executed cementing operations, https://www.offshore-mag.com/articles/print/volume-77/issue-5/engineering-construction-installation/integrated-milling-underreaming-approach-streamlines-p-a-operations-in-the-north-sea.html
Schneider von Deimling, J., Rehder, G., Greinert, J. et al. 2011. Quantification of seep-related methane gas emissions at Tommeliten, North Sea. *Continental Shelf Research* **31** (7): 867-878. https://doi.org/10.1016/j.csr.2011.02.012.
Schoell, M. 1980. The hydrogen and carbon isotopic composition of methane from natural gases of various origins. *Geochimica et Cosmochimica Acta* **44** (5): 649-661. https://doi.org/10.1016/0016-7037(80)90155-6.
Schwall, G.H. and Denney, C.A. 1994. Subsidence induced casing deformation mechanisms in the Ekofisk field. Presented at the Rock Mechanics in Petroleum Engineering, Delft, Netherlands, 29-31 August. SPE-28091-MS. https://doi.org/10.2118/28091-MS.
Shennan Jean, L. 2005. Utilisation of C2–C4 gaseous hydrocarbons and isoprene by microorganisms. *Journal of Chemical Technology & Biotechnology* **81** (3): 237-256. https://doi.org/10.1002/jctb.1388.
SINTEF. 2017. SINTEF MEMW (Marine Environmental Modeling Workbench) User's Manual, Version 9.0.0 (8 June 2017).
Skjold, M. 2017. Update alternative P&A barrier, Interwell. Presented at the Plug and Abandonment Forum (PAF) seminar, Sola, Norway, 18 October. https://www.norskoljeoggass.no/drift/presentasjonerarrangementer/plug--abandonment-seminar-2017/.
Smith, I., Olstad, D., and Segura, R. 2011. Heightened regulations create demand for well abandonment services. *Offshore* **71** (10): 70-73.
Solomon, E.A., Kastner, M., MacDonald, I.R. et al. 2009. Considerable methane fluxes to the atmosphere from hydrocarbon seeps in the Gulf of Mexico. *Nature Geoscience* **2**: 561. https://doi.org/10.1038/ngeo574.
SOS California. 2018. Natural Oil Seepage Facts. Stop Oil Seeps California, http://www.soscalifornia.org/natural-oil-seepage-facts/ (downloaded 25 May 2018)
Stolper, D.A., Lawson, M., Formolo, M.J. et al. 2018. The utility of methane clumped isotopes to constrain the origins of methane in natural gas accumulations. *Geological Society, London, Special Publications* **468** (1): 23. https://doi.org/10.1144/SP468.3.
Straume, M. 2012. Valhall P&A Challenges. Presented at the Plug and Abandonment Forum (PAF) seminar, Sola, Norway, 14 June. https://www.norskoljeoggass.no/drift/presentasjonerarrangementer/plug--abandonment-seminar-2012/.
Thiercelin, M.J., Dargaud, B., Baret, J.F. et al. 1998. Cement Design Based on Cement Mechanical Response. https://doi.org/10.2118/52890-PA.
Thomson, I. 2018. Successful Creation of Permanent Reservoir Isolation Barriers Using Coiled Tubing on the Norwegian Continental Shelf NCS. Presented at the SPE/ICoTA Coiled Tubing and Well Intervention Conference and Exhibition, The Woodlands, Texas, USA, 27-28 March. SPE-189956-MS. https://doi.org/10.2118/189956-MS.
Tissot, B.P. and Welte, D.H. 1984. *Petroleum formation and occurrence*, 2nd rev. and enlarged ed. Berlin: Springer (Reprint).
Tveit, M.R. 2018. Weathered oil found on Port Aransas Beach, Texas, in April 2018.

University of Aberdeen. 2006. The Project: Brief History of the UK North Sea Oil and Gas Industry. Department of history, https://www.abdn.ac.uk/oillives/about/nsoghist.shtml (downloaded 22 January 2018)

US Geological Survey. 2008. Tar from natural seeps floating in the ocean offshore Point Conception, California, https://soundwaves.usgs.gov/2008/04/fieldwork2.html

Vielstädte, L., Haeckel, M., Karstens, J. et al. 2017. Shallow Gas Migration along Hydrocarbon Wells–An Unconsidered, Anthropogenic Source of Biogenic Methane in the North Sea. *Environmental Science & Technology* **51** (17): 10262-10268. https://doi.org/10.1021/acs.est.7b02732.

Vielstädte, L., Karstens, J., Haeckel, M. et al. 2015. Quantification of methane emissions at abandoned gas wells in the Central North Sea. *Marine and Petroleum Geology* **68** (Part B): 848-860. https://doi.org/10.1016/j.marpetgeo.2015.07.030.

Vignes, B. 2011. Qualification Of Well Barrier Elements - Long-Term Integrity Test, Test Medium And Temperatures. Presented at the SPE European Health, Safety and Environmental Conference in Oil and Gas Exploration and Production, Vienna, Austria, 22-24 February. SPE-138465-MS. https://doi.org/10.2118/138465-MS.

Wang, B. and Socolofsky, S.A. 2015. A deep-sea, high-speed, stereoscopic imaging system for in situ measurement of natural seep bubble and droplet characteristics. *Deep Sea Research Part I: Oceanographic Research Papers* **104**: 134-148. https://doi.org/10.1016/j.dsr.2015.08.001.

Washburn, L., Clark, J.F., and Kyriakidis, P. 2005. The spatial scales, distribution, and intensity of natural marine hydrocarbon seeps near Coal Oil Point, California. *Marine and Petroleum Geology* **22** (4): 569-578. https://doi.org/10.1016/j.marpetgeo.2004.08.006.

WHOI. 2014. Image : Natural Oil Seeps, Illustration by Jack Cook, http://www.whoi.edu/oilinocean/page.do?pid=51880&tid=441&cid=139413&ct=61&article=97109

Wikimedia Commons. 2014. Thermocline Season Depth, https://commons.wikimedia.org/wiki/File:ThermoclineSeasonDepth.png - /media/File:ThermoclineSeasonDepth.png

Williams, S.M., Carlsen, T., Constable, K.C. et al. 2009. Identification and Qualification of Shale Annular Barriers Using Wireline Logs During Plug and Abandonment Operations. Presented at the SPE/IADC Drilling Conference and Exhibition, Amsterdam, The Netherlands, 17-19 March. SPE-119321-MS. https://doi.org/10.2118/119321-MS.

Yvon-Durocher, G., Allen, A.P., Bastviken, D. et al. 2014. Methane fluxes show consistent temperature dependence across microbial to ecosystem scales. *Nature* **507**: 488-491. https://doi.org/10.1038/nature13164.

APPENDIX A – FIELD A TEMPERATURE DATA

	Jan	Feb	Mar	Apr	May	Jun	Jul	Aug	Sep	Oct	Nov	Dec
1980	-	-	-	6,6	9,2	12,3	-	14,2	13,3	9,8	7,3	6,4
1981	4,8	4,1	5,0	5,3	8,7	11,0	12,9	13,7	13,7	9,2	7,0	2,6
1982	3,3	4,0	5,1	5,7	7,6	12,3	14,1	15,3	12,9	11,3	8,5	6,5
1983	6,9	3,7	5,4	-	8,1	10,6	14,5	15,2	13,6	10,8	8,0	-
1984	4,6	4,3	3,5	5,7	-	11,2	13,3	15,6	-	11,6	9,2	7,4
1985	3,0	2,8	3,9	5,2	-	9,2	12,1	12,4	11,9	12,1	-	9,5
1986	-	-	3,9	4,4	8,6	11,3	14,3	-	12,1	11,0	8,4	6,6
1987	2,4	3,9	2,4	6,1	7,3	10,1	13,2	13,4	12,9	11,0	8,3	7,0
1988	6,2	5,7	4,8	5,7	9,1	11,8	14,8	14,3	13,2	10,2	7,8	7,3
1989	6,9	6,1	6,3	5,7	9,1	12,2	14,2	14,6	-	11,8	9,2	7,3
1990	7,3	6,9	7,6	7,3	10,5	12,0	13,8	15,2	12,8	11,1	8,4	6,7
1991	7,1	3,6	5,7	6,5	8,0	10,6	15,2	15,9	13,9	11,0	8,0	7,1
1992	6,0	6,2	6,1	6,6	10,2	14,2	14,7	15,1	13,5	9,3	7,8	6,3
1993	5,6	5,1	4,6	5,9	9,0	11,3	13,1	13,6	12,0	9,5	6,4	5,3
1994	5,4	2,7	4,9	-	8,0	10,9	16,2	15,4	12,7	-	9,3	7,3
1995	5,4	5,6	4,8	6,1	8,2	11,1	15,1	16,9	14,4	13,2	9,4	5,2
1996	3,6	2,5	2,3	4,5	6,5	10,5	12,9	15,9	13,5	11,7	7,2	5,0
1997	-	-	-	6,3	8,3	11,8	15,3	-	13,6	10,5	8,5	7,0
1998	6,2	7,1	5,9	6,0	9,7	11,9	12,9	-	13,2	10,0	7,2	6,8
1999	6,6	5,2	5,6	6,8	9,1	11,7	15,0	15,3	15,7	11,2	9,0	5,9
2000	6,6	6,0	5,7	6,4	9,6	11,2	12,2	14,7	13,9	11,5	8,4	6,6
2001	5,3	3,7	3,4	5,6	9,7	11,1	15,4	15,6	12,8	12,5	8,1	5,8
2002	6,6	6,0	5,8	7,0	9,8	13,3	14,6	17,9	15,0	10,0	8,3	5,4
2003	5,4	4,5	5,9	7,1	9,8	14,0	16,1	16,8	14,8	9,9	9,5	7,3
2004	5,7	-	5,9	7,7	9,4	-	13,9	17,0	-	8,4	7,5	-
2005	-	4,7	4,9	6,7	8,5	11,2	13,9	14,3	14,4	12,9	9,1	6,9
2006	5,7	5,2	3,1	6,1	9,4	11,6	17,1	16,5	15,9	13,6	9,5	8,4
2007	7,5	6,1	7,1	8,3	9,4	13,3	14,1	14,8	12,9	11,4	8,3	7,2
2008	6,8	6,4	5,1	6,7	11,0	12,9	14,7	15,3	14,2	10,4	7,9	6,2
2009	5,3	4,6	5,9	7,5	10,0	12,4	15,6	16,0	14,1	10,9	9,6	6,0
2010	2,7	2,8	5,2	6,6	8,3	12,0	15,0	15,1	13,3	10,7	6,1	3,4
2011	5,5	4,6	5,3	7,9	10,2	12,3	13,9	14,2	13,3	11,4	10,1	7,0
2012	6,3	5,0	6,9	6,1	8,8	10,9	13,6	15,6	13,1	9,8	8,5	5,3
2013	4,3	3,5	2,3	4,9	7,6	10,9	14,9	16,2	14,0	12,0	8,3	7,4
2014	-	6,6	6,9	8,0	10,2	-	16,5	15,0	14,5	12,3	9,7	7,0
2015	6,0	5,3	5,8	6,7	8,2	11,1	13,1	15,1	13,4	11,9	9,4	8,3
2016	5,3	5,2	5,7	6,1	9,7	12,4	14,8	14,9	15,9	11,3	7,5	8
2017	5,8	4,9	6,2	6,9	9,7	13	14,4	15,2	14	11,8	7,9	6,6
2018	5,7	3,5	3	-	-	-	-	-	-	-	-	-
Mean	5,52	4,80	5,08	6,35	9,01	11,71	14,36	15,21	13,67	11,05	8,34	6,55

APPENDIX B – PYTHON PROGRAMMING SCRIPTS

Code for making gas mass flux plots:

In [1]:
```
%matplotlib inline
import numpy as np
import matplotlib.pyplot as plt
plt.style.use('bmh')
import netCDF4 as nc
```

Open a netCDF data file

In [2]:
```
datafile = 'Field.A_W-16_2w_gas.nc'
d = nc.Dataset(datafile)
```

Inspect variables

In [3]:
```
for k, v in d.variables.items():
    print(k, v.dimensions)
```

```
latitude_longitude ()
longitude ('longitude',)
latitude ('latitude',)
time ('time',)
surface_gas_flux ('time', 'latitude', 'longitude')
surface_gas_void_fraction ('time', 'latitude', 'longitude')
longitude_bounds ('longitude', 'vertices')
latitude_bounds ('latitude', 'vertices')
bathymetry ('latitude', 'longitude')
```

In [4]:
```
print(d.variables['surface_gas_flux'].units)
```

```
g m-2 s-1
```

Plot concentration

In [5]:
```
# Use cell size from simulation
# this could also be calculated from longitudes and latitudes
cell_size = 2*2

times = d.variables['time'][:] / 3600 # Convert from seconds to hours
fluxes = np.sum(d.variables['surface_gas_flux'][:].filled(0.0), axis = (1, 2))
rates = fluxes * cell_size * 1e-3 # Convert to mass rate in kg

# Calculate release rate from Gas release data
# release rate in standard cubic meter per day times density
# divided by number of seconds in a day
# to get kg/s
release_rate = 0.168 * 0.69 / (3600*24)
print('Mean gas mass flux rate: ', np.mean(rates))
print('Release rate: ', release_rate)
print('Fraction of gas that reaches surface: ', np.mean(rates) / release_rate)

#Plot rate, and average
fig = plt.figure(figsize = (6, 4))
plt.plot(times, rates, label = 'Gase rate through surface')
plt.plot(times, np.ones(len(rates))*np.mean(rates), '--', label = 'Average gas rate through surface')
plt.xlabel('Time [h]')
plt.ylabel('Gas rate through surface [g/s]')
plt.legend()
plt.title('W-16, 200m x 200m, winter')
# Lagre figur
plt.tight_layout() # Denne fjerner unødvendig whitespace rundt figuren

plt.savefig('GasMassFlux_Field-A_W-16_2w.png', dpi = 240) # lagrer png i ganske høy oppløsning
# plt.savefig('filnavn.pdf') # pdf er vektorgrafikk, så her angir man ikke oppløsning
```

```
Mean gas mass flux rate:  3.87979e-09
Release rate:  1.3416666666666666e-06
Fraction of gas that reaches surface:  0.00289176848099
```

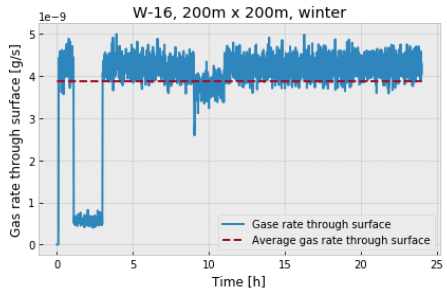

Code for analyzing mass balance results and plot them as function of time:

In [2]:
```
%matplotlib inline
import numpy as np
import matplotlib.pyplot as plt
plt.style.use('bmh')
import pandas as pd
from datetime import datetime
from collections import OrderedDict
```

In [3]:
```
namedict = {
        'outside(mt)'       : 'Outside',
        'atmosphere(mt)'    : 'Atmosphere',
        'surface(mt)'       : 'Surface',
        'submerged(mt)'     : 'Submerged',
        'biodegraded(mt)'   : 'Biodegraded',
        'stranded(mt)'      : 'Stranded',
        'sediment(mt)'      : 'Sediment',
        }

colordict = {
        'outside(mt)'       : '#FFAF59',
        'atmosphere(mt)'    : '#2C87BF',
        'surface(mt)'       : '#62C3A5',
        'submerged(mt)'     : '#AADEA2',
        'biodegraded(mt)'   : '#E6F693',
        'stranded(mt)'      : '#FFFFBC',
        'sediment(mt)'      : '#FFE185',
        }

names = [
    'outside(mt)' ,
    'atmosphere(mt)' ,
    'surface(mt)' ,
    'submerged(mt)' ,
    'biodegraded(mt)' ,
    'stranded(mt)' ,
    'sediment(mt)' ,
    ][::-1] # Flip order to get atmosphere at the top in the plot
```

```
def stackplot(df, xlabel = '', ylabel = '', normalise = False):
    fig = plt.figure(figsize = (10, 6))
    ax = fig.add_subplot(111)
    y0 = np.zeros(len(df))
    y1 = np.zeros(len(df))

    if normalise:
        df['total(mt)'] = df[names].sum(axis = 1)

    proxy_artists = []
    x = df['time(days)'].values
    for i, name in enumerate(names):
        y0[:] = y1[:]
        if normalise:
            y1[:] = df[name].divide(df['total(mt)']) + y0
        else:
            y1[:] = df[name].values + y0
        #Fill area with color
        c = colordict[name]
        ax.fill_between(x, y0, y1, color=c, alpha=1, linewidth=.5, label = name)

        #Proxy artist for labels/legend
        proxy_artists += [plt.Rectangle((0, 0), 1e-5, 1e-5, fc=c, label = name)]

    plt.legend(proxy_artists[::-1], [namedict[name] for name in names[::-1]], loc = 'upper left')
    plt.xlim(int(x[0]), int(x[-1]))
    plt.ylim(0, y1[-1])
    plt.xlabel(xlabel, fontsize = 15)
    plt.ylabel(ylabel, fontsize = 15)
    plt.tight_layout()
    return fig
```

In [4]:
```
dtofile = 'Vallhall_0.1year5z.dto'
df = pd.read_csv(dtofile)

df
```

Out[4]:

	time(days)	surface(mt)	atmosphere(mt)	submerged(mt)	sediment(mt)	cleaned(mt)	stranded(mt)	biodegraded(mt)	outside(mt)	total area(km2)	...	vol th. emul(m3)
0	0.0000	0.000000	0.000000	0.000000	0.000000e+00	0.0	0.0	0.000000	0.000000	0.000000	...	0.0
1	0.3333	0.000024	0.000095	0.000580	0.000000e+00	0.0	0.0	0.000008	0.000000	0.000027	...	0.0
2	0.6667	0.000045	0.000196	0.001143	0.000000e+00	0.0	0.0	0.000030	0.000000	0.000050	...	0.0
3	1.0000	0.000114	0.000325	0.001620	0.000000e+00	0.0	0.0	0.000063	0.000000	0.000125	...	0.0
4	1.3330	0.000102	0.000471	0.002151	0.000000e+00	0.0	0.0	0.000105	0.000000	0.000110	...	0.0
5	1.6670	0.000047	0.000594	0.002738	0.000000e+00	0.0	0.0	0.000156	0.000000	0.000052	...	0.0
6	2.0000	0.000055	0.000703	0.003268	0.000000e+00	0.0	0.0	0.000217	0.000000	0.000061	...	0.0
7	2.3330	0.000058	0.000815	0.003791	2.006000e-08	0.0	0.0	0.000286	0.000000	0.000064	...	0.0
8	2.6670	0.000057	0.000928	0.004308	2.368000e-07	0.0	0.0	0.000364	0.000000	0.000063	...	0.0
9	3.0000	0.000153	0.001062	0.004699	6.682000e-07	0.0	0.0	0.000449	0.000000	0.000167	...	0.0
10	3.3330	0.000084	0.001186	0.005261	9.624000e-07	0.0	0.0	0.000540	0.000000	0.000091	...	0.0
11	3.6670	0.000170	0.001343	0.005629	1.307000e-06	0.0	0.0	0.000636	0.000000	0.000185	...	0.0
12	4.0000	0.000154	0.001493	0.006101	1.948000e-06	0.0	0.0	0.000737	0.000000	0.000167	...	0.0
13	4.3330	0.000089	0.001641	0.006619	2.486000e-06	0.0	0.0	0.000842	0.000000	0.000097	...	0.0
14	4.6670	0.000077	0.001760	0.007106	5.135000e-06	0.0	0.0	0.000952	0.000000	0.000084	...	0.0
15	5.0000	0.000092	0.001887	0.007555	6.499000e-06	0.0	0.0	0.001067	0.000000	0.000099	...	0.0
16	5.3330	0.000053	0.001916	0.007452	8.828000e-06	0.0	0.0	0.001178	0.000000	0.000057	...	0.0
17	5.6670	0.000038	0.001935	0.007342	1.409000e-05	0.0	0.0	0.001279	0.000000	0.000041	...	0.0
18	6.0000	0.000042	0.001950	0.007221	2.277000e-05	0.0	0.0	0.001373	0.000000	0.000046	...	0.0
19	6.3330	0.000038	0.001962	0.007118	3.055000e-05	0.0	0.0	0.001460	0.000000	0.000041	...	0.0
20	6.6670	0.000034	0.001972	0.007012	4.943000e-05	0.0	0.0	0.001540	0.000000	0.000037	...	0.0
21	7.0000	0.000034	0.001981	0.006915	6.334000e-05	0.0	0.0	0.001615	0.000000	0.000037	...	0.0
22	7.3330	0.000065	0.001990	0.006794	7.598000e-05	0.0	0.0	0.001684	0.000000	0.000070	...	0.0

23	7.6670	0.000592	0.002002	0.006180	8.665000e-05	0.0	0.0	0.001748	0.000000	0.000641	...	0.0
24	8.0000	0.000159	0.002018	0.006530	9.302000e-05	0.0	0.0	0.001808	0.000000	0.000172	...	0.0
25	8.3330	0.000023	0.002026	0.006596	9.913000e-05	0.0	0.0	0.001864	0.000000	0.000025	...	0.0
26	8.6670	0.000023	0.002031	0.006520	1.181000e-04	0.0	0.0	0.001916	0.000000	0.000025	...	0.0
27	9.0000	0.000024	0.002037	0.006454	1.289000e-04	0.0	0.0	0.001965	0.000000	0.000026	...	0.0
28	9.3330	0.000023	0.002041	0.006393	1.410000e-04	0.0	0.0	0.002010	0.000000	0.000025	...	0.0
29	9.6670	0.000066	0.002046	0.006291	1.520000e-04	0.0	0.0	0.002053	0.000000	0.000071	...	0.0
...	...	...	...	...	...	...	...	...	...	...	...	...
1063	354.3000	0.000000	0.002147	0.000000	2.366000e-03	0.0	0.0	0.006080	0.000016	0.000000	...	0.0
1064	354.7000	0.000000	0.002147	0.000000	2.364000e-03	0.0	0.0	0.006082	0.000016	0.000000	...	0.0
1065	355.0000	0.000000	0.002147	0.000000	2.362000e-03	0.0	0.0	0.006083	0.000016	0.000000	...	0.0
1066	355.3000	0.000000	0.002147	0.000000	2.361000e-03	0.0	0.0	0.006085	0.000016	0.000000	...	0.0
1067	355.7000	0.000000	0.002147	0.000000	2.359000e-03	0.0	0.0	0.006087	0.000016	0.000000	...	0.0
1068	356.0000	0.000000	0.002147	0.000000	2.357000e-03	0.0	0.0	0.006088	0.000016	0.000000	...	0.0
1069	356.3000	0.000000	0.002147	0.000000	2.356000e-03	0.0	0.0	0.006090	0.000016	0.000000	...	0.0
1070	356.7000	0.000000	0.002147	0.000000	2.354000e-03	0.0	0.0	0.006092	0.000016	0.000000	...	0.0
1071	357.0000	0.000000	0.002147	0.000000	2.352000e-03	0.0	0.0	0.006093	0.000016	0.000000	...	0.0
1072	357.3000	0.000000	0.002147	0.000000	2.350000e-03	0.0	0.0	0.006095	0.000016	0.000000	...	0.0
1073	357.7000	0.000000	0.002147	0.000000	2.349000e-03	0.0	0.0	0.006097	0.000016	0.000000	...	0.0
1074	358.0000	0.000000	0.002147	0.000000	2.347000e-03	0.0	0.0	0.006099	0.000016	0.000000	...	0.0
1075	358.3000	0.000000	0.002147	0.000000	2.345000e-03	0.0	0.0	0.006100	0.000016	0.000000	...	0.0
1076	358.7000	0.000000	0.002147	0.000000	2.344000e-03	0.0	0.0	0.006102	0.000016	0.000000	...	0.0
1077	359.0000	0.000000	0.002147	0.000000	2.342000e-03	0.0	0.0	0.006104	0.000016	0.000000	...	0.0
1078	359.3000	0.000000	0.002147	0.000000	2.340000e-03	0.0	0.0	0.006105	0.000016	0.000000	...	0.0
1079	359.7000	0.000000	0.002147	0.000000	2.339000e-03	0.0	0.0	0.006107	0.000016	0.000000	...	0.0
1080	360.0000	0.000000	0.002147	0.000000	2.337000e-03	0.0	0.0	0.006109	0.000016	0.000000	...	0.0
1081	360.3000	0.000000	0.002147	0.000000	2.335000e-03	0.0	0.0	0.006110	0.000016	0.000000	...	0.0
1082	360.7000	0.000000	0.002147	0.000000	2.334000e-03	0.0	0.0	0.006112	0.000016	0.000000	...	0.0
1083	361.0000	0.000000	0.002147	0.000000	2.332000e-03	0.0	0.0	0.006114	0.000016	0.000000	...	0.0
1084	361.3000	0.000000	0.002147	0.000000	2.330000e-03	0.0	0.0	0.006115	0.000016	0.000000	...	0.0
1085	361.7000	0.000000	0.002147	0.000000	2.329000e-03	0.0	0.0	0.006117	0.000016	0.000000	...	0.0
1086	362.0000	0.000000	0.002147	0.000000	2.327000e-03	0.0	0.0	0.006118	0.000016	0.000000	...	0.0
1087	362.3000	0.000000	0.002147	0.000000	2.325000e-03	0.0	0.0	0.006120	0.000016	0.000000	...	0.0
1088	362.7000	0.000000	0.002147	0.000000	2.324000e-03	0.0	0.0	0.006122	0.000016	0.000000	...	0.0
1089	363.0000	0.000000	0.002147	0.000000	2.322000e-03	0.0	0.0	0.006123	0.000016	0.000000	...	0.0
1090	363.3000	0.000000	0.002147	0.000000	2.321000e-03	0.0	0.0	0.006125	0.000016	0.000000	...	0.0
1091	363.7000	0.000000	0.002147	0.000000	2.319000e-03	0.0	0.0	0.006127	0.000016	0.000000	...	0.0
1092	364.0000	0.000000	0.002147	0.000000	2.317000e-03	0.0	0.0	0.006128	0.000016	0.000000	...	0.0

1093 rows × 36 columns

```
In [6]: fig = stackplot(df, xlabel = 'Time [days]', ylabel = 'Fraction of released', normalise = True)
        plt.title('Winter, 5 mm droplets')
        plt.tight_layout()
        fig.savefig('Massbalance_timeseries_normalised_Valhall_0.1year5z.png', dpi = 240)
```

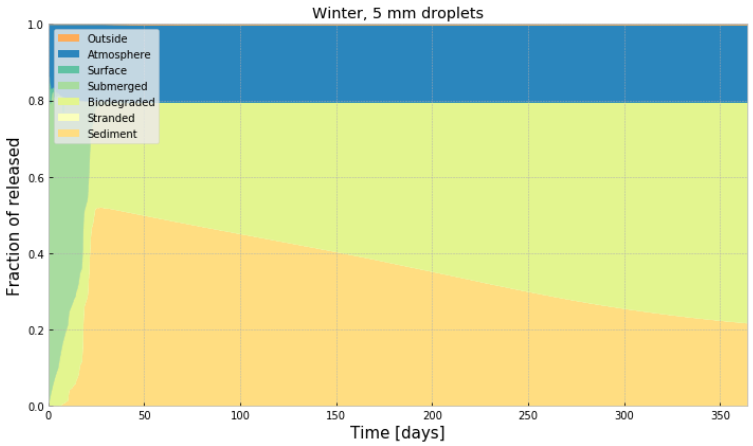

Scripts are provided by co-supervisor Tor Nordam, SINTEF Ocean.

APPENDIX C – MASS BALANCE RESULTS

The mass balance results will change with time, increasing atmospheric, sediment and biodegradation fractions and reducing surface and water column fractions. Some plots at different times t is included here for the leak rate of 1.0 l/h.

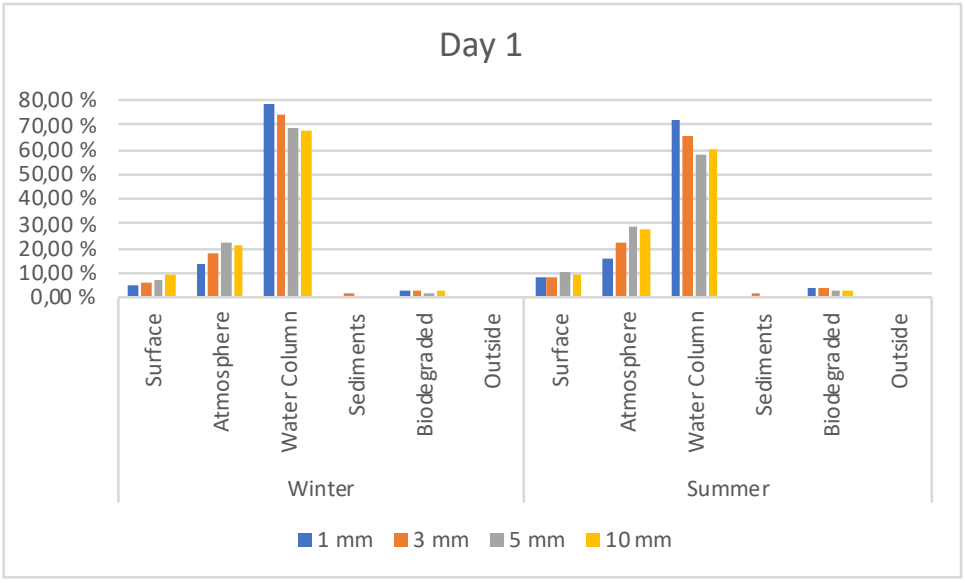

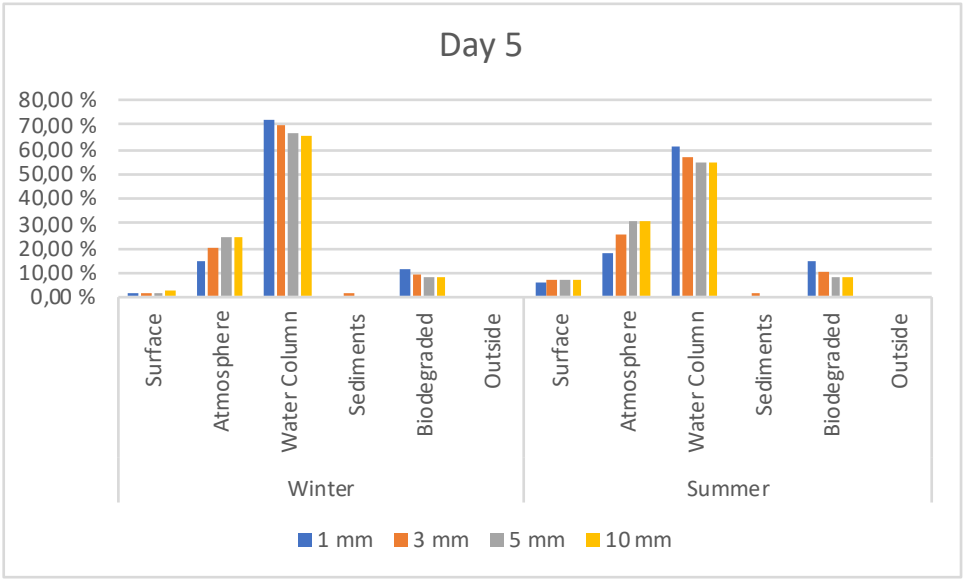

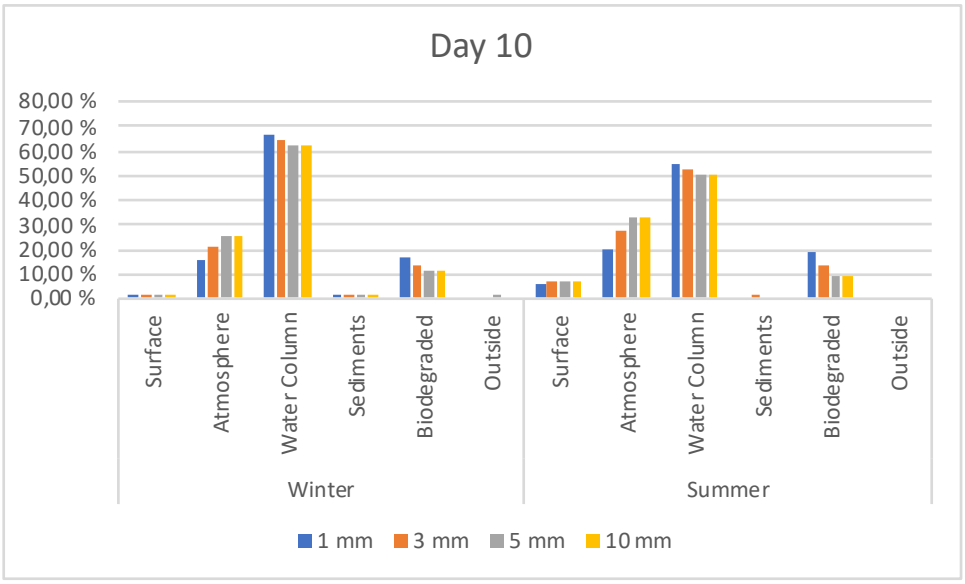
Day 10
80,00 %
70,00 %
60,00 %
50,00 %
40,00 %
30,00 %
20,00 %
10,00 %
0,00 %
Surface
Atmosphere
Water Column
Sediments
Biodegraded
Outside
Surface
Atmosphere
Water Column
Sediments
Biodegraded
Outside
Winter
Summer
1 mm
3 mm
5 mm
10 mm

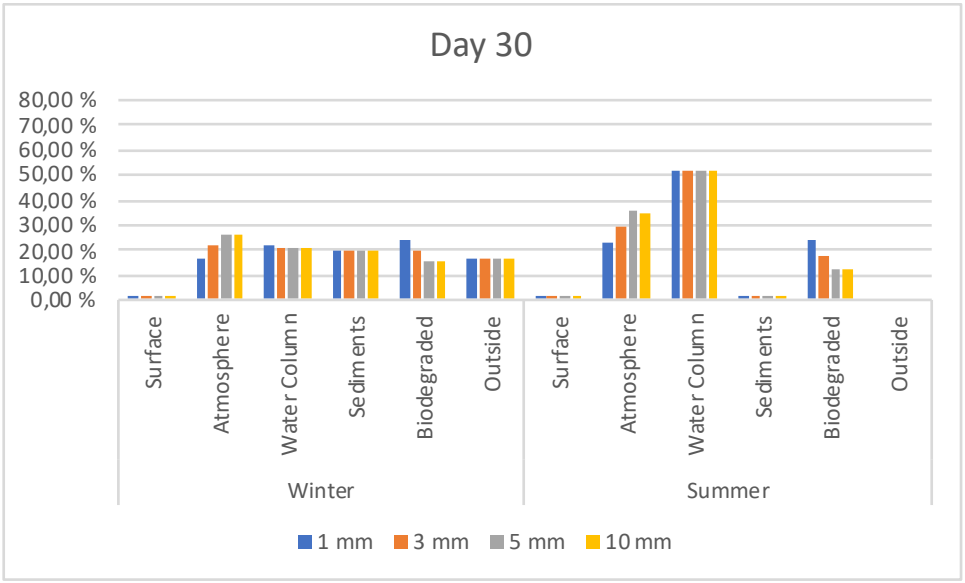
Day 30
80,00 %
70,00 %
60,00 %
50,00 %
40,00 %
30,00 %
20,00 %
10,00 %
0,00 %
Surface
Atmosphere
Water Column
Sediments
Biodegraded
Outside
Surface
Atmosphere
Water Column
Sediments
Biodegraded
Outside
Winter
Summer
1 mm
3 mm
5 mm
10 mm

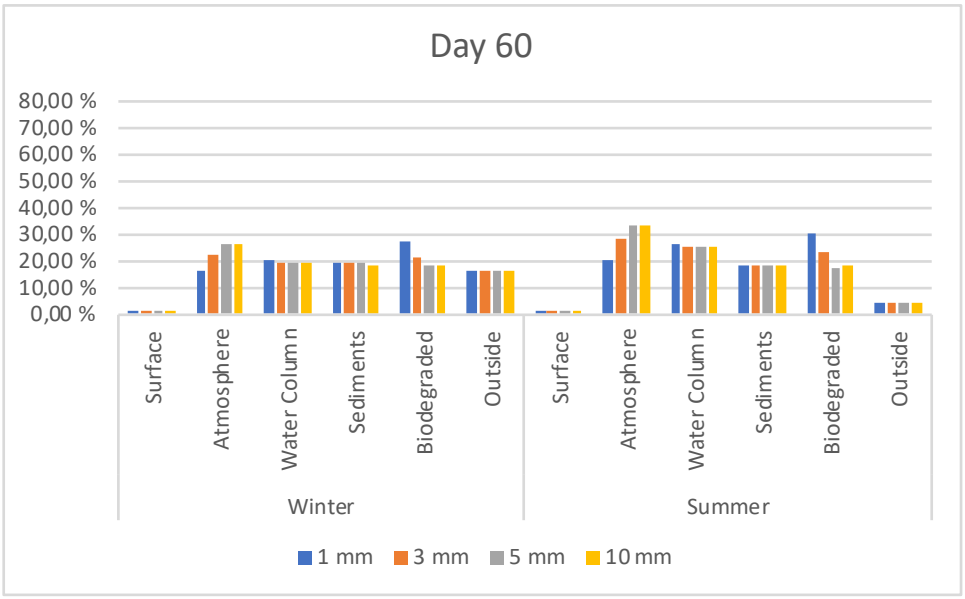
Day 60
80,00 %
70,00 %
60,00 %
50,00 %
40,00 %
30,00 %
20,00 %
10,00 %
0,00 %
Surface
Atmosphere
Water Column
Sediments
Biodegraded
Outside
Surface
Atmosphere
Water Column
Sediments
Biodegraded
Outside
Winter
Summer
1 mm
3 mm
5 mm
10 mm

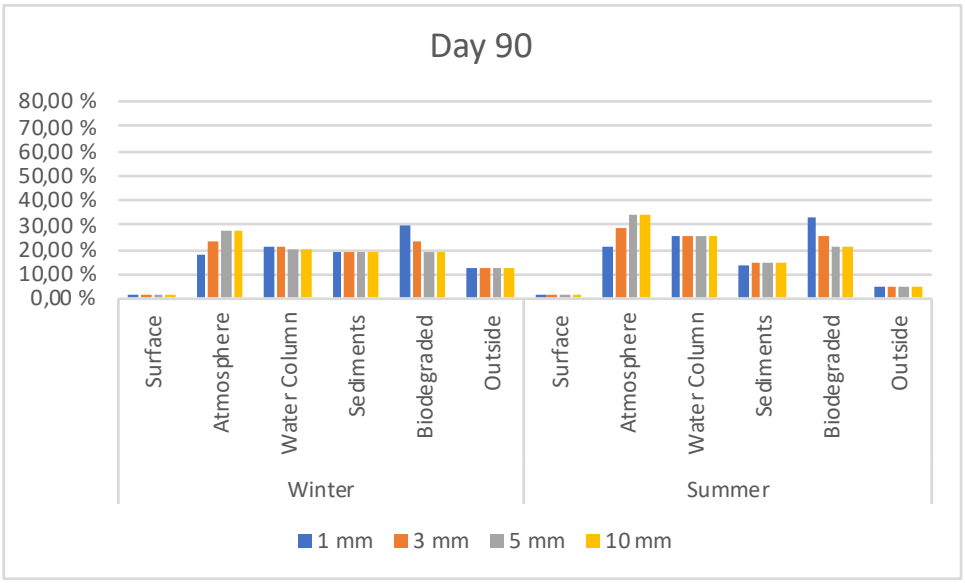
Day 90
80,00 %
70,00 %
60,00 %
50,00 %
40,00 %
30,00 %
20,00 %
10,00 %
0,00 %
Surface
Atmosphere
Water Column
Sediments
Biodegraded
Outside
Surface
Atmosphere
Water Column
Sediments
Biodegraded
Outside
Winter
Summer
1 mm
3 mm
5 mm
10 mm

APPENDIX D – MASS BALANCE RESULTS DAY 90

Leak rate	Season	Droplet size	Surface	Atmosphere	Water Column	Sediments	Biodegraded	Outside grid
0.01 l/h	Winter	1 mm	0.2 %	17.7 %	21.2 %	19.1 %	29.2 %	12.6 %
		3 mm	0.2 %	24.1 %	20.6 %	19.4 %	23.2 %	12.6 %
		5 mm	0.3 %	29.0 %	20.5 %	19.3 %	18.5 %	12.5 %
		10 mm	0.2 %	29.1 %	20.4 %	19.3 %	18.3 %	12.6 %
	Summer	1 mm	1.2 %	21.2 %	25.7 %	14.2 %	33.1 %	4.5 %
		3 mm	1.3 %	29.1 %	25.4 %	14.3 %	25.4 %	4.5 %
		5 mm	1.2 %	35.0 %	25.4 %	14.2 %	19.7 %	4.6 %
		10 mm	1.3 %	35.0 %	25.4 %	14.3 %	19.5 %	4.5 %
0.1 l/h	Winter	1 mm	0.2 %	17.6 %	21.2 %	19.0 %	29.3 %	12.6 %
		3 mm	0.3 %	23.9 %	20.6 %	19.3 %	23.3 %	12.7 %
		5 mm	0.2 %	28.8 %	20.5 %	19.2 %	18.7 %	12.6 %
		10 mm	0.2 %	28.7 %	20.6 %	19.0 %	18.6 %	12.8 %
	Summer	1 mm	1.4 %	21.3 %	25.5 %	14.2 %	33.1 %	4.6 %
		3 mm	1.2 %	28.9 %	25.4 %	14.4 %	25.5 %	4.5 %
		5 mm	1.3 %	34.6 %	25.3 %	14.4 %	19.9 %	4.5 %
		10 mm	1.3 %	34.5 %	25.5 %	14.2 %	19.9 %	4.6 %
1.0 l/h	Winter	1 mm	0.2 %	17.6 %	21.2 %	19.2 %	29.3 %	12.5 %
		3 mm	0.3 %	23.6 %	20.7 %	19.3 %	23.5 %	12.7 %
		5 mm	0.4 %	28.0 %	20.4 %	19.1 %	19.3 %	12.8 %
		10 mm	0.4 %	27.9 %	20.4 %	19.2 %	19.4 %	12.7 %
	Summer	1 mm	1.2 %	21.3 %	25.8 %	14.0 %	33.1 %	4.5 %
		3 mm	1.3 %	28.6 %	25.5 %	14.3 %	25.8 %	4.5 %
		5 mm	1.4 %	33.9 %	25.3 %	14.2 %	20.6 %	4.6 %
		10 mm	1.4 %	33.8 %	25.3 %	14.1 %	20.7 %	4.7 %